PHILIPPINE AGRICULTURAL AND BIOSYSTEMS ENGINEERING JOURNAL

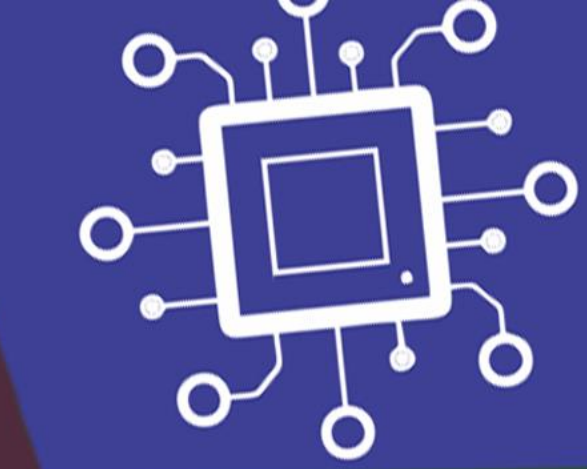

ISSN: 2619-6913
Volume 3 Issue No. 1, 2020

This journal is published by the
Philippine Society of Agricultural and Biosystems Engineers (PSABE)

The printing of this publication was funded by the Philippine Council for Agriculture and Fisheries (PCAF), a government agency attached to the Department of Agriculture (DA).

TABLE OF CONTENTS

PERFORMANCE STATUS OF SOLAR-POWERED IRRIGATION SYSTEMS TESTED BY THE AGRICULTURAL MACHINERY TESTING AND EVALUATION CENTER IN THE PHILIPPINES

Romulo E. Eusebio, Rhey Marc C. Albalos, Alphonse Regin R. Magmanlac
Arthur L. Fajardo, Darwin C. Aranguren

Agricultural Machinery Testing and Evaluation Center (AMTEC), Pili Drive,
University of the Philippines Los Baños, College, Laguna

Abstract

The Agricultural Machinery and Testing Center (AMTEC) has tested 27 sites of solar-powered irrigation systems (SPIS) all over the country. SPIS is a communal irrigation system initiated by the Department of Agriculture (DA) to increase the country's irrigable areas. This system consists of the following essential components: pumpset, photovoltaic modules, controller, water tank (optional), and irrigation pipes. The objective of the AMTEC SPIS test is to provide necessary information to the procuring entity and the contractor to evaluate the performance of the system for procurement and further system improvement. The individual performance of an SPIS was evaluated based on the photovoltaic array output, controller output, and pumpset performance. This paper presents the test summary of the systems evaluated on-site, consisting of system performance information and different installation set-up of pump sets and photovoltaic modules, various components and performance points of an SPIS, and problems encountered when designing and testing of this system.

Keywords: *Agricultural Machinery Testing and Evaluation Center, Department of Agriculture, performance, Solar-Powered Irrigation System, testing*

Introduction

Through R.A. 10601, otherwise known as the AFMEC law, the Agricultural Machinery Testing and Evaluation Center (AMTEC) shall perform testing and evaluation of all agricultural and fisheries equipment sold in the local market. As the premiere and reference testing center in the country, AMTEC has received hundreds of test applications per year. Last year, AMTEC started testing solar-powered irrigation systems (Figure 1), a project of the Department of Agriculture (DA). The system installed in Brgy. Manubuan, Matalam, North Cotabato was the first-ever SPIS tested by AMTEC. SPIS aims to increase the country's irrigable areas without the use of fuel and electricity and will be free of charge. But for an SPIS to be successful, the installed system must meet the design requirements set forth by the Regional Agricultural Engineering Division (RAED). AMTEC performs SPIS testing to assess the system performance that includes the PV module output,

inverter/controller output, pumpset output, discharge capacity, and system efficiency.

Solar-powered irrigation systems are mainly composed of four major components, namely solar photovoltaic (PV) modules, combiner box, inverter/pump controller, and the pump set. For some installations, the inverter or pump controller also acts as the combiner box. Each component should be sized appropriately and conform to each other's ratings. Figure 2 shows an actual installed SPIS unit.

The solar PV array is the main power source of an SPIS. It is composed of multiple panels configured in several strings with each string consisting of a certain number of PV modules. Each string is composed of several panels connected in series, while strings are connected in parallel. To get the array's total power, the power rating of one panel is multiplied by the number of panels in the array. On the other hand, the string configuration determines the maximum voltage and maximum current the array can deliver. The number of modules per string determines the maximum voltage the array can deliver. Assuming that all the modules used in a string are of the same rating, the maximum rated voltage of the array can be computed by multiplying the number of modules per string and the maximum voltage rating of one PV module. The maximum current of the array is determined by its number of strings. The rated maximum current of one module is simply multiplied by the number of strings.

When sizing the array, it is common practice to oversize its total power capacity. This ensures that the SPIS can operate even under cloudy conditions. Basically, the bigger the array, the more power it can harvest from the sun.

The combiner box consolidates the output of each string. It reduces the number of wires used by combining the multiple strings' output with fewer wires with bigger diameters. The output of the combiner box is then connected to the inverter or pump controller. The combiner box also contains a circuit breaker, which acts as a switch and a safety feature.

Inverters or pump controllers allow the conversion of DC output of the array into AC, which is to be used by the pump set. An inverter's performance can be measured by dividing the AC output power and the DC input power. This will tell us how efficient the inverter and controller are in converting DC power into AC power.

The pump set is the main power consumer of SPIS. Arrays are oversized depending on the capacity of the electric motor of the pump set. There are two types of pumps used in the SPIS, surface pump, and submersible pump. Surface pumps are used with shallow water sources and distant service areas, while submersible pumps are used with deep water sources and near service areas.

SPIS generates three different kinds of power. The first is DC power generated by the PV array. The second is AC power converted by the inverter from

the DC power. The last is water power, which is the equivalent power generated by the pumpset. System efficiency is computed by dividing the water power and DC power. As discussed earlier, inverter efficiency is computed by dividing AC power with DC power. Pump efficiency can also be computed by dividing the water power with AC power.

To date, AMTEC has already tested 27 units of SPIS. This paper summarizes and compares the performance of different SPISs tested by AMTEC. It is hoped that the paper will assist the procuring entity and the manufacturer/supplier on the evaluation of the system.

OBJECTIVES

The main objectives of this paper are:

1. To present and discuss the specifications of the different components and performance points of an SPIS and
2. Present the common problems encountered during the SPIS test.

MATERIALS AND METHODS

Performance **t**est data of all Solar-Powered Irrigation Systems (SPIS) tested were obtained from the AMTEC Test Reports. It consisted of 27 sites all over the country. SPIS were then grouped according to their size and analyzed for performance such as PV modules output, Controller output, Pump set input and output, and overall efficiency.

RESULTS AND DISCUSSION

Of the 27 sites already tested by AMTEC, 20 are located in Luzon, while seven are located in Mindanao. Figure 3 shows the locations of the 27 sites that were tested.

The Methods of Test for SPIS was based on the Test Protocol developed by DA-BAFE and AMTEC. SPIS's test is conducted for at least eight (8) hours from 8:00 AM to 4:00 PM with 10:00 AM to 2:00 PM as the critical period of the test where the maximum system efficiency and discharge capacity are usually observed. Before starting the test, the nameplate rating of the PV modules, controller, and pumpset, static heads (m), total pipe length (m), and PV module face direction and angle of inclination (°) are to be collected. Data are collected every thirty (30) minutes from the beginning of the test to the end. The data to be collected are solar irradiance (W/m^2), ambient temperature (°C), relative humidity (%), input current (DCA), input voltage (DCV), and input power (kW) to the controller, output current (A), output voltage (V), and output power (kW) from the controller, and system discharge capacity (L/s). Preliminary testing preparation includes making sure that

all of the pipe valves are fully opened, and test applicant system adjustments since no modifications are permitted once the test begins.

During data collection, the pyranometer is placed on the surface of the PV modules to measure the actual irradiance received by the modules. The power meter (with VFD function) is used to measure the input/output current, voltage, and power of the controller. System discharge capacity is measured by collecting the water from the pump outlet pipe using the volumetric method. The ambient was also recorded. SPIS test procedure is replicated for at least two (2) days. Data are averaged and presented in tabular and graphical format.

Component Brands

SPISs tested come from a variety of brands, from the pump and its coupled motors, controllers, and PV module. These different brands came from China, Germany, Belgium, Italy, Singapore, and others. A system is rarely composed of a single brand. Mostly pump and motors, PV modules, controllers have different manufacturers.

PV Array

A PV array consists of strings connected in parallel with each string consisting of modules connected in series. The output of the array depends on the arrangement, configuration, angle of tilt, shade, temperature, and cleanliness of the modules' surface.

Array's tilt is the angle of the inclination of the module with respect to horizontal. The Tilt angle may affect the output of the modules by 20 %. When designing a PV module's fixed angle of inclination, a good rule of thumb is equal to the location's latitude. In a Philippine setting, the modules should be facing south.

Controller

The controller is the link between the PV array and the pump set. For an SPIS that uses an alternating current (AC) pumpset, the controller is used as an inverter, which converts the direct current (DC) output of the PV array to an AC input to the pump set. For an SPIS where the DC power source is fluctuating, the controller is provided with a variable speed regulator that governs the shaft speed of the pumpset based on the DC power it receives from the PV array. A Controller can also be used as a charge controller for those sites that use batteries. It regulates the voltage and current from the PV modules to the batteries.

Pumpset

The pump set is the part of the system that delivers the irrigation water. It is usually a centrifugal pump close-coupled to an electric motor. A centrifugal pump

consists of an impeller and a casing. For SPIS, the two types of pumpset commonly in the system are surface and submersible pump set. The surface pump set is installed on the ground above the water surface, while the submersible pump is installed below the water surface. It derives its power from the controller on the system.

Pumpset Size

The size of a pump set can be determined from its discharge and suction outlet diameter. For the surface pumpset, the size is the diameter of the discharge pipe and the suction pipe's diameter. For example, a surface pumpset with a size of 100 mm x 150 mm (4" x 6"), the 100 mm is the diameter of the discharge pipe, and the 150 mm is the diameter of the suction pipe. For a submersible pump set, the diameter of the discharge outlet is its size. To categorize the SPISs tested by AMTEC, the pump set discharge outlet size is used. The following are the common discharge outlet size of SPISs tested by AMTEC: 63 mm (2.5"), 75 mm (3"), 100 mm, 127 mm (5"), 150 mm, and 200 mm (8").

The performances of the test SPISs are categorized into different pump outlet sizes since it is directly proportional to the pump input power to the pumpset, the number of panels, and rated PV array output power. Tables 1, 2, 3, 4, and 5 summarize the maximum system performances of the tested SPISs. The overall average maximum system efficiency of the tested SPISs is 48.79 %, with Site 6D obtaining the highest maximum system efficiency of 87.73 % and Site 8A acquiring the lowest maximum system efficiency of 12.67 %. Out of the 27 sites tested by AMTEC, 19 sites used a surface pump while eight sites used submersible pumps. Furthermore, 22 sites had an open water source while 5 had groundwater source

The systems with 3" and below pump outlet size had a number of panel range of 16 to 54 pieces, and array output power range of 2418.00 W to 2764.89 W. Site 3A is deemed to be over-designed in terms of the number of panels because the pump only drew 2435.93 W from the rated array power of 14580 W, which is only 16.71 % of the power utilized by the system. For the 4" pump outlet sized SPISs, the number of panels ranges from 48 to 60 pieces and array output power range of 6317.20 W to 11959.43 W. The SPISs with 5" pump outlet size had a panel number range of 32 to 105 pieces and array output power range of 5001.66 W to 20031.44 W. Sites 5B1 and 5B2 are designed to have small safety factor, but high array power utilization since the sites have 80.51 % and 92.47 % system power consumption, respectively. SPIS sites with 6" pump outlet size had a panel number range of 54 to 140 pieces and array output power range of 7132.36 W to 33017.40 W. Lastly, there is only one unit of SPIS tested with an 8" pump outlet size. This site had 108 pieces of panels with a maximum array output power of 12691.40 W.

Performance

The performance of the SPIS depends on the output of the PV array, efficiency of the controller, height of the pump set from the source to the delivery outlet (Total Head), size of the inlet and outlet pipes, number of pipe bends, water quality, and efficiency of the pump set. The performance of the system is also highly affected by the available solar irradiance. The performance of the SPIS can improve even under overcast conditions by increasing the design capacity of the PV array.

The efficiency of Controller / Inverter

The inverter is an electronic device which converts DC that comes from the PV panels into AC. Like any such device, there are some energy losses commonly in the form of heat. Therefore, an efficiency rating for the inverter is required to calculate how much power is actually produced. A typical inverter should have an efficiency of about 94 %, with 6 % of the energy lost in the conversion process. The input capacity of the inverter should be properly sized to accommodate the output of the PV array. The controller/inverter efficiencies of the tested SPISs by AMTEC are summarized in Tables 1 to 5. The average controller / inverter efficiency of tested SPIS with 3" and below, 4", 5", 6", and 8" size pump sets are 71.51 %, 62.47 %, 72.55 %, 67.93 %, and 70.00 %, respectively.

Total Head

The Total head is the equivalent height by which the pump set can raise a certain amount of water. It is the combination of suction, discharge, velocity, and frictional heads. For a centrifugal pump, as the total head increases, the discharge decreases and vice versa. Surface pumps have a maximum suction lift capacity wherein the pump can draw from the source. For areas where surface pumps would incur high suction heads, submersible pumps are used. Submersible pumps are also recommended for flood-prone areas. The friction head increases with the pipe's length from the pump outlet to the discharge pipe outlet. Velocity head also increases as discharge capacity increases. Determining the total head is very important in pump selection and maximizing pump efficiency. The total head of the tested SPISs by AMTEC is summarized in Tables 1 to 5.

Water Quality

There are different pumps for different applications. There are low head but higher discharge pumps or high head low discharge pump. Also, pumps designed to pump clear liquid or pumps can be used to pump liquids with solids in suspension, sewage, and any other type of liquid. While pumps are designed to be used in all types of liquids, the water quality still affects the performance of the pump. Some SPISs have water sources wherein river sand is drawn along with water during discharge. This can heavily affect the discharge capacity and efficiency of the pump

as well as shorten the life of the pump set. River sand can also accumulate in the discharge tank if not drained properly.

Efficiency of the Pumpset

Different pumps have different efficiencies, which were determined in the laboratory. Pump performance curves show the performance of a pump in varying head and discharge. For a given pump, there is an optimum setting for head and discharge where the efficiency is maximum. For the prime mover, usually an electric motor for SPIS, it also has a performance curve based on laboratory tests. The pump and the motor's performance curves are used to properly combine the pump and the motor where the efficiency is maximized. The best operating point of the pump should match the best operating point of the motor. Figure 4 shows an example of a pump performance curve. The maximum pumpset efficiencies of the SPISs tested by AMTEC are summarized in Tables 1 to 5. The average pump set efficiency of the tested SPIS with 3" and below, 4", 5", 6", and 8" size pump sets are 53.61 %, 63.71 %, 41.94 %, 60.45 %, and 17.96 %, respectively.

Discharge Capacity

Discharge capacity is the most important performance characteristic of an SPIS. It is the culmination of all the other SPIS performance characteristics. It is the primary data needed for the procuring entity to assess the acceptability of an SPIS site. Discharge capacity is directly proportional to the pump outlet size, motor and pump capacity, inverter capacity, and PV array output and is inversely proportional to head. The discharge capacities of the SPISs tested by AMTEC are summarized in Tables 1 to 5. The average discharge capacities of tested SPISs that used pumpset outlet sizes of 3" and below, 4", 5", 6", and 8" are 35.08 m^3/h, 85.33 m^3/h, 92.69 m^3/h, 213.94 m^3/h, and 207.02 m^3/h, respectively. It should be noted that there is only one site tested with an 8" size pumpset.

Common Problems Encountered During Testing

Some of these recurring problems encountered during testing can be addressed to prevent future occurrences. Apart from the usual problem that is the presence of overcast, there are several issues encountered which affects the methods of test.

The testing methods for SPIS require the continuous operation of the system, ideally from 8:00 am to 4:00 pm. One problem encountered involves the sustainability of the water source. In some cases, the SPIS derives more water than the source can replenish, may it be groundwater or open water source. In such cases, the SPIS is temporarily shut down to facilitate groundwater recharge or to preserve the open water source.

The second limit to continuous SPIS operation is the capacity of the discharge tank. In some sites, the discharge tank output is smaller than the discharge tank input. In such cases, the overflow sensor is triggered, and the system shuts down. For sites without overflow sensor, the discharge tank overflows and makes it impossible for the technician to measure the discharge of the pump.

Observations with the System Design

As mentioned earlier, certain aspects of the design have affected the execution of the test methods for SPIS. Apart from the design of the discharge tank and selection of water sources, other problems have been observed with the system design.

The type of pump used is a very important aspect of system designing. The designer should have a clear criterion on whether to use a surface pump or submersible pump. Some sites have implemented a surface pump when a submersible pump would have been much more effective in terms of performance and even survivability in floods. Surface pumps also have an inherent limit in terms of suction lift, which must be considered in the selection of pumps. The performance of surface pumps whose actual suction lift is higher than the rated suction lift will suffer.

Proper PV array configuration is also very important. Some sites had an unequal number of modules per string. This will reduce the effective designed voltage to the voltage of the string with the least number of modules. By reducing the effective voltage of the array, the total output power of the array is reduced. It is also important to properly mount the PV array corresponding to the site where it is installed.

There is also an instance of an improperly sized controller/inverter against the PV array. The rating of the inverter must always be greater than the PV array output. It is recommended that the procuring entity is present during the delivery and installation of the components on-site to verify the specifications prior to commissioning to prevent damage to equipment.

Proper piping specifications should also be considered. There was an incident wherein the suction pipe collapsed due to incorrect pipe thickness. The surface pump created a vacuum pressure that is greater than the strength of the pipe resulting in a collapse, which resulted in a termination of the test.

The designer must also consider the possible shadows that may be generated upon the complete implementation of the design. On one site, the discharge tank casted a shadow over the PV array, which resulted in an abrupt drop in performance. Nearby trees can also cast shadows over the PV array that can affect the PV array output power.

CONCLUSION

AMTEC has tested a total of 27 sites of Solar-powered irrigation systems. The average maximum system efficiency of the SPISs tested by AMTEC is 48.79 %. Based on the summarized data of the tested sites, the number of PV modules, array output power, and pump discharge are directly proportional to the pump size while the total head, controller/inverter efficiency, pump set efficiency, and system efficiency vary across pump size as shown in Table 6. It is recommended to design SPIS appropriately to attain high system performance. Some system properties to address when designing solar-powered irrigation systems are appropriate type and specification of a pump, proper PV array configuration, and installation, controller/inverter that is suited to the PV array and pumpset, correct pipe size and material, and nearby structures that could cast shadows to the PV array.

ACKNOWLEDGMENTS

The assistance of Russel Capunpon in searching and summarizing the data from previous AMTEC test reports is appreciated.

REFERENCES

Philippine Agricultural Engineering Standards. 2000. PAES 115:2000 – Centrifugal, Mixed Flow, and Axial Flow Water Pumps – Methods of Test. In Philippine Agricultural Engineering Standards Volume 1, Section A

Philippine Agricultural Engineering Standards. 2002. PAES 130:2002 – Electric Motor – Methods of Test. In Philippine Agricultural Engineering Standards Volume 3, Section A

Agricultural Machinery Testing and Evaluation Center & Department of Agriculture – Bureau of Agriculture and Fisheries Engineering. 2018. Protocol: Solar-Powered Irrigation System – Methods of Test. Protocol in Preparation

Agricultural Machinery Testing and Evaluation Center. 2018 & 2019. Various AMTEC Test Reports. AMTEC-UPLB, Los Baños, Laguna

Table 1. Maximum Performance Data of SPISs with Pump Outlet Size of 3" and Below

Site	Number of Panels	Rated Array Output Power (W)	Type of Pump	Type of Water Source	Maximum Data Points							
					Total Head (m)	Discharge Capacity (m^3/h)	Array Output Power (W)	Input Power to Pumpset (W)	Pumpset Output Power (W)	Controller/ Inverter Efficiency (%)	Pumpset Efficiency (%)	System Efficiency (%)
3A	54	14580	Surface	Ground Water	8.81	54.63	2435.93	2163.63	1310.84	88.82	60.59	55.05
3B	16	4960	Submer-sible	Ground Water	15.93	24.61	2418.00	1590.21	1067.38	65.77	67.12	51.12
3C	16	4960	Submer-sible	Ground Water	12.96	25.99	2764.89	1657.70	549.01	59.96	33.12	21.42

Table 2. Maximum Performance Data of SPISs with Pump Outlet Size of 4"

Site	Number of Panels	Rated Array Output Power (W)	Type of Pump	Type of Water Source	Maximum Data Points							
					Total Head (m)	Discharge Capacity (m^3/h)	Array Output Power (W)	Input Power to Pumpset (W)	Pumpset Output Power (W)	Controller/ Inverter Efficiency (%)	Pumpset Efficiency (%)	System Efficiency (%)
4A	60	18600	Surface	Open Water	9.63	110.13	11959.43	7198.73	5510.00	60.19	76.54	48.78
4B	54	14580	Submer-sible	Ground Water	11.31	67.55	9080.38	5645.99	3817.25	62.18	67.61	68.23
4C	48	15600	Surface	Open Water	9.07	78.30	6317.20	4108.88	1930.00	65.04	46.97	41.55

Table 3. Maximum Performance Data of SPISs with Pump Outlet Size of 5"

Site	Number of Panels	Rated Array Output Power (W)	Type of Pump	Type of Water Source	Maximum Data Points							
					Total Head (m)	Discharge Capacity (m^3/h)	Array Output Power (W)	Input Power to Pumpset (W)	Pumpset Output Power (W)	Controller/ Inverter Efficiency (%)	Pumpset Efficiency (%)	System Efficiency (%)
5A	105	33075	Submer-sible	Open Water	28.79	118.42	20031.44	ND	9276.90	ND	ND	72.46
5B	32	11200	Submer-sible	Open Water	16.90	95.91	9018.11	6249.27	4413.97	69.30	70.6317698	53.21
5C	32	11200	Submer-sible	Open Water	16.84	92.69	10356.42	6875.68	4250.28	66.39	61.8161404	49.04
5D	45	14175	Submer-sible	Open Water	12.77	107.89	10640.80	ND	3752.49	ND	ND	46.08
5E	56	16520	Surface	Open Water	9.95	99.22	8831.82	6848.89	2687.73	77.55	39.2432934	47.57
5F	36	11340	Surface	Open Water	6.96	98.93	5001.66	3590.28	1873.89	71.78	52.1934222	38.25
5G	56	17640	Surface	Open Water	8.76	72.04	7323.53	5503.95	1718.63	75.15	31.2253927	38.60
5H	56	17640	Surface	Open Water	8.73	69.81	7386.64	5443.50	1658.88	73.69	30.4745109	31.86
5I	56	17640	Surface	Open Water	6.04	93.13	8186.60	5614.60	1531.22	68.58	27.272112	28.78
5J	56	17640	Surface	Open Water	5.76	78.83	7004.82	5457.64	1236.70	77.91	22.6599776	20.74

Note: Site Codes 5B1 and 5B2, 5F1 and 5F2, and 5G1 and 5G2 denotes two pumps on a single SPIS site.

Table 4. Maximum Performance Data of SPISs with Pump Outlet Size of 6”

Site	Number of Panels	Rated Array Output Power (W)	Type of Pump	Type of Water Source	Maximum Data Points							
					Total Head (m)	Discharge Capacity (m³/h)	Array Output Power (W)	Input Power to Pumpset (W)	Pumpset Output Power (W)	Controller/ Inverter Efficiency (%)	Pumpset Efficiency (%)	System Efficiency (%)
6A	140	43400	Submer-sible	Open Water	22.50	230.47	33017.40	17605.50	14122.90	53.32	80.22	67.13
6B	68	22440	Surface	Open Water	10.83	316.00	19002.10	13358.89	9323.31	70.30	69.79	65.93
6C	120	37200	Surface	Open Water	14.62	217.51	26382.30	16880.18	8660.00	63.98	51.30	65.72
6D	54	17820	Surface	Open Water	8.34	320.28	9532.15	6311.25	5272.31	66.21	83.54	87.73
6E	54	17820	Surface	Open Water	11.31	213.23	10458.64	6562.05	5565.42	62.74	84.81	63.15
6F	78	23400	Surface	Open Water	9.51	231.02	11792.22	10006.00	5982.06	84.85	59.78	51.58
6G	60	18600	Surface	Open Water	11.68	168.09	12481.94	7816.84	5346.89	62.63	68.40	53.08
6H	60	19500	Surface	Open Water	10.65	179.70	11474.78	8897.78	5212.63	77.54	58.58	61.81
6I	54	17820	Surface	Open Water	8.23	209.10	9483.10	6257.44	4686.18	65.99	74.89	54.47
6J	60	18600	Surface	Open Water	8.50	149.79	11269.63	7192.25	3469.06	63.82	48.23	44.79
6K	60	18600	Surface	Open Water	6.88	145.26	9647.77	6662.73	2722.21	69.06	40.86	33.20
6L	60	18900	Surface	Ground Water	6.24	152.54	7132.36	5453.68	2590.00	76.46	47.49	59.09
6M	140	46200	Submer-sible	Open Water	3.91	248.18	21674.05	14344.10	2570.00	66.18	17.92	30.51

Table 5. Maximum Performance Data of SPISs with Pump Outlet Size of 8”

Site	Number of Panels	Rated Array Output Power (W)	Type of Pump	Type of Water Source	Maximum Data Points							
					Total Head (m)	Discharge Capacity (m³/h)	Array Output Power (W)	Input Power to Pumpset (W)	Pumpset Output Power (W)	Controller/ Inverter Efficiency (%)	Pumpset Efficiency (%)	System Efficiency (%)
8A	108	34020	Surface	Open Water	2.83	207.02	12691.40	8883.91	1595.14	70.00	17.96	12.67

Table 6. Summary of Average Performances of SPISs Based on Pump Outlet Size

Average	≥ 3"	4"	5"	6"	8"
Discharge Capacity (m³/h)	35.08	85.33	92.69	213.94	207.02
Controller / Inverter Efficiency (%)	71.51	62.47	72.55	67.93	70.00
Pumpset Efficiency (%)	53.61	63.71	41.94	60.45	17.96
System Efficiency (%)	42.53	52.85	42.66	56.78	12.67

Note: There is only one data point for 8” size pumps.

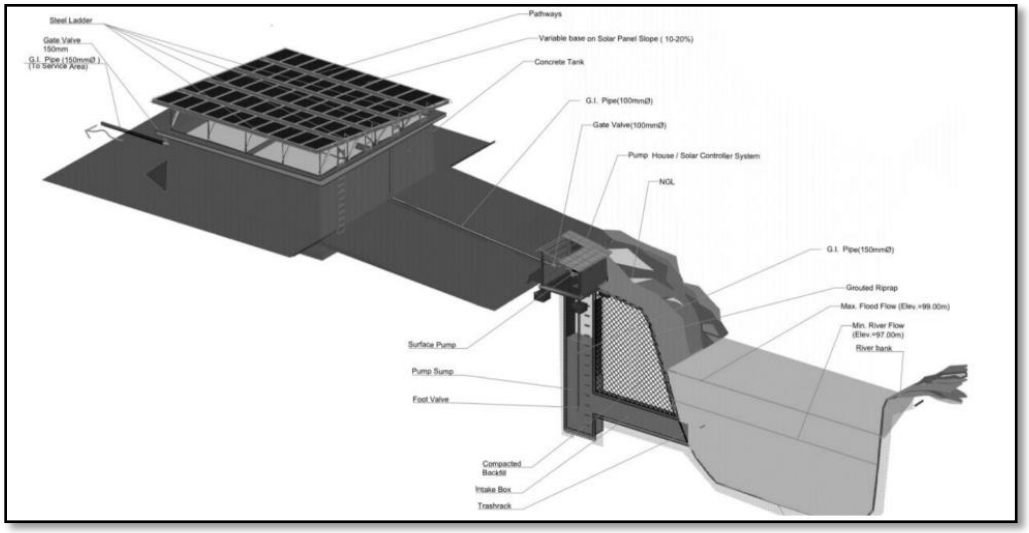

Figure 1. Typical Design of SPIS

Figure 2. Actual Installed SPIS

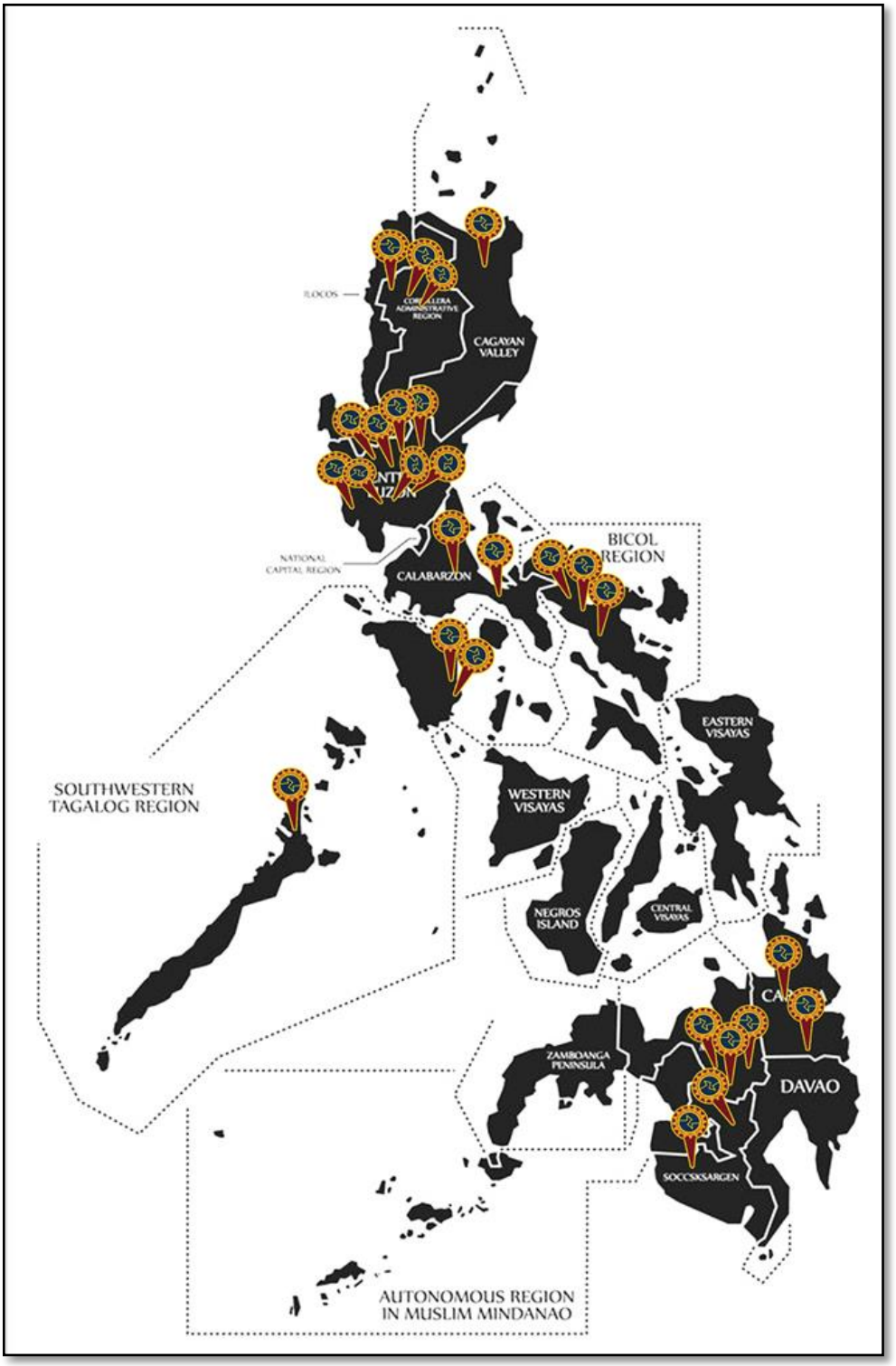

Figure 3. The 27 SPIS Sites Tested by AMTEC.

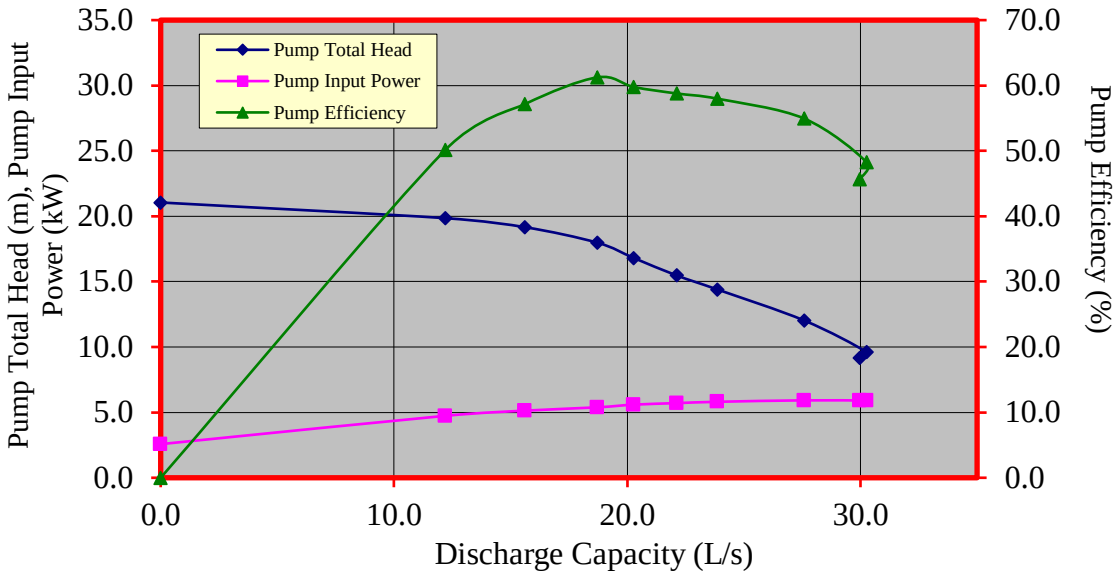

Figure 4. Sample Pump Performance Curve

QUANTIFYING THE IMPACT OF LAND USE CHANGE AS AFFECTED BY GROUNDWATER HYDROLOGY USING SWAT- MODFLOW MODELING

C.M. Pascual[1] and J.I. Jimenez[2]

[1]Department of Agricultural and Biosystems Engineering, College of Engineering
Mariano Marcos State University, Batac City 2906 Ilocos Norte
[2]College of Agriculture, Forestry and Sustainable Development
Mariano Marcos State University, Batac City 2906 Ilocos Norte

Abstract

Comprehensive planning on land-use change and water resources development to maximize human consumption is important for meeting the demand of increasing competing consumers. However, there is a need for physically-based modeling tools to assist with identifying successful water management strategies, especially groundwater hydrologic responses. This research presents the newly-coupled SWAT-MODFLOW model that allows application at Quaioit River watershed in the northern Philippines, specifically in quantifying the agricultural expansion on the land use plan of Paoay as affected by the groundwater hydrology was explored. The study showed the impact of the conversion of potential undisturbed land areas suitable for crop production with groundwater use. The SWAT-MODLFOW model showed that the area had groundwater recharge ranged from 69 to 350m^3/d with the varying hydraulic head from 96 to 40masl at the observation grid cells of the area. Geospatial analysis on the impact of land-use change, particularly on agricultural expansion due to groundwater hydrology where groundwater discharge, water yield, deep percolation, total soil water, and lateral flow were considered. Results revealed that the conversion of undisturbed land to agricultural land reduced the quantity of water underground; groundwater discharge decreased by 1%-2.15%. The same trend was observed on lateral groundwater flow that significantly decreased by 5.51%-7.23%. The SWAT-MODFLOW model was an indispensable tool for agricultural and biosystem engineers and other professionals in the updating the comprehensive land-use plan of any towns or cities, incorporating the conjunctive use of surface and groundwater resources toward a sustainable supply of water resources to the community.

Keywords: *Agricultural and biosystems engineer, Comprehensive land use plan Groundwater hydrology, Land use change, SWAT-MODLFOW*

INTRODUCTION

Often there is a hostile competition within a single river basin from the municipal, agricultural, industrial, environmental, and recreational sectors over the use of the limited supply of surface water and groundwater. Groundwater in rural

areas is most vulnerable as the transfer of surface water rights to urban areas increases dependence on groundwater resources, leading to a decrease in groundwater levels and overall groundwater storage (Knapp and Baerenklau, 2003). Also, removing surface water irrigation decreases seepage from earthen irrigation canals and deep percolation from applied surface water irrigation, thereby removing a source of groundwater and leading to additional groundwater storage depletion. In such a complex water resources network, wherein both surface water and groundwater resources are managed conjunctively to satisfy all social sectors, physically-based distributed hydrological models can be used to quantify water availability under current and future conditions and determine appropriate integrated water management policies. Hydrological models typically are developed based on (i) surface runoff models that consider groundwater in a simplistic manner, such as the Hydrologiska Byråns Vattenbalansavdelning [HBV] (Bergstrom and Forsman, 1973; Bergstrom, 1992), the Sacramento Soil Moisture Accounting Model [SAC-SMA] (Burnash et al., 1973), TOPMODEL (Beven and Kirby, 1979), the Variable Infiltration Capacity [VIC] (Liang et al., 1994), the Hydrologic Modeling System [HEC-HMS] (William et al., 1995; U.S. Army Corps of Engineers, 2016), the Soil and Water Assessment Tool [SWAT] (Arnold et al., 1998), among others and just lately is the new coupled SWAT-MODFLOW model (Chunn et al., 2019; Park and Bailey, 2017).

Based on the simulation studies (Arceo et al., 2018) in two watersheds, changes in climate and land cover, including increased precipitation and conversion of range/brushland to the forest, affecting the present hydrologic balance of a watershed. Given the current condition of the test watersheds, an increase in precipitation tended to significantly increase surface runoff, which could cause serious erosion, sedimentation of the reservoirs, depletion of soil nutrients, and even flooding in low-lying areas within the watershed. Furthermore, an increase in forest cover decreases surface runoff, increases evapotranspiration, and decreases baseflow. The flux in baseflow is significant for the test watersheds as they provide water for irrigation and domestic use in the area. The impacts of land cover and climate changes on hydrologic responses are non-uniform from one watershed to another. A sound watershed management scheme can have potential benefits to improve water availability and reduce flood-risks downstream. However, quantifying groundwater hydrologic responses have not considered and needs further investigation.

Within river basins, water resources competition often exists between agricultural, municipal, and industrial sectors, particularly in semi-arid regions where surface water and groundwater are managed conjunctively to sustain urban areas and food production. There is a need for physically-based modeling tools to assist with identifying successful water management strategies in these basins. This paper presents an updated version of SWAT-MODFLOW that allows the application to large agro-urban river basins in semi-arid regions of Quaioit River Watershed (QRW).

The study aimed to quantify the impact of land-use change (agricultural expansion) to groundwater hydrology of the QRW using SWAT and SWAT-MODFLOW. Specifically, the study aimed to: (1) simulate and calibrate a model for streamflow and other hydrologic processes of the watershed using the Soil and Water Assessment Tool (SWAT); (2) to characterize the groundwater state of the watershed using SWAT-MODFLOW; (3) evaluate the effectiveness and efficiency of SWAT-MODFLOW model to simulate groundwater hydrology link to SWAT model and (4) quantify the impact of agricultural expansion to groundwater discharges and other groundwater processes.

MATERIALS AND METHODS

Research Framework of the Study

To better understand the step by step of the study, the research framework is presented in Figure 1. The study involved computer applications that can simulate the projected impact of land-use change, particularly agricultural expansions in the study area. The first work is to collect raw data needed in the simulation e.g., meteorological data, land use map DEM and soil map. It is further analyzed and prepared in proper format as required by the ArcGIS-ArcSWAT application. These processed maps and data were used to simulate streamflow runoff using the SWAT model. It is further calibrated using a reliable statistical tool. Simulated data developed by the SWAT model were then used as input to the coupled SWAT-MODFLOW model to quantify and characterized groundwater hydrology responses to different land-use change scenarios.

Data Gathering and Compilation

Data needed in the study were gathered and compiled into the proper format required by the subsequent geospatial analysis. Spatial data required by the model include the digital elevation model (DEM), land use map, and soil map. These data were used to delineate the watershed boundary, generate the stream network, and the hydrologic response unit (HRU), the basis of the SWAT model. The SAR DEM with 90 x 90 m resolution was used in the study. Land use mapping exposes the pattern of land use and provides a basis for characterizing landscape and understanding land management practices. Land use maps used in the study were classified into land-use classes recognized by the SWAT database. A soil map is a geographical representation showing the diversity of soil types and/or soil properties in the area of interest. Like Land use, soil map will be classified generally that recognizable by the SWAT database. The weather data, including rainfall, maximum and minimum temperature, relative humidity, solar radiation, and wind speed, were compiled as a text file as required by the SWAT model (Jimenez and Galeon, 2016).

SWAT–MODFLOW Model

SWAT-MODFLOW is a newly coupled hydrologic model that combines the land surface and stream hydrologic processes of SWAT and the groundwater hydrologic processes of MODFLOW to provide a comprehensive coupled hydrologic model for watershed systems (Park and Bailey, 2017). Transport of contaminants in this coupled system also can be simulated by including the RT3D (Reactive Transport in 3 Dimensions) model into the MODFLOW groundwater routines. The processes simulated by each model are shown in Figure 2 using some general assumptions of basic groundwater flow conditions. Processes simulated by SWAT are shown with green text, those simulated MODFLOW in blue text, and those simulated by RT3D (if desired; in red text). SWAT performs operations for land surface hydrology, soil hydrology, and surface water hydrology; MODFLOW performs operations for groundwater hydrology and interactions between groundwater and surface water. Data needed in the SWAT-MODFLOW model were the outputs that were simulated in basic SWAT models such as HRUs, river flows, and sub-basins. These were used to create and process linkages, and other needed data for the simulation was readily available provided by the SWAT-MODFLOW interface. It includes MODFLOW input files, swatmf_link.txt, and mapping files (linking text files). It includes executable files that contained the simulation procedure with other needed data for the simulation that was readily available provided by the SWAT-MODFLOW interface. It included MODFLOW input files, swatmf_link.txt, and mapping files (linking text files). It also included executable files that were contained in the simulation procedure.

Evaluation of Land Use Change

Land-use change was based on the Comprehensive Land Use Plan (CLUP) of the two biggest localities within the boundary of the watershed, the Batac City and the Municipality of Paoay. To exposed and project the futuristic consequences of intensive land-use change in the watershed towards food productions, evaluated land-use change was used to simulate the different states of groundwater hydrology in the area. Table 1 shows the formulated land-use change scenarios at two stages. **Scenario 1** shows the two combination effects of converting Range to Brushland and Forest land into Agricultural land about 25% of their total area in the watershed. **Scenario 2** the same with the later scenario; it is just increased by 50% of their total area.

RESULTS AND DISCUSSION

Study Area

The Quiaoit River Watershed (QRW) has a total land area of 17,362.76 hectares covering Batac City and Municipality of Paoay, Cirrimao, Banna, and Sarrat Ilocos Norte (Figure 3). About 61% of the total watershed area was located within

the city and the second-largest contributor of its area and almost covering its downstream is the municipality of Paoay which contributed 18% from the total area of the QRW, about 44.48% of the total area of the municipality It summits as high as 520masl. The watershed falls within Latitude 17° 07' North and Longitude 120° 32' to 120° 28' East. The area is about 18 km to Laoag City, the province capital; 225km to the regional center (San Fernando, La Union), and about 472km to Metro Manila (Manzano and Alibuyog, 2014; Jimenez and Galeon, 2016).

Calibration of the SWAT Model

The simulated streamflow runoff using the SWAT model was further calibrated to validate the effectiveness of the model. The r-value and the Nash and Sutcliff Coefficient (NSE) were used to test the adequacy of the model. Calibrated streamflow of the stations in figure 6 gathered from the Crop Research Laboratory of Mariano Marcos State University was requested as the foundation of the calibration. Table 2 shows the varying values of correlation, r, and NSE with respect to stations. Correlation r values ranged from 0.63 to 0.93, which proves that as the simulated streamflows increase, observed streamflows also increase, and vice versa. NSE values were range from 0.34 to 0.87, in which NSE values indicated that the model is a better predictor than the mean. This means that the SWAT model simulated was efficient and effective in simulating the relationship of water behavior to land conversion (Arceo et al., 2018; Jimenez and Galeon, 2014). Figure 4 shows the response of streamflow peaks (calibrated and simulated) during heavy rains.

Groundwater Characterization of QRW

To perform groundwater simulation using SWAT-MODFLOW, various essential files are needed (Figure 5). Data needed in the SWAT-MODFLOW are simulated in SWAT and used as hydrologic response units (HRUs), river, and sub-basins. These files were created and processed linkages to grid files such as (a) swatmf_dhru2hru.txt - relates HRUs to DHRUs; (b) swatmf_dhru2grid.txt- relates DHRUs to Grid Cells; (c) swatmf_grid2.dhru.txt- relates Grid to DHRUs, and (d) swatmf_river2grid.txt- relates Grid to DHRUs of the QRW study area.

Initial simulation of the SWAT-MODLFOW model shows that groundwater recharge ranges from 69m^3/d to 350 m^3/d (Figure 6). It is also noticed that the watershed has a groundwater hydraulic head of 96.1 up to 140.4masl (Figure 6) along the vicinity of the watershed, which varying geographical characteristics. It also shows the variation of groundwater head of the watershed at different observation cell of the watershed (Figure 7). Upstream location shows a higher head while lower areas have a smaller head. It is also noticed that due to time groundwater head is decreasing throughout the watershed.

Quantifying the Impact of Agricultural Expansion to Groundwater Responses

This aims to display the impact of land-use change, particularly on agricultural expansion, to groundwater hydrology responses. Groundwater discharge, water yield, deep percolation, total soil water, and lateral flow were considered in the quantifying effect. Results show that the conversion of undisturbed land to agricultural land decreases the quantity of water underground (Figure 6). Table 3 shows that groundwater discharge decrease by about 1% in **Scenario 1** and 2.15% decrease in **Scenario 2**. It is the same as through with lateral flow, which shows a significant decrease at the two levels of conversion: 5.51% to 7.23%, **Scenarios 1** and **2**, respectively. With the study of Manzano and Alibuyog (2014), the estimated total capacity of about 336,100.8m^3/day of the QRW where the simulated groundwater responses adequately, considering the hydraulic connection of the groundwater from the Quiaoit River to its adjoining areas that can be irrigated using shallow wells (Figure 7).

The model was run for the 2005–2014 periods and by tested against groundwater elevation and streamflow discharges at monitoring wells and stream gages, respectively, located throughout the basin. The results of the coupled SWATMODFLOW model are adequate as regards to simulating streamflow and groundwater elevation hydraulic heads. The existing model can be useful for management purposes, qualifying the water resources managers to quantify spatial groundwater vulnerability in the studied QRW or other similar watersheds. However, such investigation needs further hydrogeological characterization and well logs in the study area on more groundwater hydrology parameters and improved irrigation coding of the SWAT-MODFLOW model.

CONCLUSION

The coupled SWAT-MODFLOW model was successfully applied in the QRW to quantify land-use changes and groundwater hydrologic responses at differing scenarios. The results of the coupled SWAT-MODFLOW model are adequate with regards to simulating streamflow and groundwater recharge and hydraulic heads. The existing model can be useful for management purposes, qualifying the water resources managers to quantify the area's spatial groundwater vulnerability.

Moreover, the study shows the impact of judicious land-use changes, though it does not consider water usage in the watershed, considering the huge increase in crop production. It is recommended that a follow-up study should be done to quantify the effect of agricultural expansion to groundwater hydrologic responses considering the huge requirements of water for irrigation considering groundwater as the second most reliable water source in the watershed for agricultural and other uses. Such an irrigation coding program of SWAT-MODFLOW is recommended for further computer programming development and evaluation and can be applied in other similar watersheds.

REFERENCES

Arceo M.G.A., R.V.O. Cruz, C.L. Tiburan Jr., J.B. Balatibat and N.R. Alibuyog. 2018. Modeling the Hydrologic Responses to Land Cover and Climate Changes of Selected Watersheds in the Philippines Using Soil and Water Assessment Tool (SWAT) Model. DLSU Business & Economics Review.

Arnold J.G., R. Srinivasan, R.S. Muttiah, J.R. William. 1998. Large area hydrologic modeling and assessment part i model development. JAWRA 34 (1), 73–89.

Beven K.J., M.J. Kirkby. 1979. A physically based variable contributing area model of basin hydrology. Hydrol. Sci. Bull. 24 (1), 43–69.

Bergstrom S., A. Forsman. 1973. Development of a conceptual deterministic rainfall-runoff model. Nordic Hydrol 4, 147–170 (Munksgaard, Copenhagen, Denmark).

Bergstrom S. 1992. The HBV Model-Its Structure and Applications. SMHI Rep.s Hydrol., S-601 76 Norrkoping, Sweden.

Burnash R.J.C., R.L. Ferral, R.A. Mcguire. 1973. A Generalized Streamflow Simulation System Conceptual Modeling for Digital Computers. U.S. Department of Commerce, National Weather Service, and State of California, Department of Water Resources.

Chunn D., M. Faramarzi, B. Smerdon, and D.S. Alessi. 2019.Application of an Integrated SWAT–MODFLOW Model to Evaluate Potential Impacts of Climate Change and Water Withdrawals on Groundwater–Surface Water Interactions in West-Central Alberta. Water, 11, 110

Jimenez J. and N.J. Galeon. 2016. Evaluation Of The Effects Of Land Use Change In The Hydrologic Water Balance Of The Qiuaoit River Watershed. Unpublished Undergraduate Thesis.

Keith C., K.C. Knapp and K.A. Baerenklau. 2006. Ground Water Quantity and Quality Management: Agricultural Production and Aquifer Salinization over Long Time Scales. Journal of Agricultural and Resource Economics 3 1 (3):6 16-641

Liang X., D.P. Lettenmaier, E.F. Wood, S.J. Burges. 1994. A simple hydrologically based model of land surface water and energy fluxes for general circulation model. J. Geophys. Res. 99 (D7).

Manzano Jr. V.J.P. And N.R. Alibuyog. 2014. The hydrological capacity of the Quiaoit River Watershed. MMSU Science and Technology Journal. Vol. 4, No. 1/Jan-June 2014. ISSN:2012 0060.

Park S. and R.T. Bailey. 2017. SWAT-MODFLOW Tutorial: Documentation and preparing model simulations. Colorado State University and TAMU, USA.

William C., A. Pabst, J. Peters. 1995. The Hydrologic Modeling System (HEC-HMS): Design and Development Issues. Institute for Water Resources, Hydrol. Eng. Center, Davis, CA.

Table 1. Scenario development on land-use changes for SWAT-MODFLOW.

Scenario	Converted From	Converted To	Percent of the Total Area
Scenario 1	Range to Brush Land	Agricultural Land	25%
	Forest Land	Agricultural Land	25%
Scenario 2	Range to Brush Land	Agricultural Land	50%
	Forest Land	Agricultural Land	50%

Table 2. Statistical indicator during calibration using SWAT model

Statistical Parameters	Correlation, r	NSE
STAT 1	0.63	0.34
STAT 2	0.76	0.41
STAT 3	0.93	0.87
STAT 4	0.75	0.64
STAT 5	0.91	0.71

Table 3. Groundwater hydrology response in different scenarios

Groundwater Parameter	Baseline	Scenario 1	Percent Change	Scenario 2	Percent Change
Groundwater Discharge (mm)	897,944.05	888,942.87	1.00	878,638.25	2.15
Water Yield (mm)	1,876,751.23	1,876,650.92	0.01	1,876,650.92	0.01
Percolation (mm)	947,740.30	938,302.01	1.00	919,781.96	2.95
Total Soil Water (mm)	156,786.30	156,790.25	0.00	156,786.30	0.00
Lateral Flow (mm)	30,773.18	29,079.06	5.51	28,548.28	7.23

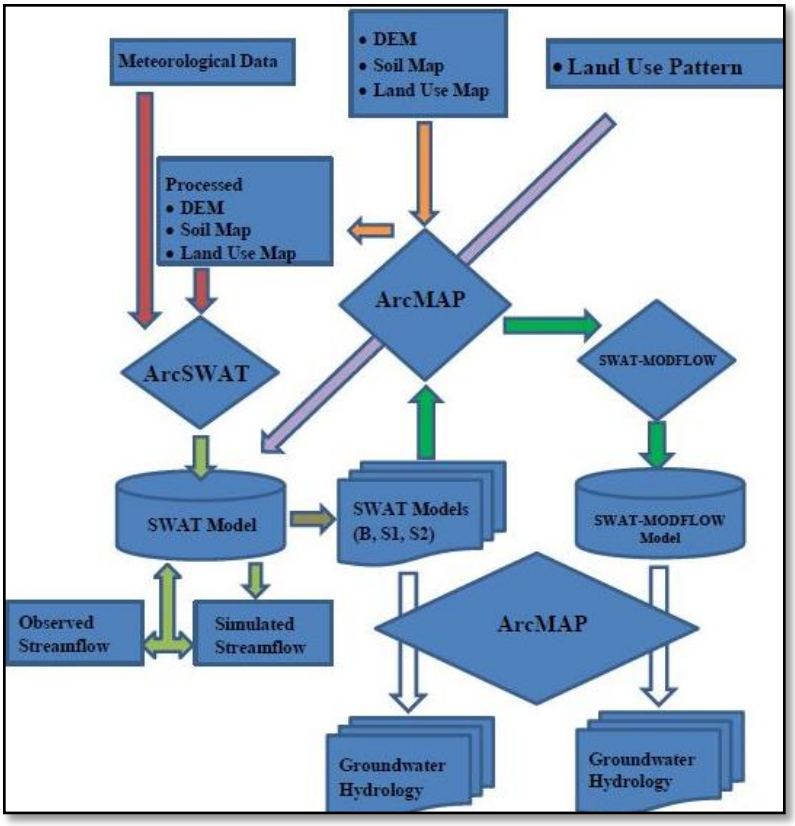

Figure 1. Process framework of the study.

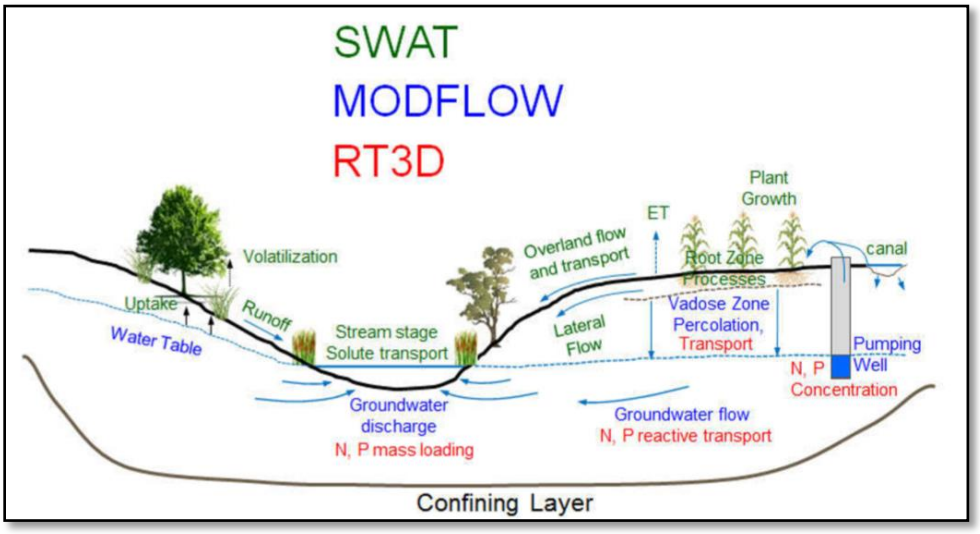

Figure 2. Framework of SWAT-MODFLOW modelling (Park and Bailey, 2017).

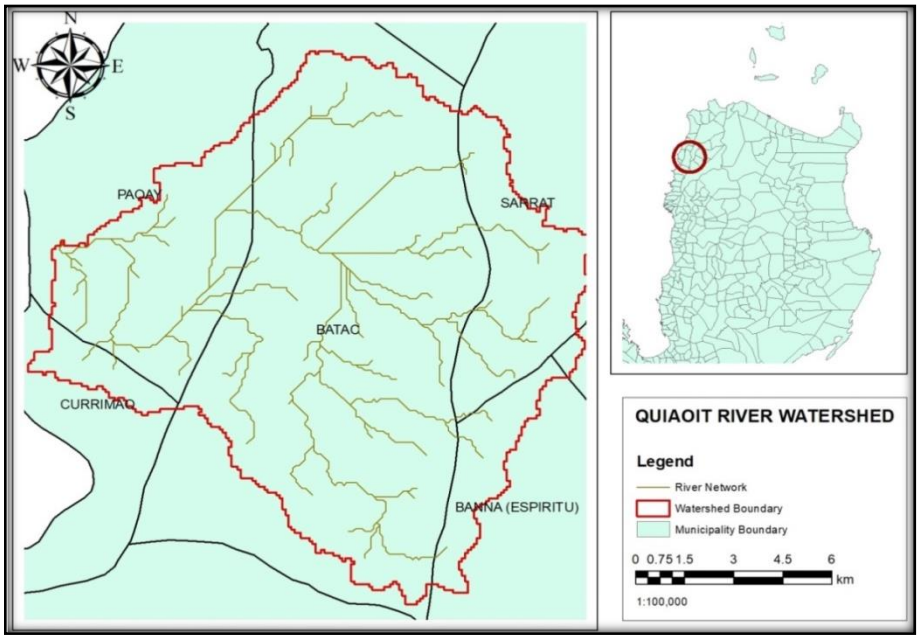

Figure 3. Location of Quiaoit River and watershed boundary, Ilocos Norte.

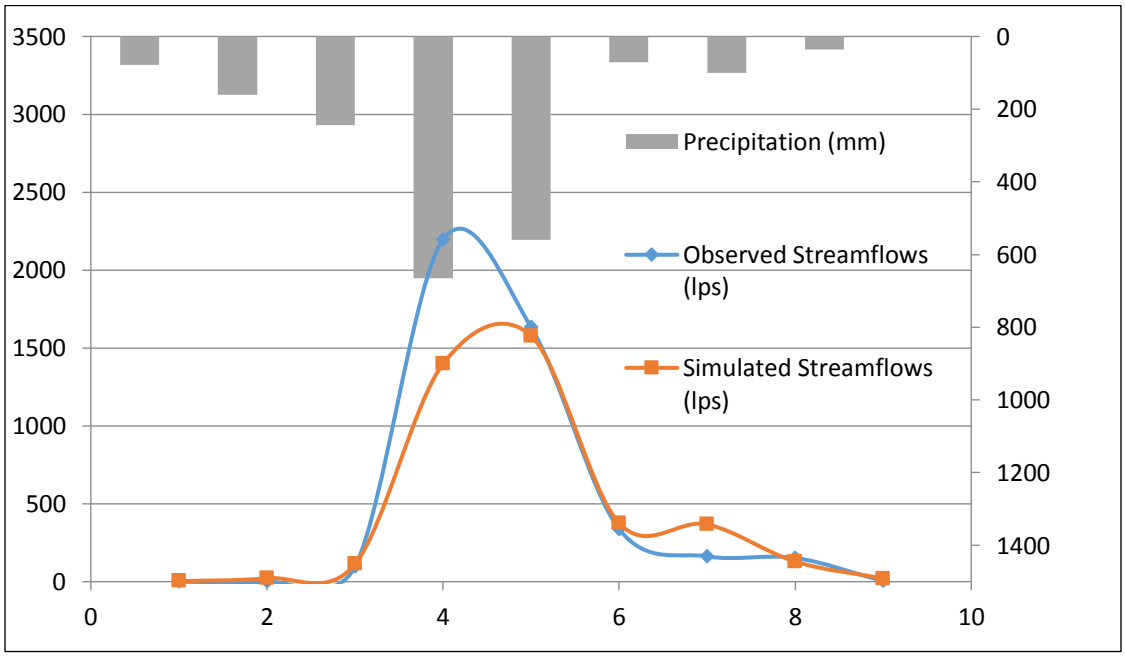

Figure 4. Response of streamflow runoff to peak rainfall using SWAT model

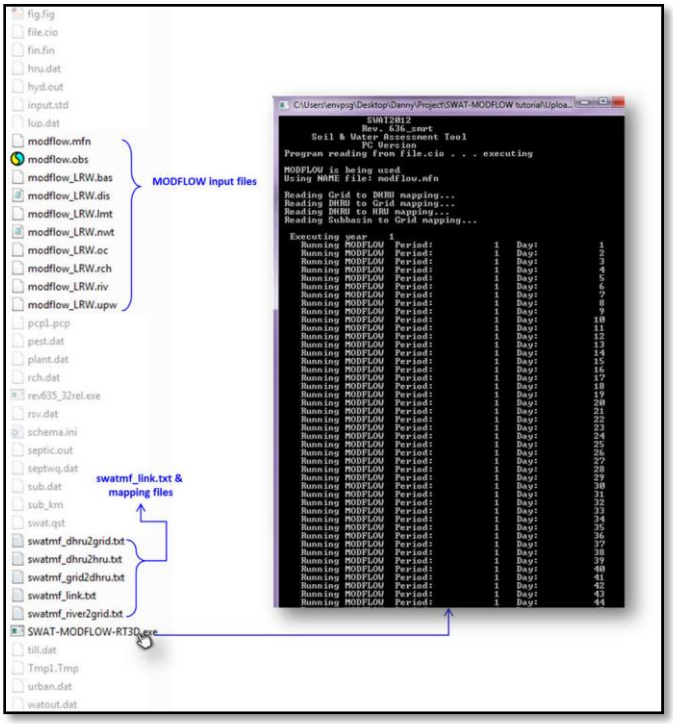

Figure 5. Essential files needed in running SWAT-MODFLOW simulation.

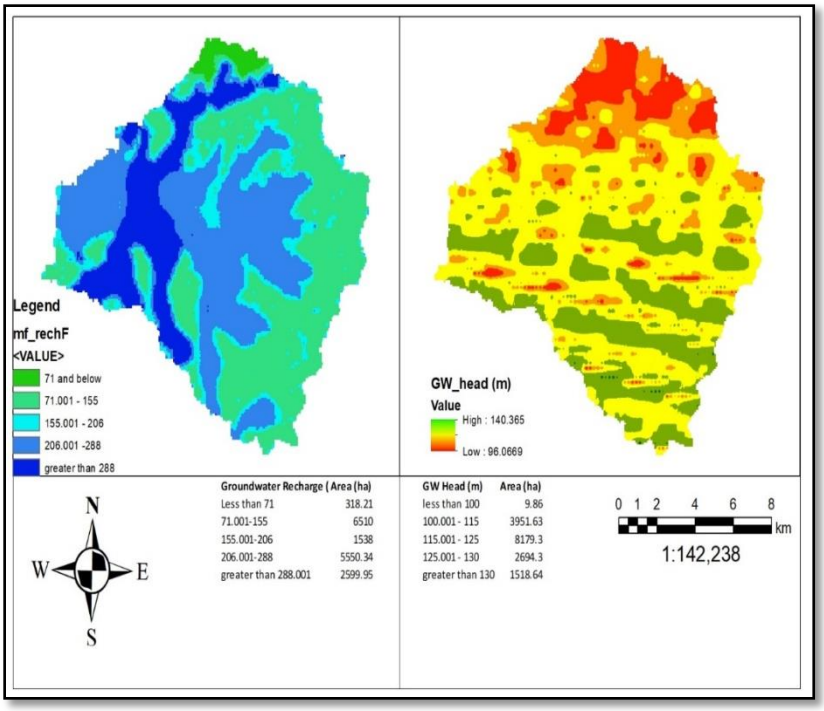

Figure 6. Simulated groundwater recharge spatial coverages and groundwater hydraulic head of the Quiaoit River watershed using SWAT-MODFLOW.

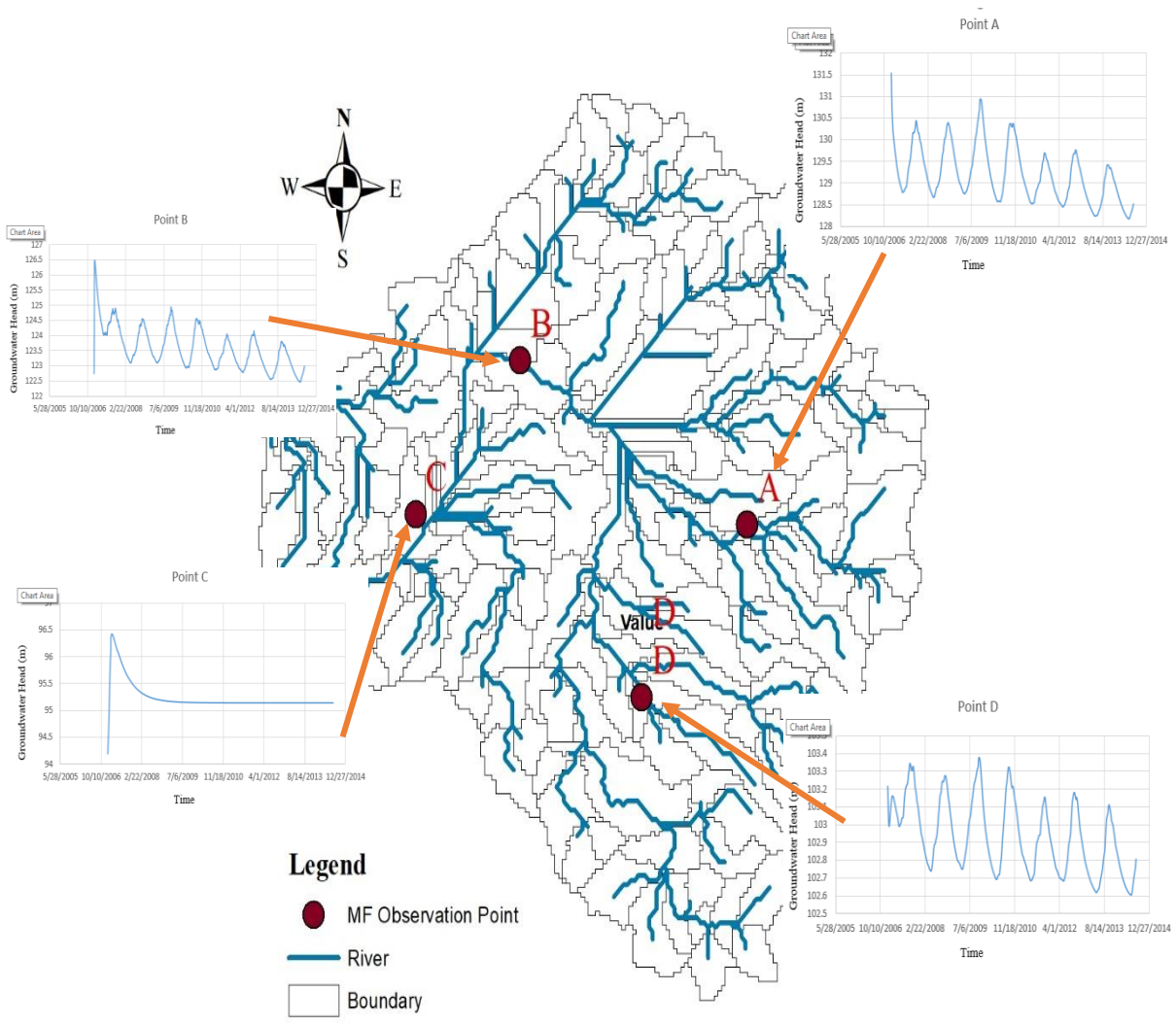

Figure 7. Simulated groundwater recharge at different groundwater head time series of aquifer at observation points of the Quaioit River networks using SWAT-MODFLOW.

FLOOD RISK ASSESSMENT AS AFFECTED BY LAND USE CHANGE FOR POLICY INTERVENTION: A CASE STUDY OF QUAIOIT RIVER WATERSHED

C.M. Pascual[1] and J.I. Jimenez[2]

[1]Department of Agricultural and Biosystems Engineering
College of Engineering, Mariano Marcos State University
Batac City 2906, Ilocos Norte
[2]College of Agriculture, Forestry and Sustainable Development
Mariano Marcos State University, Batac City 2906, Ilocos Norte

Abstract

Flooding is a main environmental calamity threat in Quaioit River Watershed (QRW) with risks that are probable to increase in the future if not mitigated. Land use and land cover (LULC) have a strong influence on flood risk. The main projected land-use change processes are forest expansion and urbanization, which have a contradictory impact on flood risk, which makes the future impact of LULC changes on flooding in the QRW hard to estimate. This study examined the impact of the projected LULC changes on probable flood risk areas at different land-use change scenarios. Geospatial techniques were used, such as the Soil and Water Assessment Tool (SWAT), Multi-Criteria Analysis – Analytical Hierarchial Process (GIS-AHP), and Conversion of Land Use and its effects (CLUMondo model) showed convincing assessment results and scenario pathways for mitigation. Results revealed that problems in flooding could always be quantified and assessed for proper compiling decision maps and can be used in hazard risk assessment. Conversion of agricultural land into commercial land caused a tremendous increase of flood extent up to 2.41% of the total watershed exposed to very highly prone to flooding. Moreover, converting forest land and grassland areas of about 50% of its total area would dramatically decrease safe areas of about 7.69%. For proper management, the study recommended alternative solutions by constructing small water impounding systems and to increase river network water holding capacity to reduce overflow by adding some river networks as policy intervention in the affected flood-prone areas.

Keywords: *Assessment, CLUMondo model, Flood risk, Land use/land cover change, GIS-AHP, SWAT model*

INTRODUCTION

Flood is known as one of the most destructive natural disasters due to its various kinds of casualties, from disease diffusion to loss of life. Flash flooding in urban and its tangential areas resulted from blocked or inadequate storm sewers and are flooded due to increased urbanization (Ajin et al., 2013). Urban areas have a

high risk of flash flooding due to the presence of large impervious areas and sometimes inefficient drainage system (Chen et al. 2009; Danumah et al., 2016).

Land use and land cover (LULC) disturbed both the probability of flood and its magnitudes in several ways. Land cover affects different elements of the water balance; evaporation, ground temperatures, an interception (Stonestrom et al. 2009). In addition, LULC impacted climate systems, and, in turn, the frequency and characteristics of rainfall (Cornelissen et al. 2013; Boysen et al. 2014; Mitsova 2014). Moreover, there is a direct impact of LULC on the formation of runoff from a particular rainfall event (Tellman et al. 2015). Finally, the land cover in river channels affects hydraulic flow conditions and contributes to, for example, woody debris jams on bridges (Stoffel et al. 2016). LULC changes have implications for the consequence component of flood risk through increased development of settlements on flood-prone areas (Kundzewicz et al. 2010). Numerous studies have considered the general impact of land-use change on flooding; however, there are fewer studies of the projected (simulated) impact of future land use on flood risk.

The Municipal of Paoay, Ilocos Norte, covering almost all the downstream areas of the Quaioit River watershed, faced a great challenge on flooding. The municipality is almost self-sufficient because of its very attractive tourist spots (the UNESCO heritage Augustine Paoay Church and Paoay Lake). But because of flooding during peak season, casualties plus the decrease of potential return from its attractive spots due to sever urban floods, unaccesible roads, crop productivity degradation, and sedimentation. Unless a very comprehensive land use plan of the municipality addressing the issue of flooding, this problem will be increasing annually.

Flood hazard mapping served a vital component for appropriate land use planning in flooded areas and mitigation measures (Bhatt et al. 2014). It provided accessible charts and maps which can be easily read and, therefore, facilitated the identification of hotspot risk areas by planners, enabling them to prioritize their mitigation efforts (Bapalu and Sinha, 2005; Ajin et al., 2013). Flood management is necessary not only because it imposes huge damage to society but also for the optimal exploitation of the land and its proper management. This cannot become technically feasible without effective flood hazard and risk maps (Bhatt et al. 2014; Danumah et al., 2016).

The study mainly focused on the assessment of flood risk mapping, simulating flood response to land use/land cover (LULC) conversion. Such an assessment will lend support for further evaluation of possible solutions for policy intervention to address the issues.

MATERIALS AND METHODS

Locale of the Study

The Quiaoit River Watershed (QRW) has a total land area of 17,362.76 ha covering the City of Batac and Municipality of Paoay, Cirrimao, Banna, and Sarrat, Ilocos Norte (Figure 1). About 61% of the total watershed area is located within Batac City. The second-largest contributor to its area and almost covering its downstream is the municipality of Paoay, which contributed 18% from the total area of the watershed, about 44.48% of the total area of the municipality. It is located in the northwest corner of the island of Luzon, about 11km from the eastern shores of the South China Sea. It summits as high as 520m above sea level. The watershed falls within latitude 17° 07' North and longitude 120° 32' to 120° 28' East. The climate is Type I, with two pronounced seasons – dry (from Nov to Apr) and wet (June to Oct). The average annual rainfall is 2390mm.

At present, the pattern of cultivation is closely related to the slope or landform. The level lowland areas are intensively cultivated and planted to rice during the wet season. During the dry season, corn, tobacco, and vegetables are planted. In upland and hilly areas, agricultural activities are also common along the river, tapping water for irrigation, especially during the dry season. Most of the commercial activities are concentrated in the central and western parts of the watershed.

The municipality of Paoay Ilocos Norte, located in the downstream of the watershed, is frequently visited by typhoons because of its geographical locations. Devastations due to flooding are experienced since the municipality is the gateway of floodwaters from the towns of Ilocos Norte towards the West Philippine Sea.

Conceptual Framework

Three (3) essential GIS-based tools were used in the study, namely: (1) SWAT; (2) –GIS-AHP; and (3) CLUMondo models (Figure 2). The application of SWAT to simulate the different relationships between land and water, especially runoff volumes and streamflow, is important. Ancillary maps (DEM, soil, and land use) were gathered from various implementing agencies. The resulting simulated runoff of the model was further calibrated using observed streamflow. Numerical values of soil and water relation maps and parameters were further extracted to come up with the list of criteria essential in GIS-AHP and suitability maps as independent input in the CLUMondo model. Criteria were reclassified into a uniform format from **1** to **5**, **5** as the most flooded areas, and one as not affected by the flood. Using these reclassified criteria, it was further simulated using the GIS-AHP to derive the flood extent of the watershed. CLUMondo was ultimately used to come up with a land-use change, probably the expansion of inland water, to increase the water storage capacity of the watershed so it could reduce the runoff during peak season.

Data Gathering

The Digital Elevation Model (DEM) with a pixel size of 90 by 90 meter resolution was gathered from the Quiaoit River Watershed Project of the Mariano Marcos State University, including the land use and soil map of Ilocos Norte. The Comprehensive Land Use Plan (CLUP) of the two municipalities that comprised the biggest contributor in terms of ancillary data was also gathered. Meteorological data such as rainfall, humidity, solar radiation, wind, and temperature were arranged and prepared according to the required format by the SWAT model.

Preparation of Criteria Maps/Suitability Maps Needed in GIS-AHP and CLUMondo

Based on the results of SWAT simulation, some essential parameters were extracted and processed using GIS spatial toolkit to derive the different criteria, suitable maps needed in the simulation to GIS-AHP and CLUMondo, for flood hazard maps and alternative land-use change for policy recommendation, respectively. The criteria used in the flood hazard mapping were: Flow Accumulation, Flow Direction, Land Slope, Elevation, Drainage Density, and Runoff Volume (Figure 3). All of these thematic maps were gathered in the calibrated SWAT model. Processed maps were used for CLUMondo suitability maps, and reclassified maps were used for GIS-AHP simulations. The dependent map used in CLUMondo simulation for policy interventions was the General Land Use (Figure 4).

Development of Land Use Scenarios

Projected land-use patterns are expected to happen in the future. Due to the increasing demand for human needs, based on the CLUP of two involved municipalities were derived to predict the response of floodwater behavior when there is the conversion of land use without proper allocation. Table 2 shows the scenarios of land-use conversion to showcase the effect of land-use change to runoff depth. **Scenario 1** involved the projected land-use conversion of the two municipalities in the watershed, Paoay, and City of Batac. About 25% percent was projected to convert from Agricultural Land to Commercial Land in the Urban Areas due to urban commercialization that is mandated in the CLUP of both municipalities. **Scenario 2** involved the projected land-use conversion of the urban areas plus the demand of an abrupt increase of population by converting shrubland into productive agricultural land by about 50% and the forest areas into grassland and shrub areas by about 50 % due to deforestation.

RESULTS AND DISCUSSION

Calibration of Streamflow Using SWAT Model

The simulated streamflow using the SWAT model was further calibrated to validate the effectiveness of the model. The correlation **r**-value and the Nash and Sutcliff Coefficient (NSE) were used to test the adequacy of the model. Calibrated streamflow of the stations gathered from the Crop Research Laboratory of Mariano Marcos State University was requested as the basis of the calibration (Alibuyog et al. 2009). Table 3 shows the variation of correlation, **r,** and **NSE** with respect to stations. Correlation **r** values ranged from 0.63 to 0.92, which proves that as the simulated streamflows increases, observed streamflows also increases, and vice versa. **NSE** values ranged from 0.34 to 0.87, which indicated that the model was a better predictor than the mean. This meant that the SWAT model simulated was efficient and effective in simulating the relationship of the water behavior to land conversion. Figure 5 shows the variation of response of peak flows (calibrated and simulated) during heavy rains.

Flood Hazard Mapping Using GIS-AHP

Essential processed six (6) thematic maps as a set of criteria by the resulting calibrated SWAT model were further extracted from the model to simulate the flood hazard map. Using the MCA-AHP with resulting percent weights at consistency ratio of less than 1%; the flow direction (10.1%), flow accumulation (10%), slope (22.6%), elevation (31.5%), drainage density (21.7%), and annual runoff (4.1%) were all gathered and prepared to required format from the calibrated SWAT model. For such a GIS-AHP model, elevation had the highest weight to look for the low lying areas. Next is the land slope to find the areas wherein there are great flows. Drain density was also considered to showcase the effect of low draining density to flood behavior. Other criteria used were flow accumulation, flow direction, and of course, annual runoff as a product of land use pattern, precipitation, and land cover. Figure 6 shows the resulting flood hazard of the QRW, and the two flood hazards are the Municipality of Paoay extracted from the map. The upper left figure is the modeled flood map, and the right one is the existing flood map of Paoay Ilocos Norte. Both of these maps have little similarities but show significant areas of Paoay exposed to floodings.

Flood Response at Different Land Use Pattern

This section demonstrated the effect of land change with the response to the aggregate conversion of land-use change into more susceptible to flooding, e.g., agricultural land to commercial. As stated before, for a society to improve its economic status is to maximize its resources, minimizing the casualties. But with the traditional conversion of land into a productive one, which is maximizing the land resources but maximizing casualties. In this section, one disaster was used to demonstrate the effect of land-use change, e.g., floods. Figure 7 shows the extent of

flooded areas in different scenarios. To come with the objective of this section, Typhoon *Pepeng* in 2009 was considered in the simulation to showcase the most possible occurrence of floods during peak season. It drops of 843.40 meters in the watershed. At **Scenario 1** (conversion of agricultural land into commercialize land), an increase of 2.41% from the total areas was added as very susceptible areas, while a reduction of 2.16% was not merely affected. In **Scenario 2** (additional conversion of grassland into agricultural land and forest land into grassland), a very high reduction did not affect about 7.69% of those not affected or very low affected. Most of the susceptible areas to flooding risks were located in the urban areas and agricultural land areas. These areas will give the very high cost of casualties due to flooding.

Policy Intervention for Land Use Change

Every conversion of agricultural land into commercial land will adversely affect the extent of floodwater, increasing the affected and could increase casualties in the watershed. In this section, some solutions were presented to address the issue of floodwater in response to the conversion of water. The first solution is to provide alternative stream networks to increase the stream discharge capacity of the watershed, considering those with very low drainage density. This intervention is to decrease overflow in the stream bed in the watershed that contributed to flooding water.

Figure 8 shows the best location in the watershed to construct additional stream networks. One network was located in the vicinity of Paoay, and the other one is located in the area of the City of Batac. These locations are the area that is mostly affected by floodwater during peak seasons.

Another solution is by locating areas that are potential sites for constructing small water impounding projects (SWIPs). SWIPs are artificial reservoirs that can impound water during peak seasons that can be used during water-scarce months, mostly in the summer time. Figure 9 shows the possible locations in the watershed that have a high possibility of constructing SWIPs for future use. There are suitable areas simulated using the CLUMondo. Most of these SWIPs are located on the upstream of the watershed located in the upper area in the City of Batac. But one vast site that could have a great volume of water can impound is located in the municipality of Paoay. The land use that can be converted into water bodies is from pasture land, which is not utilized and could maximize its purpose of constructing SWIPs.

CONCLUSION

The combined-use of GIS-based tools such as SWAT, GIS-AHP, and CLUMundo are indispensable tools in integrating, organizing, processing, and visualizing the comprehensive land-use plan for policy interventions. Its application is fundamental to the efficient and effective creation of thematic maps in a GIS

environment. It has been a very effective way of conveying the flood risk assessment as impacted by land-use changes at different scenarios for policy intervention on updating their CLUPs.

With more and high resolution, multi-spectral, and temporal of spatial data are captured, and improved land-use models, results, and decision maps become available. Developing and improving geo-referenced data and information management of land and water resources in the comprehensive land-use plan of towns and cities to effectively handle all the information will remain a challenge to agricultural and biosystems engineers as future land-use planners. Thus, enhancing courses to incorporate more topics in GIS and remote sensing tools in schools and various training-workshops are recommended.

REFERENCES

Ajin R.S., R.R. Krishnamurthy, M. Jayaprakash and P.G. Vinod. 2013. Flood hazard assessment of Vamanapuram River Basin, Kerala, India: An approach using Remote Sensing & GIS techniques. Advances in Applied Science Research 4(3): 263–274.

Alibuyog N.R., V.B. Ella, M.R. Reyes, R. Srinivasan, C. Heatwole and T. Dillaha. 2009. Predicting the Effects of landuse Change on Runoff and Sediment Yield in the Manupali River Sub watersheds Using the Swat Model. International Agricultural Engineering Journal 2009, 18(1 2):15-25.

Bapalu G.V. and R. Sinha. 2005. GIS in flood hazard mapping: a case study of Kosi River Basin, India. GIS Development Weekly 1(13):1-3.

Bhatt G.D., K. Sinha, P.K. Deka and A. Kumar. 2014. Flood Hazard and Risk Assessment in Chamoli District, Uttarakhand Using Satellite Remote Sensing and GIS Techniques. International Journal of Innovative Research in Science, Engineering and Technology 3(8): 9.

Boysen L.R., V. BROVKIN, V.K. ARORA, et al. 2014. Global and regional effects of land-use change on climate in 21st century simulations with interactive carbon cycle. Earth Syst Dyn 5:309–319. https://doi.org/10. 5194/esd-5-309-2014.

Brandt J.S. and P.A. Townsend. 2005. Land Use–Land Cover Conversion, Regeneration and Degradation in the High Elevation Bolivian Andes. Landscape Ecology–Volume 21, Issue 4, pp 607-623.

Chen J., A.A. Hill and L.D. Urbano. 2009. A GIS-based model for urban flood inundation. Journal of Hydrology 373: 184–192.

Cornelissen T., B. Diekkru, S. Giertz. 2013. A comparison of hydrological models for assessing the impact of land use and climate change on discharge in a tropical catchment. J Hydrol 498:221–236.

Danumah J.H., S.N. Odai, B.M. Bachir Mahaman Saley, J. Szarzynsk, M. Thiel, A. Kwaku, F.K. Kouame and L.Y. Akpa. 2016. Flood risk assessment and mapping in Abidjan district using multi-criteria analysis (AHP) model and geoinformation techniques, (cote d'ivoire). Geoenviromental Disasters. Danumah et al. Geoenvironmental Disasters 3:10

Djokic D. 2012. Hydrologic and Hydraulic Modeling with ArcGIS-Technical Workshops. ESRI International User Conference. San Diego, California

Hartnet M. and S. Nash. 2016. High-resolution Flood Modeling of Urban Areas using MSN Flood- Volume 10.

Jimenez J. and N.J. Galeon. 2016. Evaluation Of The Effects Of Land Use Change In The Hydrologic Water Balance Of The Qiuaoit River Watershed. Unpublished Undergraduate Thesis.

Kim B.S. and H.S. Kim. 2014. Evaluation of flash flood severity in Korea using the modified flash flood index (MFFI). Journal of Flood Risk Management 13.

Kundzewicz Z.W., N. Lugeri, R. Dankers, et. al. 2010. Assessing river flood risk and adaptation in Europereview of projections for the future. Mitig Adapt Strateg Glob Change 15:641–656.

Mitsova D. 2014. Coupling land-use change modeling with climate projections to estimate seasonal variability in runoff from an urbanizing catchment near Cincinnati, Ohio. ISPRS Int J Geo-Inf 3:1256–1277.

Pedersen A.N., P.S. Mikkelsen And K. Arnbjerg-Nielsen. 2012. Climate change induced impacts on urban flood risk influenced by concurrent hazards. Journal of Flood Risk Management 5: 203–214.

Sharma S. et. al. 2017. Flood risk assessment using multi-criteria analysis: a case study from Kopili River Basin, Assam, India. Informa UK Limited, trading as Taylor & Francis Group.

Singh Y.K., Et. Al. 2017. Flood Response System–A case Study. MDPI. www.mdpi.com/journal/hydrology.

Stoffel M., T. Nied, V. Ruiz-Villanueva et. al. 2016. Flood risk in the Upper Vistula Basin. Springer, New York, pp 23–38.

Stonestrom D.A., B.R. Scanlon, L. Zhang. 2009. Introduction to special section on impacts of land use change on water resources. Water Resour Res 45:1–3.

Tellman B, J.E. Saiers, O.A.R. Cruz. 2015. Quantifying the impacts of land use change on flooding in data poor watersheds in El Salvador with community-based model calibration. Reg Environ Change.

Table 1. Land use, soil types and slope distribution in the study area

Thematic Map	Description /Name	Symbol	Area (Ha)	Percent of Total Area
LANDUSE				
	Agricultural Land-Generic	AGRL	8949.35	51.54
	Residential	URBN	571.11	3.29
	Water	WATR	8.37	0.05
	Pasture	PAST	3.34	0.02
	Forest-Mixed	FRST	338.31	1.95
	Agricultural Land-Row Crops	AGRR	66.99	0.39
	Range-Brush	RNGB	6848.29	39.44
	Forest-Deciduous	FRSD	576.97	3.32
		Total	17362.75	100
SOILS				
	Bantay	Bantay	7749.35	44.63
	Bantog	Bantog	1786.18	10.29
	Beach	Beach	453.87	2.61
	Bolinao	Bolinao	5.02	0.03
	Faraon	Faraon	503.28	2.9
	Malitbog	Malitbog	201.81	1.16
	San Fernando	San Fernando	2996.23	17.26
	San Manuel	San Manuel	3666.99	21.12
SLOPE:		(%)		
	Flat	0-2	5148.36	29.65
	Relatively flat	02-08	6764.56	38.96
	Undulating	08-18	3959.25	22.8
	Steep	18-30	1089.46	6.27
	Very Steep	> 30	401.11	2.31

Table 2. Land use scenarios used in the flood assessment

Scenario	Land Use	Convert To	Percent of Area
Scenario 1	Agricultural Land	Commercial Land	25
Scenario 2	Agricultural Land	Commercial Land	25
	Shrub to Grass Land	Agricultural Land	50
	Forest Land	Shrub to Grass Land	50

Table 3. Statistical Indicator during calibration

Statistical Parameter	Correlation, r	NSE
STAT 1	0.63	0.34
STAT 2	0.76	0.41
STAT 3	0.92	0.87
STAT 4	0.75	0.64
STAT 5	0.91	0.71

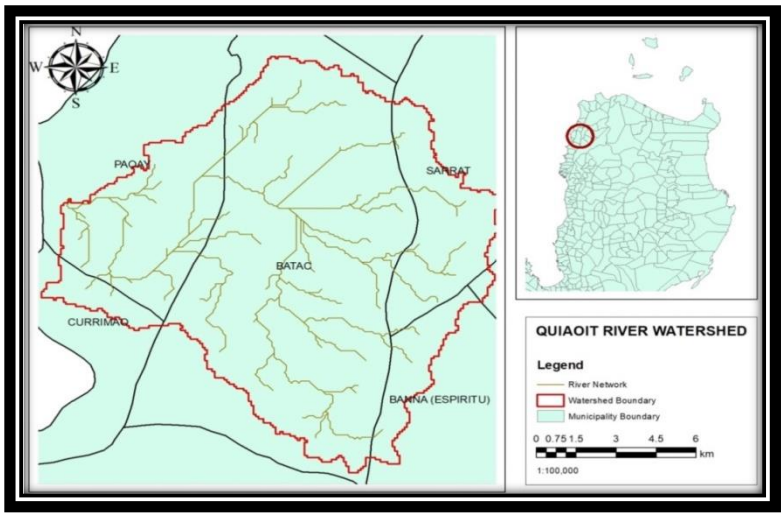

Figure 1. Location of Quiaoit River and watershed boundary, Ilocos Norte (Source: JIMENEZ AND GALEON, 2016).

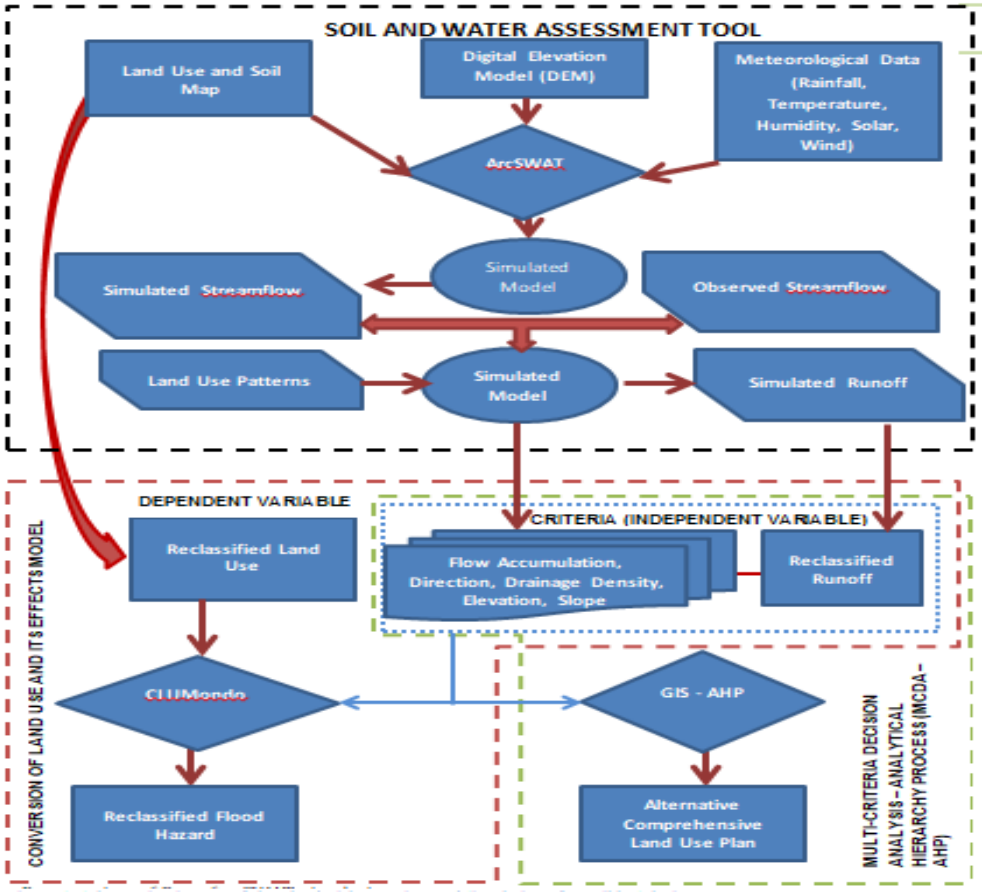

Figure 2. Research framework of the flood risk mapping assessment using GIS-based tools and land use model.

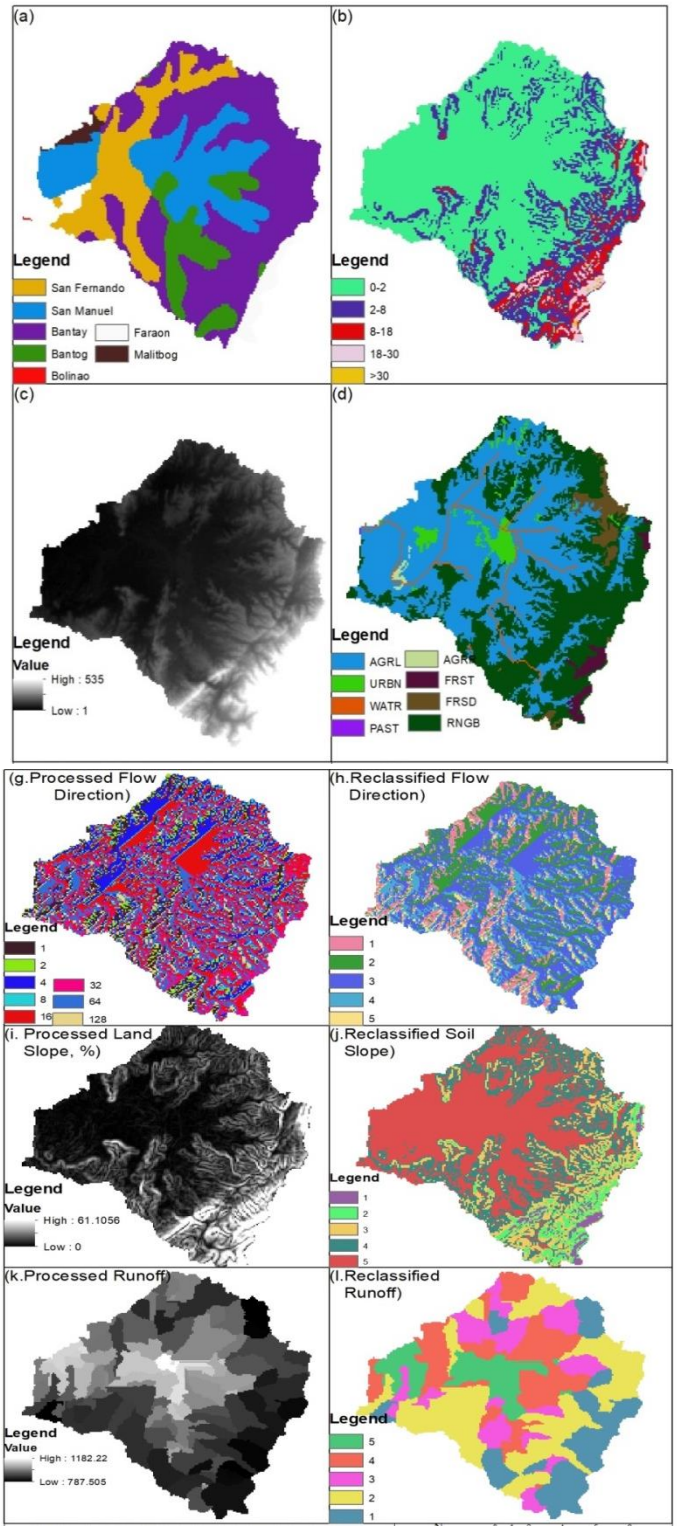

Figure 3. Thematic maps of (a) soils; (b) slope; (c) digital elevation model; and (d) land use and reclassified simulated results of SWAT of Quaioit River watershed for GIS-AHP and CLUMondo Maps/Criteria.

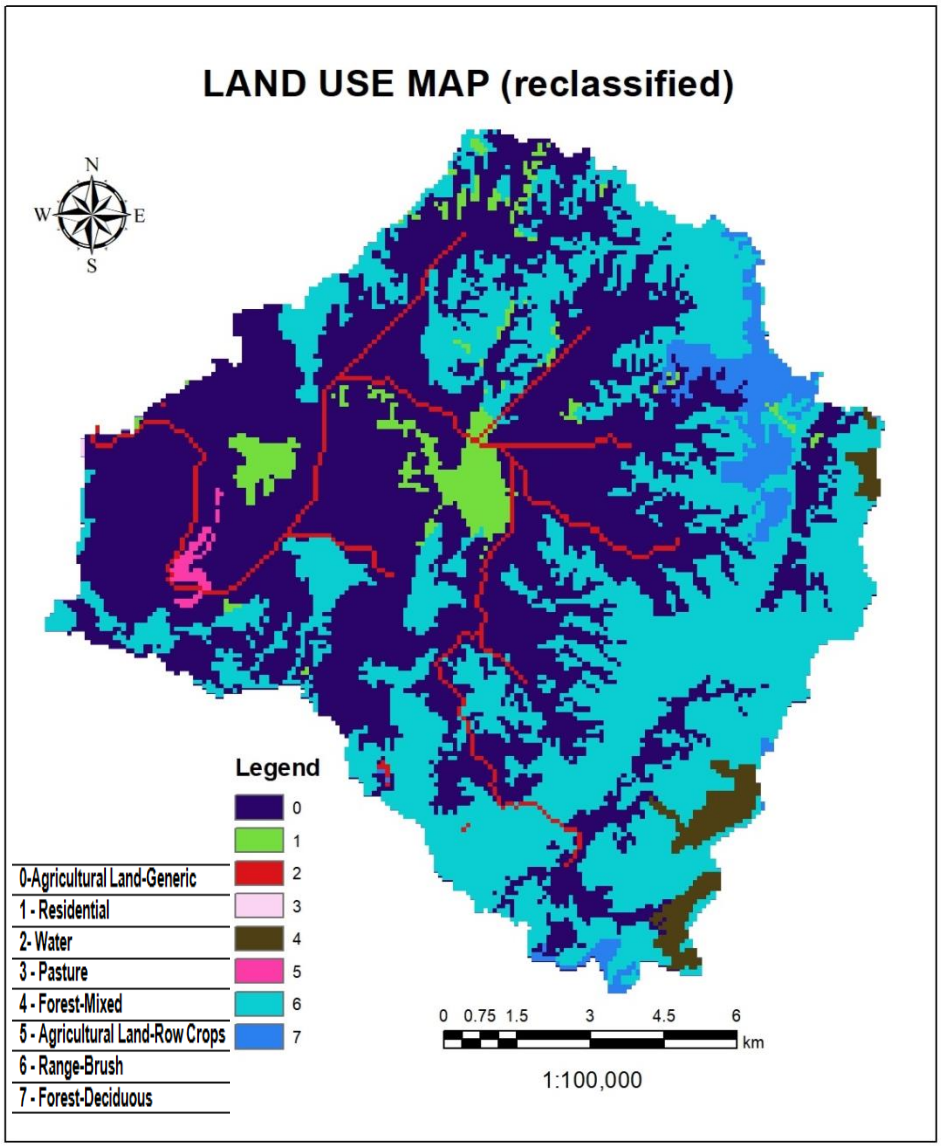

Figure 4. Land use thematic map result of the Quaiot River watershed using CLUMondo model.

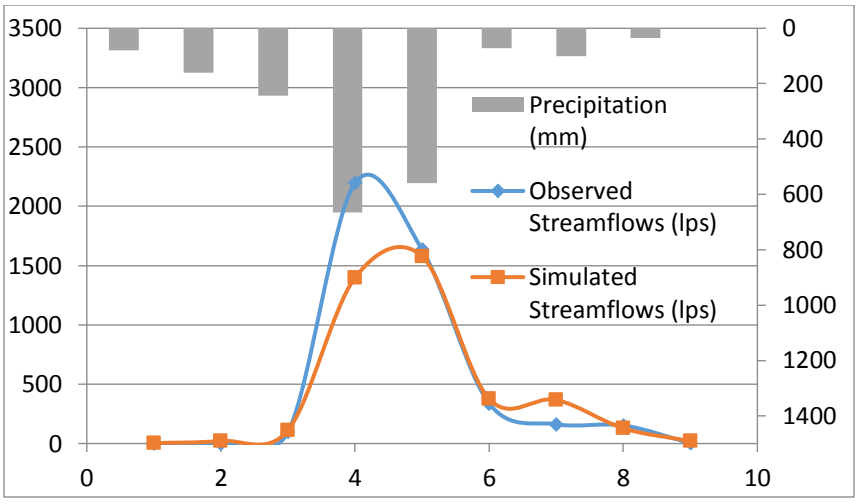

Figure 5. Response of streamflow runoff to peak rainfall using SWAT model.

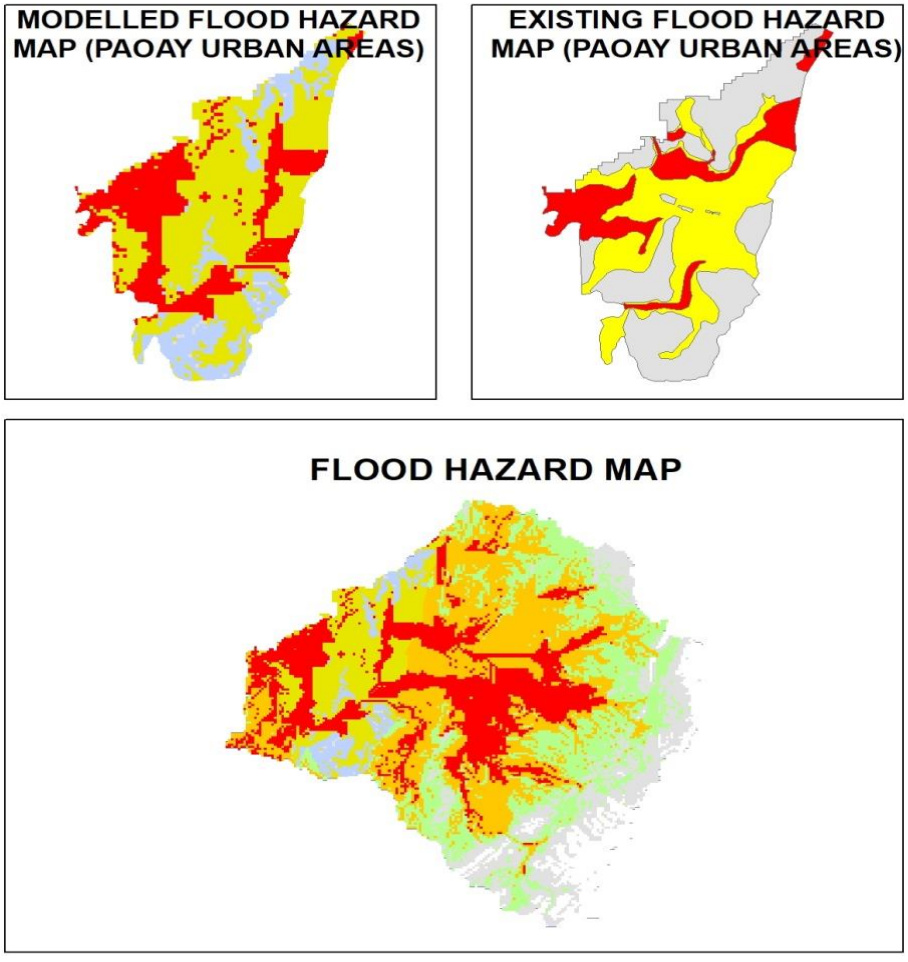

Figure 6. Flood risk assessment of the Quiaoit River watershed and urban areas of Paoay, Ilocos Norte.

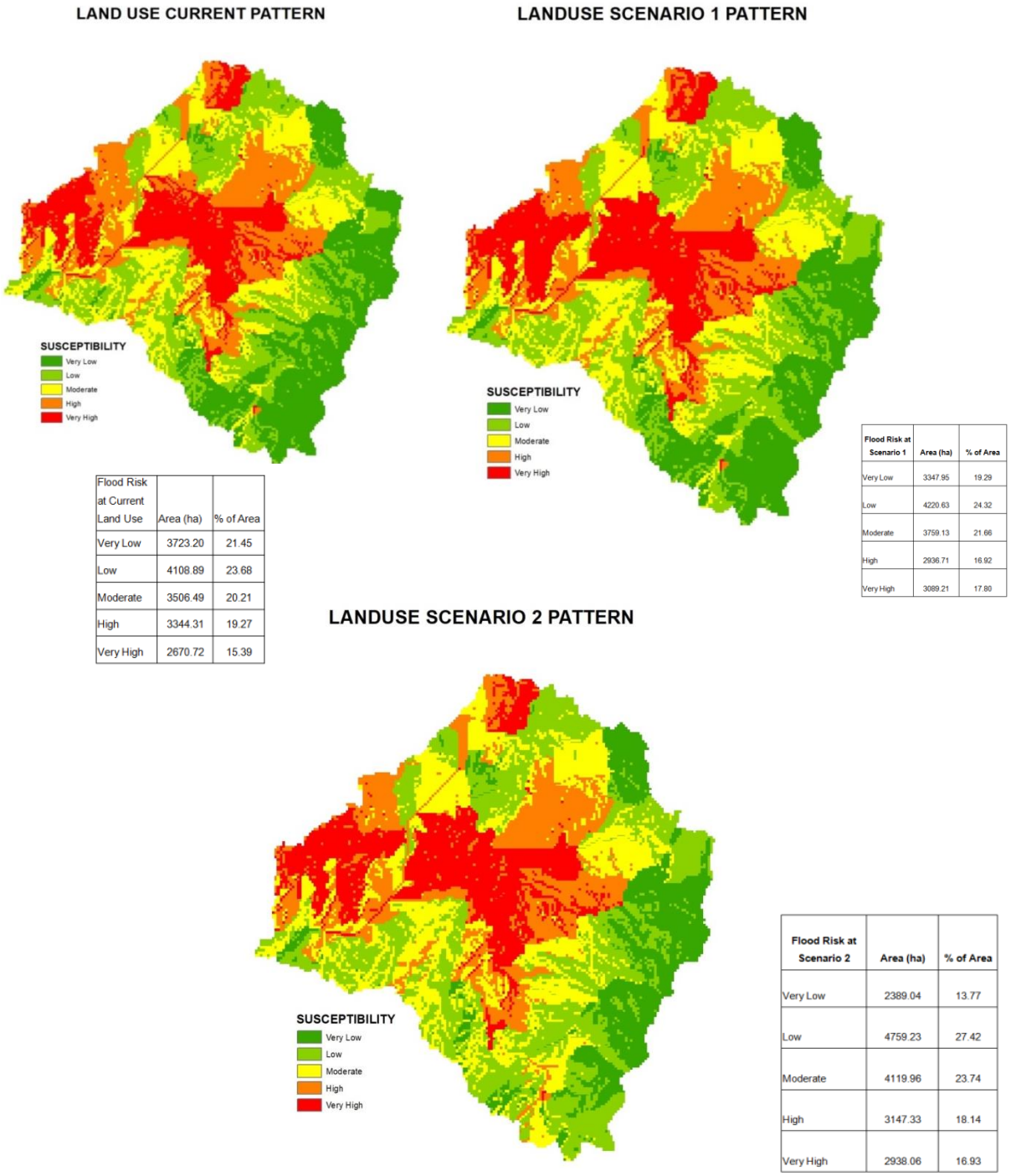

Flood Risk at Current Land Use	Area (ha)	% of Area
Very Low	3723.20	21.45
Low	4108.89	23.68
Moderate	3506.49	20.21
High	3344.31	19.27
Very High	2670.72	15.39

Flood Risk at Scenario 1	Area (ha)	% of Area
Very Low	3347.95	19.29
Low	4220.63	24.32
Moderate	3759.13	21.66
High	2936.71	16.92
Very High	3089.21	17.80

Flood Risk at Scenario 2	Area (ha)	% of Area
Very Low	2389.04	13.77
Low	4759.23	27.42
Moderate	4119.96	23.74
High	3147.33	18.14
Very High	2938.06	16.93

Figure 7. Flood risks at different land use pattern scenario at the Quaioit River watershed.

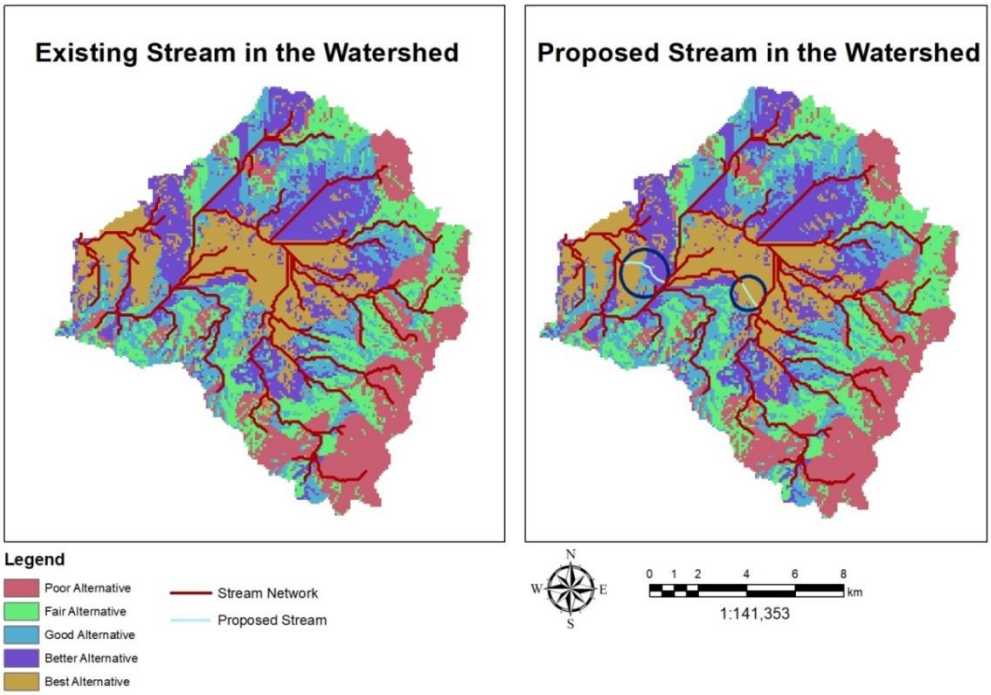

Figure 8. Existing and proposed alternative stream networks at the Quiaoit River watershed.

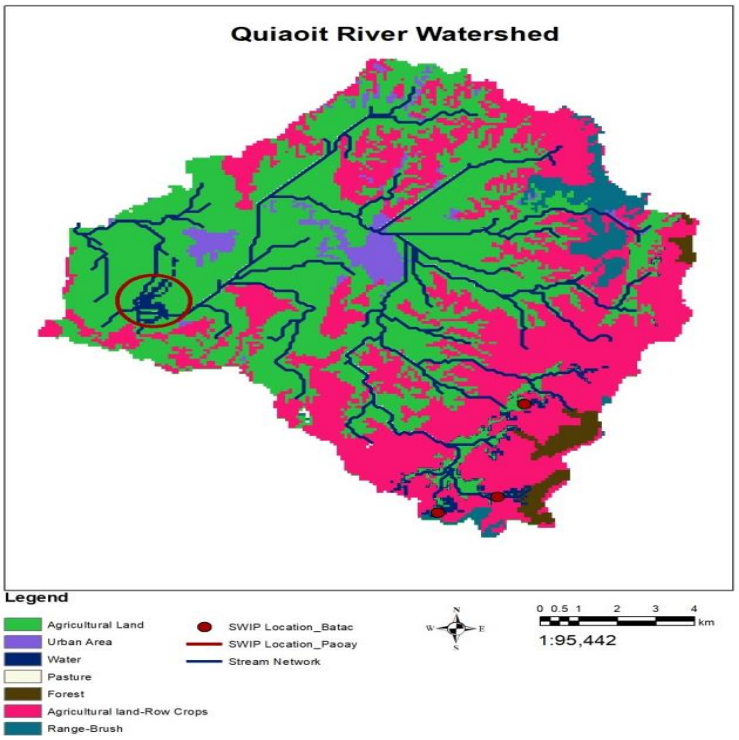

Figure 9. Proposed location of small water impounding projects at the Quaioit River Watershed.

DESIGN, FABRICATION, AND PERFORMANCE TESTING OF MOBILE CACAO BEAN FERMENTER

Nila B. Oñate, Marife L. Pesino, Ma. Carmela N. Llovit

Central Bicol State University of Agriculture
San Jose, Pili, Camarines Sur, Philippines

ABSTRACT

Fermentation is one of the most important processes in the production of chocolate. However, it is done in a no controlled process for 5-7 days. In this method, the turning of beans is done by transferring the beans from one set up to another or transfer manually using hands, making the work more laborious. The researchers designed and fabricated a mobile cacao bean fermenter, which can speed up the fermentation process and reduce the drudgery of human labor in turning the cacao beans during fermentation. Machine parts that have direct contact on the beans were made of stainless steel food-grade materials to ensure that the fermented cacao beans and the product derived from the juice collected will be safe for human consumption. Performance test using 40 kg of fresh cacao beans had recovered 35 kg fermented beans. Results showed that the machine has an 87% fermenting recovery and 88% fermenting efficiency. Using the fabricated mobile cacao bean fermenter, fermentation lasted only for three (3) days. Cut test of dried fermented beans using the machine produced fermented cacao beans, which was classified as grade 1A. Cost and return analysis showed that using the machine yielded a higher net income amounting to Php 334,470 compared to the traditional method. Partial Budget analysis likewise showed that using the machine had an incremental change in income amounting to Php 20,039. Hence, the designed mobile cacao bean fermenter is considered an economically viable technology for cacao bean fermentation.

Keywords: *cacao beans, fermentation, cacao bean fermenter*

INTRODUCTION

Cacao (*Theobroma* cacao L.) belongs to the family of Malvaceae, generally known to have originated from Central and Southern America.

Cacao becomes an economically important crop and an important agricultural export commodity in the world. It forms the backbone of the economy due to its valuable seeds, commonly known as cocoa beans.

When cacao beans are fully fermented and processed, the beans produce one of the most desired flavors in the world - chocolate. The fermentation of the beans is one of the most important processes in the production of chocolate. It is a process with catalyzing several enzymes and microorganisms to increase the speed of biochemical reactions in pulp and cotyledon. Cocoa fermentation also helps remove the tannins present in the cacao bean. Tannins bring an astringent flavor to the final chocolate and must be removed.

To fully develop a cacao bean's flavor, the fermentation process must be done properly since fermentation is a crucial step in the processing of high-quality cacao, which will produce the desired flavor and aroma of chocolates. Chocolate is in such high demand throughout the world today, and cacao trees must be grown. Beans harvested and processed sustainably in a safe way for wildlife, people and the environment.

Traditionally, cacao seed fermentation is a no-controlled process done in fermentation boxes usually made of wood, in plastic tarpaulin, plastic crate, and in perforated baskets in small quantities. Another existing method is the heap-type fermenter, which is no longer practiced in most cacao farms. In these methods turning of beans is done by transferring the beans from one set up to another. If not, beans are mixed manually using hands, making the work more drudging and time-consuming even for small scale operations. There were studies conducted using juice from cacao, termed as liquefied pulp juice, which can be processed as vinegar and wine. However, the extracted juice from the traditional fermentation method is normally considered a liquid waste due to the typical design without a sweat collecting vessel.

Thus, to improve quality and achieve global standards of the cacao industry, the development of appropriate cacao bean fermenting equipment should be done to maximize benefits and give high quality dried fermented cacao beans gender-friendly and affordable to small scale farmers aside from utilizing waste during fermentation.

OBJECTIVES

The study generally aimed to design and establish the operating conditions of a cacao bean fermenter. Specifically, the study aimed to:

1. design and fabricate a cacao bean fermenter with a manual stirring/mixing mechanism;
2. determine the fermenting time, fermenting recovery and fermentation efficiency of the machine;
3. determine the quality of the dried fermented beans in terms of cacao bean aroma, pH of the liquefied pulp, odor, chocolaty taste, temperature of bean mass, cut bean color after drying of fermented beans,

fermentation efficiency, input and output capacity, bean count, and fermentation recovery; and to

4. determine the economic viability of the equipment.

Significance of the Study

Improving the quality of commercially available chocolate may increase the economic value of cocoa, resulting in the promotion of the cacao industry in the country.

The result of the study will serve as a reference for further development of technology on appropriate cacao fermentation that will support the production and processing system and withstand the growing demand for quality chocolate worldwide.

Enabling the farmers to produce high-quality cacao beans will give them an equivalent increase in income, which will also benefit cocoa processors and likewise make the Philippines as one of the potential exporter of high quality dried fermented cacao beans.

METHODOLOGY

Design

In the design of the equipment, the desired quantity of batch of cacao beans to be fermented, ease of turning, ease in the monitoring of the changes during the process, and ease of fabrication were considered. All parts that have contact with the beans and liquefied pulp was made of stainless steel. Sketch-up modeling was employed in the production of working drawings (Figure 1).

Fabrication and Performance Testing

The machine designed was fabricated at JPS Agri Inputs and Technology at San Jose, Pili, Camarines Sur. One skilled welder from the shop, as mentioned above was responsible for the fabrication of the machine with the researcher's supervision. The fabrication shop provided all the labor and equipment used for construction. The fabricated machine is shown in Figure 2. Performance testing was done at the College of Engineering and Food Science of CBSUA.

Fermentation Process

The equipment was subjected to a thorough cleaning and sterilization before the wet beans were loaded. The materials and equipment were also checked and

prepared before the testing. Cacao beans were loaded in the equipment and allowed to ferment. The first turning of beans was done after attaining the 45˚C temperature mark of the bean mass and was turned regularly every 12 hours to maintain a uniform temperature inside the fermenter. The beans were left in the bin until constant temperature reading was attained, which indicates that the samples were already fully fermented. Juice from the fermenting beans was also collected; its volume was determined.

Drying of Fermented Beans

After the end of the fermentation process, fermented beans were immediately subjected to drying to avoid deterioration. Drying of fermented beans was done using the sun-drying method. The reduction in bean moisture content was monitored using moisture analyzer until optimum moisture content for safe storage of cacao ranged to 7% - 7.5% was achieved.

Data Gathered

During and after the fermentation process, test parameters were obtained and recorded, evaluation of the quality of dried fermented cacao beans was undertaken.

Measurement of Parameters

A. <u>During the fermentation process</u>

1. pH of the sample

The pH of the liquefied pulp was monitored daily using a pen type pH meter initially calibrated with buffer 4 and 7. Three (3) trials were performed for each sample.

2. Temperature of bean mass

Temperature of the fermenting bean mass was monitored at 3-hour intervals from the start to the end of the fermentation process. The temperature was obtained at three points (top, middle, bottom) inside the fermenter using a multi-purpose dial thermometer (Figure 6).

<u>B. Post-Fermentation Evaluation</u>

Five (5) panelists consisted of one (1) cacao expert, three (3) cacao farmers, one (1) chocolate processor were invited to assess the sensory attributes of the fermented dried beans, including the cut bean color and odor after drying, as well as the aroma and chocolatey taste of the beans after roasting.

1) Bean Odor

Bean odor was rated using a hedonic scale of the sour or acidic odor of the beans divided into categories as follows:

(1) Extremely sourly or acidic;
(2) Sourly or acidic;
(3) Moderately sourly or acidic;
(4) Slightly sourly or acidic; and
(5) Not sourly or acidic

Bean Acidic odor was due to the changes in the acid formation, together with residual lactic and acetic acid that can be used as an index for evaluation of fermentation success and seed quality.

2) Bean Color

Bean color was assessed through the nib's color after the bean was cut. Its results were further discussed in the evaluation of fermentation efficiency.

3) Bean Aroma

Since cacao bean aroma can only be assessed after roasting, the dried fermented beans were manually roasted and evaluated using the following 9-point hedonic scale.

(1) Dislike extremely
(2) Dislike very much
(3) Dislike moderately
(4) Dislike slightly
(5) Neither like nor dislike
(6) Like slightly
(7) Like Moderately
(8) Like very much
(9) Like extremely

Performance Testing

The following parameters were computed and evaluated from the gathered data to determine the machine's performance.

1. Fermentation Efficiency

The quality of fermented beans was entirely assessed after drying them as fermentation continued through the drying process.

Fermentation efficiency was computed through a cut test consisting of 100 beans per trial, which were done randomly, the bean was cut lengthwise, laterally

using a bean cutter. Both splits of each bean were examined in full daylight according to the cross-sectional color of the beans and placed in one of the following categories: Through Philippine National standard and; Code of practice for Philippine cacao beans.

(1) fully brown (fully fermented)
(2) partly brown, partly purple (moderately fermented)
(3) purple (under-fermented)
(4) slaty (not fermented)
(5) insect-damaged
(6) moldy
(7) germinated

The equation determined fermentation efficiency:

$$Fe = \frac{Nf}{Nt}\ x\ 100$$

Where:

F_e = fermentation efficiency, %
N_f = number of dried fermented (fully brown to partly brown, partly purple) beans, pcs.
N_t = number of dried bean samples, pcs.

2. Fermentation Recovery

Fermentation recovery was determined using the equation:

$$Fr = \frac{Wf}{Wi}\ x\ 100$$

Where:

F_r = fermentation recovery, %
W_f = weight of fermented beans, kg
W_i = weight of beans prior to fermentation, kg

Data Analysis

Data obtained from the performance testing of the mobile cacao bean fermenter and the evaluation of the quality of dried fermented cacao beans were summarized using simple statistical tools as mean and percentage.

Economic and Financial Analysis

The cost and return analysis was determined to compare the profitability of the mobile cacao bean fermenter versus the traditional fermentation method. The following profitability criteria were used. The partial budget was used to compare

the additional benefits of using the Mobile cacao bean fermenter versus the traditional method of cacao bean fermentation.

The following profitability indicators were likewise computed:

a. Return on investment (ROI)

It measures the return on the owner's investment, which shows profitability if its value is greater than the current bank investment. It was conducted to determine the viability of the machine.

$$\textbf{Return on Investment (ROI)} = \frac{\textbf{Annual Net Income}}{\textbf{Annual Operating Cost}} \textbf{ X 100}$$

Where:

Annual Net Income = Annual Gross Income – Annual Operating Cost

Annual Operating Cost = Fixed Cost + Variable Cost

b. Payback period

It refers to the time required for the return and amount of expenses in utilizing the system to be equally expressed in years.

$$\textbf{Payback Period} = \frac{\textbf{Annual Operating Cost}}{\textbf{Annual Net Income}}$$

c. Break-even cost (BEC)

It is the condition of the enterprise at which revenues equal to expenses.

$$\textbf{Break-even cost (BEC)} = \frac{\textbf{Annual Operating Cost}}{\textbf{Volume of Production}}$$

d. Benefit-cost ratio (BCR)

The BCR measures the benefits of utilizing the machine. Where in associated with costs. A BCR greater than or equal to one (1) indicates that the machine under consideration is economically advantageous.

$$\textbf{Benefit-cost Ratio (BCR)} = \frac{\textbf{Annual Gross Income}}{\textbf{Annual Operating Cost}}$$

RESULTS AND DISCUSSION

Design

The design and the fabricated machine, as reflected in Figure 3 were composed of the following components:

a. Main frame

The machine frame was fabricated from 3/16" x 1 1/2" angle bars connected by ordinary welding rods. It was designed to support the loading bin and to withstand the movement caused by the stirring process. Including the caster wheel attached, the machine's frame height was 550 mm which was designed to provide ease of mixing the beans. It measured 500 mm x 500 mm width based on the cylinder casing to allow a container or an at least 500 ml bottle to be placed below the discharge chute to facilitate juice collection.

b. Loading bin

The portion where the beans were loaded to ferment was designed to control the fermentation process initiated by the fermenting organism, by securing an anaerobic condition. It was connected to the sweat's discharge funnel. Thus, a perforated bottom surface, which was intended for liquid drainage and was made detachable for easy cleaning and removal of placenta and other impurities stucked on the funnel. It was fabricated from 1mm thick stainless steel sheet bent in a cylindrical shape and was oriented vertically with a diameter of 430 mm and a 500 mm high, connected to the main frame through bolts and nuts.

c. Stirring/ assembly

It consisted of a 1/4" ø stainless steel (SS) shaft which was formed in a helical shape and was welded by a stainless steel welding rod to the main shaft made of a 1/2" ø SS shaft which was vertically oriented. It was designed to turn the beans from top to bottom and vice-versa to facilitate aeration in the aerobic phase and helped equalize the temperature to break bean clods. The stirrer was supported by a stainless steel bearing attached to the bin cover. The mixing operation was done by manually rotating the maneuver on the top portion of the machine.

d. Juice outlet

The juice outlet of the machine is a funnel attached under the loading bin that served as a drainage for the sanitary collection of the liquefied pulp through a stainless steel valve

Fabrication of the machine

The machine and its entire components were fabricated at the JPS Agri- input and technology at San Jose, Pili, Camarines Sur. To ensure the precision of the stainless steel sheet components, it was subjected to a laser cutting and joined together by an inert tungsten gas (TIG) welding using stainless steel welding rods. All the machine parts that have direct contact on the beans were made of stainless steel food-grade materials to ensure that the fermented cacao bean and the product derived from the juice collected will be safe for human consumption.

Performance Testing

The performance characteristics and machine specification of the mobile cacao bean fermenter were indicated in Table 1. The machine follows a batch type loading system and fermentation lasted for three (3) days period. The machine has a 40 kg loading capacity and a 50 kg full load capacity per batch (Figure 5). Fermenting recovery was calculated at 88 %. An approximately ten (10) rotation of maneuver was observed and recorded. Performance test showed that the stirrer proved to equalize the bean mass's temperature at the top, middle and bottom of the loading bin measured. This indicated that an efficient turning of beans carried out adequate aeration during the aerobic phase of the fermentation. The use of the machine also attested a great reduction in the effort of turning the beans, compared to when the traditional method of fermentation was used.

The controlled condition of the process allowed the achievement of the ideal bean mass temperature which was recorded at 38°-39°c on the first 24 hours and was observed to increase even more every after the stirring process. The liquefied pulp collected on the first day of fermentation was still sweet-smelling indicative that fermenting organisms were not yet active. On the second day, the sweet smell of the collected juice decreased, a formation of bubbles and a presence of alcohol were detected in the collected liquefied pulp, an indication that the alcohol forming organism has converted the fermenting sugar component of the bean mucilage into ethanol; a fermentation evidence, these continued up to the third day. Aside from the fermented cacao beans, due to controlled and sanitized collection of juice an additional product was derived from the collected liquefied pulp such as vinegar, wine and process cacao juice all of which offer good market value. On the third day as the fermentation terminates, the bean turned to brown color and was observed to be slightly dried but still sticky due to the mucilage residual.

Temperature

The temperature monitoring was done at a three (3) hours interval until five consecutive constant readings were recorded, wherein it indicates the termination of the fermentation process. The initial temperature of the bean mass was 30°c up to

the maximum of 44°c attained on the thirty-sixth (36th) hour which also signals the first turning of beans. The maximum temperature achieved each day of fermentation reading were 39°C, 44°C and 39° on the first, second and third day respectively, whereas the fermentation terminated at 35°C.

Figure 6 shows the temperature of the bean mass and the ambient temperature during the fermentation process using the Mobile Cacao Mean Fermenter (MCBF). It was noticed that there were a sudden increase in the temperature after twelve (12) hours of fermentation, wherein most of the volume of liquefied pulp has already been drained off. The 44°c maximum temperature was considered to be high enough also to produce good quality cocoa.

pH

Samples of liquefied pulp were collected daily and subjected to pH value determination using a pen pH meter. It was noted that the pH value of the degrading pulp surrounding the beans decreases as the fermentation progress. A decrease in pH value ensured that the fermenting sugars in the pulp were converted into lactic and acetic acids that are important in the biochemical changes of the beans during fermentation. Lower pH indicated higher acidity. Figure 7 presents the trend of the pH value of liquefied pulp through the fermentation process from the MCBF. The stable or rapid decrease in pH indicates a fast fermentation rate. The initial pH recorded in MCBF was 3.7, that increase to a maximum of 4.4 but decreased eventually to 3.9 on the third day of fermentation.

Drying of the fermented cacao beans

Prior to the fermentation progress, the moisture content of the fresh beans was taken to determine the amount of water present in the cacao beans. Calculations were recorded at 39 % of the oven drying method. The bean's moisture content after the fermentation and the moisture content during drying were analyzed using the 5 g chopped samples which were subjected to the moisture analyzer calibrated at 95% precision in ten (10) minutes reading timer as required for accuracy. Fermented beans were found to be at 35.33% moisture content. A 4.05 % moisture loss after fermentation was due to loss of the mucilage surrounding the beans while another 28. 23% decrease was after drying. The fermented beans were subjected to sun drying immediately (Figure 8) after the fermentation process until 7. 1% moisture was attained.

Fermentation recovery

The recovered fermented beans after fermentation was 35 kg thus, resulted in 88% fermentation recovery. The reduction of weight was mainly caused by the deterioration and drainage of pulps surrounding the beans. Aside from the dried

fermented cacao beans, the liquefied pulp was also collected and recorded to be 2.600 ml, which was computed to be 65 ml per kg wet beans.

A. **Evaluation of the Quality of Dried Fermented Cacao Beans**

The success in fermentation success was obtained after the drying of beans as fermentation continues during the drying process. Sensory evaluation was determined in terms of the bean odor and color after the drying of beans. Likewise, dried beans were roasted for aroma and chocolatey taste sensory evaluation.

Cut test on the beans was done to determine the fermentative quality of the dried fermented cacao beans. One hundred pcs of the dried beans fermented using the mobile cacao bean taken at random and evaluated using the procedures discussed in the methodology.

The fermentation of cacao continues during the drying process until the full brown color is achieved, indicating that it was well fermented. Thus, Different varieties of cacao required different fermentation times as well as drying. A fully fermented bean ranges from partly - purple and brown to an even chocolate - brown color with cotyledons open and dried to 7.1% moisture content. Table 4 shows that the machine attained 88% fermenting efficiency.

Odor

The bean odor of dried fermented cacao beans was evaluated and found to have a slightly sour odor indicating that there was an acetic acid retained in the beans. It is normal under commercial standards shown in Tables 4 and 5.

Chocolatey Taste and Aroma

The chocolatey taste and aroma of the dried fermented cacao beans were found after the beans were roasted. The result of the sensory evaluation using the 9-point hedonic scale was found to be moderately like.

Bean count

The bean count was the main basis in grading the dried fermented cacao beans. The bean samples fermented using the mobile cacao bean fermenter were compared to the commercial dried beans. The weight of beans per 100 pcs and the number of beans to make 100 g, or the bean count was determined. The result is presented in Table 6.

Data shows that the cacao beans fermented using the mobile cacao bean fermenter has a high weight per 100 pcs, which was 156 g and required 64 beans to make 100 g.

Bean count determination is one of the main parts of bean grading. In general, bean count result combined with the count of the fully fermented bean ranged from partly - purple and brown to an even chocolate - brown color showing that the dried fermented cacao bean using the mobile cacao bean fermenter passed the standards of the top class dried cacao bean quality or Grade 1A. Based on the Philippine National Standard's grades and standards, Code of practice for Philippine cacao beans, Grading of cacao (Table 7).

Economic Analysis

Cost and return analysis shows that the net return of the machine for a total of 2,268.6 kg wet beans processed for a year amounted to PhP 154,098 which was higher than the returns using the traditional plastic drum method. Assumptions used in calculating the economic/financial analysis of the machine shown in Tables 8 and 9.

Aside from the fermented beans, the machine created another source of returns, which is the collected cacao juice or liquefied pulp.

CONCLUSIONS

Based on the data gathered the following conclusions were established:

1. The mobile cacao bean fermenter has an 88 % fermenting recovery, 87% fermenting efficiency and fermentation time of three (3) days.
2. Quality of dried fermented cacao beans was graded as Grade 1A which passed the set standards by Code of Practice for Philippine Cacao Beans, Grading of Cacao Beans (PNS/BAFPS 58:2008).
3. The partial budget analysis showed that the designed mobile cacao bean fermenter is economically viable.

RECOMMENDATIONS

Based on the result of the study, conducting a similar study to the machine's performance with the full loading capacity is strongly recommended

REFERENCES

Tagro Guehi S. et al. 2010. Effect of Turning Beans and Fermentation Method on the Acidity and Physical Quality of Raw Cocoa Beans.

Australian Government AusAID. Cocoa Processing Methods for the Production of High Quality Cocoa in Vietnam.

Emmanuel O.A. et al. 2012. Influence of pulp-preconditioning and fermentation on fermentative quality and appearance of Ghanaian cocoa (Theobroma cacao) beans.

Afoakwa E.O. et al. 2013. Changes in acidification, sugars and mineral composition of cocoa pulp during fermentation of pulp pre-conditioned cocoa (Theobroma cacao) beans

Galvez J.C. et al. 2016. Design and Development of Cacao (*Theobroma Cacao L.*) Bean Fermenter.

Bray J. 2012. From cacao tree to bean: the Beginning of fermentation.

Mikkelsen L. 2010. Quality Assurance along the Primary Processing Chain of Cocoa Beans from Harvesting to Export in Ghana.

Philippine National Standard, Code of Practice for Philippine Cacao Beans (Pns/Bafps 104:2011Ics 67.020)

A Primer on PEF's Priority Commodities: Industry Study on Cacao, International Cocoa Organization (ICCO) Quarterly Bulletin of Cocoa Statistics, Mar 2013).

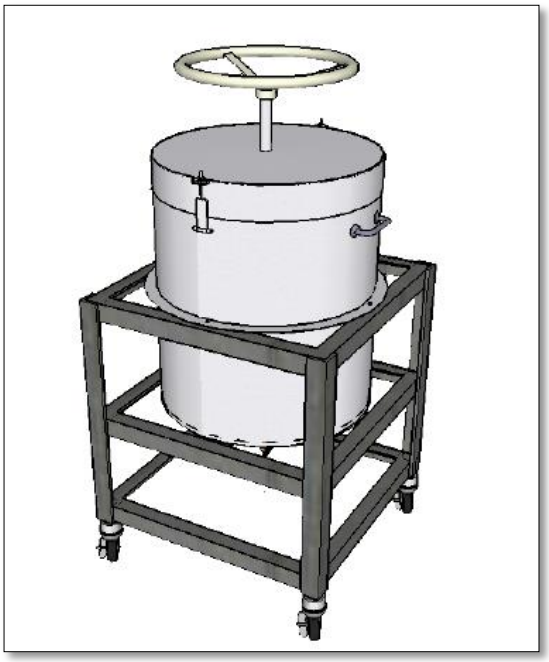

Figure 1. The designed mobile cacao bean fermenter

Figure 2. The fabricated mobile cacao bean fermenter

Figure 3. The fabricated mobile cacao bean fermenter

Figure 4. Cacao beans loaded in the mobile cacao bean fermenter.

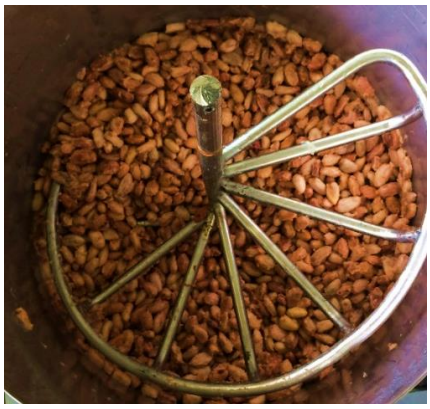

Figure 5. Fermented cacao beans after fermentation process.

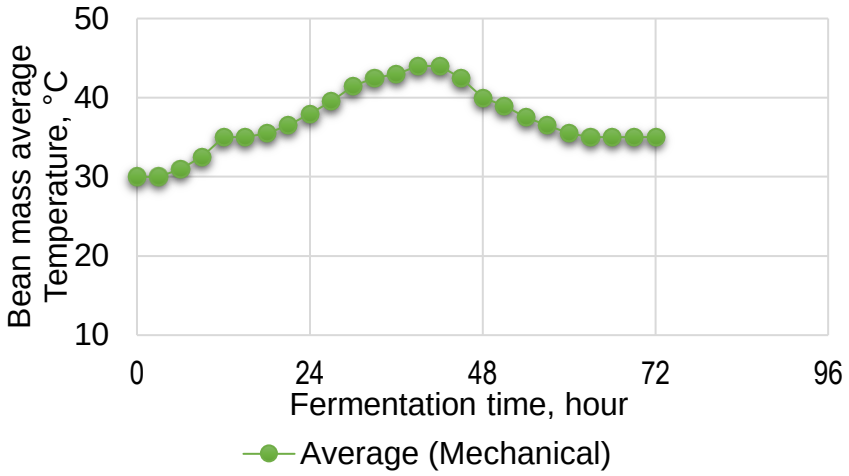

Figure 6. Average temperature of bean mass during the fermentation process using the mobile cacao bean fermenter.

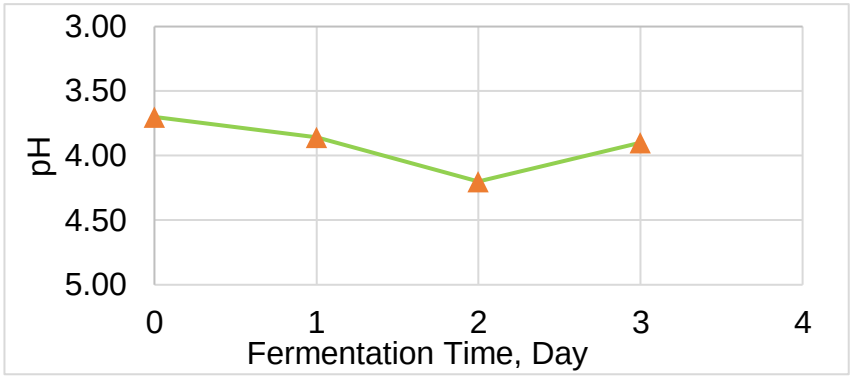

Figure 7. pH value of liquefied pulp

Figure 8. Sun drying of the fermented cacao beans

Figure 9. The extracted liquefied pulp collected during the fermentation process.

.

Table 1. Specification of the mobile cacao bean fermenter.

Machine Specification	Parameters
Dimensions, mm	
Length	550
Width	550
Height	900
Diameter of the bin	450
Weight of the machine, kg	18
Loading Capacity, kg	40
Labor requirement, person	1
Fermentation duration, days	3
Fermentation recovery, %	88
Fermentation efficiency, %	87
Number of maneuver's rotation required to equalize the bean mass temperature, rotation	10

Table 2. Data gathered from the performance testing of mobile cacao bean fermenter.

Parameters	Specification
Weight of fresh beans, g	28,700
Weight of fermented beans, g	35,000
MC of fresh beans, %	39.48
MC of fermented beans, %	35.33
Volume of liquefied pulp collected, li	1.8
Fermentation recovery, %	88
Duration of fermentation, days	3

Table 3. Sensory Result for Cut Bean Color.

	APPEARANCE					
CACAO BEAN SAMPLES	**FB**	**PB/ PP**	**P SB**	**ID**	**MB**	**GB**
	45	43	6 3 0		0	2

*(FB) fully brown, (PB/PP) partly brown/ partly purple, (P) Purple, (SB) Slatty beans, (ID) -Insect damage, (MB) moldy beans, (GB) Germinated beans

Table 4. Chocolatey taste rating of roasted dried fermented bean samples.

Samples	Judge No.					Ave.
	1	2	3	4	5	
R1	6	7	8	7	6	6.8
R2	7	8	7	6	7	7.2
R3	7	7	8	8	6	7.2
						7.07

* (1) Dislike extremely, (2) Dislike very much, (3) Dislike moderately, (4) Dislike slightly, (5) Neither like nor dislike, (6) Like slightly, (7) Like Moderately, (8) Like very much, (9) Like extremely

Table 5. Aroma rating of dried bean samples.

Samples	Judge No.					Ave.
	1	2	3	4	5	
R1	6	8	8	7	8	7.4
R2	6	9	7	9	7	7.6
R3	7	7	7	6	6	6.6
						7.2

* (1) Dislike extremely, (2) Dislike very much,(3) Dislike moderately,(4) Dislike slightly, (5) Neither like nor dislike, (6) Like slightly, (7) Like Moderately, (8) Like very much, (9) Like extremely

Table 6. Weight of beans per 100 pcs and bean count.

CACAO BEAN SAMPLES	TRIALS	WEIGHT PER 100 pcs (g)	MEAN	BEAN COUNT (pcs/100g)	MEAN
Mechanical	1	157.6	156	64	64
	2	156.4		64	
	3	153.7		64	

Table 7. Grading of Dried Cacao Beans

GRADE	BEAN COUNT	PERCENTAGE OF BEANS		
		MOLDY	SLATY	DAMAGED, INFESTED, AND GERMINATED BEANS
1A	≤100	3	3	2.5
1B	101-120	3	3	2.5
2A	≤100	4	8	5
2B	100-120	4	8	5
Substandard	>120	>4	>8	>5

* Note: The percentages are maximum; the percentages are given in the last column apply to all defects mentioned therein, taken together. Code 1-2 denotes grade based on defective characteristics. Code A and B stand for bean counts.

Source: PNS/BAFPS 104:2011 ICS 67.020; Code of practice for Philippine cacao beans, Grading of cacao beans (PNS/BAFPS 58:2008)

Table 8. Cost and Return Analysis Comparing the Traditional Method and the Mobile Cacao Bean Fermenter Based on Annual Production

PARTICULARS	MOBILE CACAO BEAN FERMENTER	TRADITIONAL FERMENTATION
A. RETURN		
SALES:		
Dried fermented beans	408, 348	245,008
Vinegar	43, 200	-
TOTAL RETURNS	451, 548	245, 008.
B. COST		
1. FIXED COST		
Fermenter	15,000	200.00
Depreciation	2700	-
Interest on investment	2700	-
Taxes, licenses and insurance	300	-
Land rental	6000	6000
Repair and management	750	-
TOTAL FIXED COST	27,450.00	6200.00
2. Variable cost		
Labor cost	90,000	90,000
Raw material cacao beans	180,000	108,000
Total Variable cost	270,000	204,200
3. TOTAL COST (PhP)	**90450**	**51616**
C. Net Income (PhP)	**334,470**	**190,736**

Table 9. Partial Budget Analysis Comparing the Mechanical and the Traditional Plastic Crate Method of Cacao Bean Fermentation Based on the Annual Production.

	PARTIAL BUDGET ANALYSIS	
	A	B
	Added cost, Php	Added return, PHP
	93,250.00	113,289.2
	Reduced return	Added return
	0	0
Incremental change in income(B-A), php	20,039.2	

DEVELOPMENT OF COMPUTER VISION SYSTEM FOR MANGO SORTING AND GRADING

Arlene C. Joaquin, Maria Elizabeth V. Ramos, Romualdo C. Martinez, Richard P. Avila, Rolando A. Almerol

Philippine Center for Postharvest Development and Mechanization (PHilMech), Science City of Munoz, Nueva Ecija

ABSTRACT

Traditional manual sorting of fruits and vegetables in the Philippines is inaccurate, time-consuming, laborious and expensive. It requires high operating costs and vulnerable to damage due to inappropriate handling and inconsistent human skills. The computer vision system is one of the promising advancements in the sorting and grading of crops and has been successfully used in most developing countries. The computer application allows sorting and grading to be executed in an objective, rapid and precise manner. In 2017, Philmech attempted to develop a computer vision system (CVS)-based machine to address the problems associated with the current practices of mango sorting in the country. The technology aimed to sort and grade green mangoes in two stages; physical defects and weight classification, and eventually classify the mangoes based on standard references. Initial testing conducted to assess the performance of the initial prototype unit CVS-based mango sorting machine revealed that the technology has an accuracy of 98.58% or an estimated error of 1.42 % in classifying green "Carabao" mangoes. Both findings indicate acceptable sorting error based on the 10% maximum error tolerance per pack of any size, set by the Codex Alimentarius International Food Standards (CODEX). Also, initial validation tests conducted between actual weights and predicted weights using the laboratory set-up CVS-based mango sorting machine generated a relatively high coefficient of determination (R^2) at 0.99 and mean square error of 3.66% which is an indication of the technical feasibility of the developed system.

Keywords: *machine vision, green mango, sorting, digital imaging*

INTRODUCTION

Mango or *Mangifera Indica* L. is one of the most important fruit crops of the Philippines. The Carabao mango is also known as Manila super mango is the most popular variety not only in the Philippines but also in the international market. The fruit is mostly eaten fresh or in several processed forms such as juices, nectars, purees, frozen, dehydrated/dried and preserved (Philippine Statistics Agency, 2014; Tharanaj et al., 2009 as cited by Sivakuma et al., 2010). Philippine mangoes are marketed locally and internationally as fresh or processed, but the bulk of mango

exports is in the fresh form (Sivakuma et al., 2010). About 3% of the country's average annual total production of mango was exported from 2004-2013 amounting to an annual average volume of 22,338 metric tons. It is the third leading fruit exports of the country and contributed about Php 14.02 billion (2%) in the Gross Value Added (GVA) of Agriculture and Fishing sector in 2013 at constant prices (Philippine Statistics Office, 2014; Fresh Plaza, 2014; Espino and Espino, 2014)

Grading of fruits, like mango,is a very important activity before marketing whether in local or in the export market because it increases the value of the product, improves packaging, handling, reduces handling losses during transportation and an overall improvement in the marketing system (Londhe et al., 2013).

Very few mango growers in the country are GAP accredited and the majority of these growers practice manual grading. Mostly, it is at the trader-wholesaler or exporters who practice grading. Briones et al. (2013) noted that along the marketing channels for the mango value chain, mango growers sell directly to an exporter because of the relatively higher price but the most prevalent route was through a contract buyer then mangoes passes through either a wholesaler or wholesaler-retailer until the product reached the retailer or the exporter. Meanwhile, the widespread practice of "all in pricing" wherein domestic and export grades mangoes are marketed under a single price indirectly affects the average price along the chain. Mango growers should opt for classified pricing when marketing their produce wherein mango prices are sorted for export and local grades to increase their unit revenue.

The Philippine mango exports face strict quality requirements and cautious adherence to quality and size provisions by importing countries and have to comply with the international market (Altmera et al., 2007). However, like in most developing countries, grading of fruits like mango is usually done manually using human eye judgment and perception. This practice is time-consuming, labor-intensive and very costly and not standardized. From their research works, Rehkugelr and Throop (1976) stated that a manual sorter was able to remove bruised apples from sound fruit with acceptable sorting efficiencies at a rate of approximately one fruit per second per inspector. Similarly, Stephenson (1976) showed that rates for sorting tomatoes into immature and mature lots did not exceed one fruit per second per inspector. A slightly faster rate, 1.2 fruits per second, was identified as the maximum rate for an inspector to reject 72% of serious defects in oranges. Furthermore, a personal interview with Arenas (2016); a mango trader, processor and was an exporter of fresh mango from Pangasinan, validated this manual sorting rate of trained and experienced workers. From the data given, an average manual sorter has a sorting capacity of 0.8 to 1.0 fruit per second.

The inherent variability in the visual appearance of fruit and its quality-determining features is often challenging in sorting and grading. Quality perception

varies from person to person hence, the non-uniformity of the graded product in the manual method. Also, manual grading is subjective and inefficient because visual inspection might be affected by the individual's health and psychological condition, light in the working area, fatigue and so on (Shahir, 2009; Gao, 2014). Amores (2015), president of Hilas Marketing Corporation, a leading Philippine exporter of fresh mangoes, also expressed the need for automation in their manual sorting operation. Slow, tedious and lack of human labor to meet their required volume were the reasons given. These findings demonstrated the shortfalls of manual inspection and re-enforced the need for a more consistent grading system.

To address the shortfalls of manual sorting and grading, classification has changed from humans to automatic weight-based and size grading machines for fruits and vegetables such as apples, oranges and mangoes (Ganiron Jr. 2014). Computer vision technology has also been explored and becomes more potential and important in addressing the problems in manual sorting and strict demands of the international market for quality agricultural products.

For mango, computer vision systems have been developed for grading applications. Nandi et al. (2014) explored the computer vision system for mango fruit grading while monitoring of color changes of mango color peel using computer vision applications was done by Nagel et al. (undated). A preliminary investigation on the use of a simple computer vision system for sorting mango size, conducted by Altamera et al. (2007), also yielded promising results. These initial researches resulted in commercially available automatic sorting and grading machines. While the international market offers these cutting-edge technologies on sorting and grading and may benefit the Philippine mango industry, prohibitive costs prevent our local exporters from acquiring such technologies. Online costs of a size-based classification sorting machines were estimated at the range of PhP 300,000 to PhP 2,000,000.00 while the more sophisticated CVS-based fruit sorters can cost as high as P 5,000,000.00, with a sorting capacity of 0.5 tons to 5 tons per hour.

This project thus proposed the development of a less expensive computer vision system sorting and grading machine for the mango that will address the subjectivity and slow process of manual fruit sorting and grading specifically, mango.

OBJECTIVES

Generally, the project aimed to develop a computer vision system (CVS) mango quality sorting and grading machine at the exporters level of operation.

Specifically, the project aimed to *(1)* determine the technical requirements of mango quality sorting machine, as well as the socio-economic issues in the adoption of the proposed machine; *(2)* come-up with a laboratory set-up computer vision system based mango sorting and grading that, will establish the technical

requirements needed in the development of the prototype unit computer vision system mango quality sorting and grading; and *(3)* assess the technical viability of the computer vision system-based pilot-scale mango quality sorting and grading machine.

MATERIALS AND METHODS

Establishment of a laboratory imaging system for mango sizing and textural characteristics

Phase 1 of the project aimed to establish a laboratory set-up to characterize individual mango samples based on weight, size, shape and external bruises. Initial technical requirements and sorting parameters were established and resulted in the fabrication of laboratory unit CVS for fresh mango.

The laboratory set-up (**Figure 1)** consisted of two main components: an imaging chamber and a programming component provided by RoboRealm (**Figure 2**). The imaging chamber facilitates image acquisition of fresh mango fruits. It is composed of three (3) units high-definition cameras; two (2) units modulated LED lights and semi-automated mango turning assembly which exposes the mango surfaces into three different angles. The RoboRealm software expedites image processing and statistical correlations.

Development of prototype unit mango sorting machine and grading

In 2017, Philmech attempted to explore computer imaging and machine vision to address the problems associated with the current practices of mango sorting in the country. *Figure 3* shows the initial prototype unit CVS-based mango sorting machine installed at PHilMech. It was aimed at sorting green mango samples in two stages; selected external defects and size classification.

The system used a single-board raspberry pi microcontroller where USB ports are attached to the camera, keyboard, mouse and monitor. *Python* programming and modules are used for the entire sorting process.

Description of the System

The hardware of the CVS – based mango sorting machine primarily consisted of a motor-driven belt conveyor, imaging chamber and classification bins. It was also provided with a brushing mechanism to wipe off dust and dirt before it entered the imaging chamber. The imaging chamber was covered and placed between the brushing area and sorting unit to factor out the shading effect. Autofocus, 1080p/30 frames per second camera, is mounted on the center of the imaging chamber to capture rotating mango samples videos. Two-6000K daylight surface-mount device light-emitting diode module (SMD-LED) lamps provide the necessary lighting

intensity. Pneumatic actuators were used to clean and direct the mango samples to trigger transport to the imaging chamber. Actuators were also used to direct mango fruits to its respective size classification bins. Time delays were programmed for the brushing process, during image capturing and processing. Initially, a single mango fruit can be sorted in five (5) seconds, but this could be increased and targeted to be competitive to existing mechanical sorters. An Arduino Mega was provided to run the actuators.

Figure 4 shows the laboratory unit of the CVS-based mango sorting machine initially installed and tested at the PHilMech laboratory. Green mango samples used for training the system in predicting external defects are pre-sorted and were sourced from different mango producing areas specifically, Davao, Cebu, Pangasinan, Zambales and Nueva Ecija. A total of 2,314 mango fruits of varied sizes and physical defects were trained.

Image processing module

The process flow of the system is detailed in *Figures 5a* and *5b*. The system adopted a two-stage sorting method for physical quality and size classification using image classification models. The grading system started with live video capture of individual mango fruits, rotating and fed manually through the conveyor. The mango fruits were pre-sorted by trained classifiers. They were classified either bad or good quality based on pre-harvest and transport damages like bruises, latex stains and mechanical damage as defined by the Philippine National Standard/Bureau of Agricultural and Fishery Product Standards (PNS/BAFPS, 2004). The system was programmed to count the number of good and bad quality mangoes based on given conditions and tolerances provided (CODEX, 2005). Bad quality mangoes are labeled as "Rejected" fruits and were ejected to the specific bin for other purposes while good mango fruits were labeled as "Accepted" and conveyed for 2nd stage processing.

The second and final stage of sorting is based on size (weight) classification as calibrated with the mango fruit's geometric characteristics, in pixels. Measurements in pixels were then converted into volume computed to weight equivalent. As shown in *Figure 6*, the video captured images that underwent pre-processing to convert the red, green and blue (RGB) color space into hue, saturation values (HSV) color space to separate the background from the real mango images. A grayscale image was then constructed. After pre-processing, the estimated volume of mango is determined by the sum of the volume of 10 transverse cuts along the length of the mango (*Figure 7*). The analysis was derived from computing the semi-axes *a* and *b* at different points along the length of the mango and relationship between the values of the semi-axes called Depth Factor (DF). This method was adopted from the works of Bermudez et al. (2013).

RESULTS AND DISCUSSION

Existing mango sorting practices

All of the mango stakeholders used manual sorting of mangoes based on size and quality, except one consolidator-processor-exporter from Manila. Respondents who used manual sorting in sorting-grading mangoes reported that even experienced labor-sorter sometimes failed in their task and resulted in numerous market rejects.

At the farm level, sorting was done by separating the marketable mangoes from an unmarketable/defective one. Real grading and sorting were done off-farm which consider size, weight and quality (color and skin condition of mangoes). It was the consolidator-trader-exporters who were knowledgeable about the size and quality requirements of the importing countries. Thus, growers and grower-consolidators were left with sorting the rejects from marketable mangoes prior to marketing. At the market place, mangoes were given an all-in price. Then trader-exporters sorted the mangoes by size, weight and quality and sold for different prices.

Japan markets were more discriminating than other foreign markets with quality and acceptable chemical residue. Japan also preferred mangoes with medium size. On the other hand, Korea prefers medium and bigger sized mangoes while Hongkong prefers small to medium-sized mangoes. The sizes reported by the respondents were the following; Extra Large (350g and up); Large (301-350)g; Medium (252-300g); small (201-250g); Super small (165-200g). Mostly, mango exporters follow the CODEX international.

Problems cited with manual sorting were the following:

1. No standard size followed at the local market. During peak season of harvest, the large-sized mangoes become medium-sized, while the medium-sized mangoes become large-sized during lean months.
2. Sorter-graders are subjective in grading the quality of mangoes.
3. Buyers sometimes tricked/cheated the sellers in terms of size, weight and quality.

Among the 15 respondents, six (40%) cited that they were not interested in the CVS mango sorter-grader because they have only a small volume of mangoes handled and there are still available laborers for sorting. The remaining 60% were interested in CVS mango sorter-grader provided that the following will be considered in the equipment design.

1. The CVS should consider the size, color, weight and physical defects of mangoes
2. It must be fast and accurate.

3. With cleaning features (soft brush) for latex.
4. Spare parts of the CVS should be locally available
5. Test which parts are easily worn out or need replacements
6. Should include VHT and floatation
7. The CVS should have a selector on grades and standards for different importing countries such as Japan, Hongkong, Vietnam, and other potential exporting countries
8. The CVS should include in its feature to identify the insect infestation (fruit fly) and internal breakdown (*bugbog*).

The average volume handled by consolidator-exporters ranged from 200 tons to 600 tons per month. The lone exporter with a mechanical sorter reported a sorting capacity of 5 tons/hr. One high-end exporter who did not want to be interviewed reported that their new mechanical sorter-grader could sort about one fruit per second, but the price was more than half a million.

Meanwhile, manual sorting capacity was reported at 260-500 kg/day, depending on the quality of mangoes. Manual sorting-grading fee reported ranged from Php 0.70/kg to Php1.44/kg.

Performance Evaluation of the prototype unit CVS-based mango sorter

Initial testing was conducted to assess the performance of the developed technology. Table 1 below presented the prototype unit CVS-based mango sorter's initial performance in predicting the pre-sorted mango samples based on mango's external defects. The test was conducted for a total of 370 and 617 for good and rejected mango fruits, respectively, pre-selected by trained classifiers. For good mangoes, 14 was erroneously classified to be rejected or 3.78% error was estimated. On the other hand, a 100% accuracy prediction was observed for rejected mango samples. Both findings were an indication of an acceptable sorting error based on the 10% maximum error tolerance per pack of any size (CODEX, 2005).

Figure 5 shows the calibration tests conducted between actual weights and volume (in pixels) of mango samples. A calibration model was established with a relatively high correlation coefficient (R^2) of 0.9204 and a relatively low standard error of estimate (SEE) at 0.538 which indicated adequacy and fitness of the system.

Furthermore, initial validation tests conducted between actual weights and predicted weights of 28 mango fruits using the laboratory set-up CVS-based mango sorting machine is shown in *Figure 6*. Results obtained from the tests revealed a relatively high coefficient of determination (R^2), computed at 0.9913 and mean square error of 3.66% which indicated the technical feasibility of the developed system.

CONCLUSION AND RECOMMENDATIONS

Results of the project revealed that all mango stakeholders are doing manual mango sorting based on size and quality, except one consolidator-processor-exporter from Manila. Respondents who used manual sorting reported that even experienced labor-sorter sometimes failed in their task and resulted in numerous market rejects. It was also found out that no standard size followed at the local market.

The developed CVS-based mango sorting machine is aimed to sort and grade green mangoes in two stages; physical defects and weight classification. Initial testing conducted to assess the performance of the initial prototype unit CVS-based mango sorting machine revealed that the technology has an accuracy of 98.58% or an estimated error of 1.42 % in classifying green "Carabao" mangoes. These findings were an indication of acceptable performance based on the 10% maximum error tolerance per pack of any size, set by the Codex Alimentarius International Food Standards (CODEX). Also, initial validation tests conducted between actual weights and predicted weights using the laboratory set-up CVS-based mango sorting machine generated a relatively high coefficient of determination (R^2) at 0.99 and mean square error of 3.66% which is an indication of the technical feasibility of the developed system. To validate its initial performance, the developed system is recommended to undergo field testing.

REFERENCES

Altamera M.R.L. and T.G. Aguinaldo. 2007. Preliminary Study on Mango (Mangifera indica L.) Fruit Grading Using Digital Image Technology. In: Agricultural Mechanization Bulletin. January to June 2007 Issue. Volume XIV No 1.

Arakeri M.P and Lakshama. 2016. Computer Vision Based Fruit Grading System for Quality Evaluation of Tomato in Agriculture Industry. In: 7th International Conference on Communication, Computing and Visualization 2016. Procedia Computer Science 79.

Bermúdez A.M., D. Padilla, G. Torres. 2013. Image analysis for automatic feature estimation of the Mangifera indica fruit. Ingeniería y Desarrollo. Universidad del Norte, Columbia. Vol. 31 n.° 1: 84-104.

CODEX STAN 184. Amended. 2005. Standard for Mangoes. Codex General Standard for the Labelling of Prepackaged Foods.

Espino R.R.C. and M.C. Rafael. 2014. The Status of the Fruit Industry in the Philippines. Accessed at www.agnet.org/library.php? func=view&style=type&id= 20150810090507.

Gao H., J. Cai and X. Liu. 2014. Automatic Grading of the Post Harvest Fruit: A Review. Accessed athttps://hal.inria.fr/hal-0160507

Ganiron Jr. T.U. 2014. Size Properties of Mangoes using Image Analysis. In: International Journal of Bio-Science and Bio-Technology Vol.6, No.2, pp.31-42

Londhe D., S. Nalawade, G. Pawar, V. Atkari and S. Wandkar. 2013. Grader: A review of different methods of grading for fruits and vegetables. In: Proceedings of the Agricultural Engineering Institute: CIGR Journal

Nagle S. J., K. Intani, G. Muller, B. Mahayothee, V. Sarsud and J. Muller. 2016. Determination of surface color of 'all yellow' mango cultivars using computer vision. In: International Journal of Agricultural and Biological Engineering. Vol. 9 No.1.

Nandi S.C., B. Tudu, and C. Koley. 2014. Computer vision based mango fruit sorting system. In: Proceedings of the International conference on Innovative Engineering Technologies (ICIET'2014) Dec. 28-29, 2014 Bangkok, Thailand.

Philippine Statistics Agency (PSA). 2014. Accessed at http:// www.countrystat.psa.gov.ph

PNS/BAFPS 13:2004. Philippine National Standard. Fresh Fruits – Mangoes. Department of Trade and industry.

Rehkugler G.E. and J.A. Throop. 1976. Optical-mechanical bruised apple sorters. PP. 185-188, 192. In: J.J. Gaffney(ed). Quality Detection in Foods. ASAE. St. Joseph, MI.

Shahir S. 2009. Performance evaluation of divergent roller grader for selected vegetables. Agricultural mechanization in Asia, Africa and Latin America. Vol. 20 No. 460. Accessed at http://www.academia.edu/3457548; Performance Evaluation of a Divergent Roller Grader for selected vegetables.

Sivakuma D, Y. Jiang and E.M. Yhia. 2010. Maintaining mango (Mangifera indica L.) fruit quality during the export chain. Food research International. Vol. 44 (2011) 1254-1263. Accessed at www. Elsevier.com/locate/foodres.

Stephenson K.Q. 1976. Color sorting system for tomatoes. ASAE. PP. 199-201.

U.S. Department of Agriculture. 1996. Agricultural Marketing Service, Fruit and Vegetable Division, FPB, General Market Inspection instructions, Washington, DC, July 1966.

Table 1. Confusion matrix for rejected and good mango samples using the developed CVS-based mango sorting machine

		Predicted Classification (count)		Accuracy (%)
		Reject	**Good**	
Actual Classification (count)	**Reject**	617 (TP)	0 (FN)	**98.58**
	Good	14 (FP)	356 (TN)	

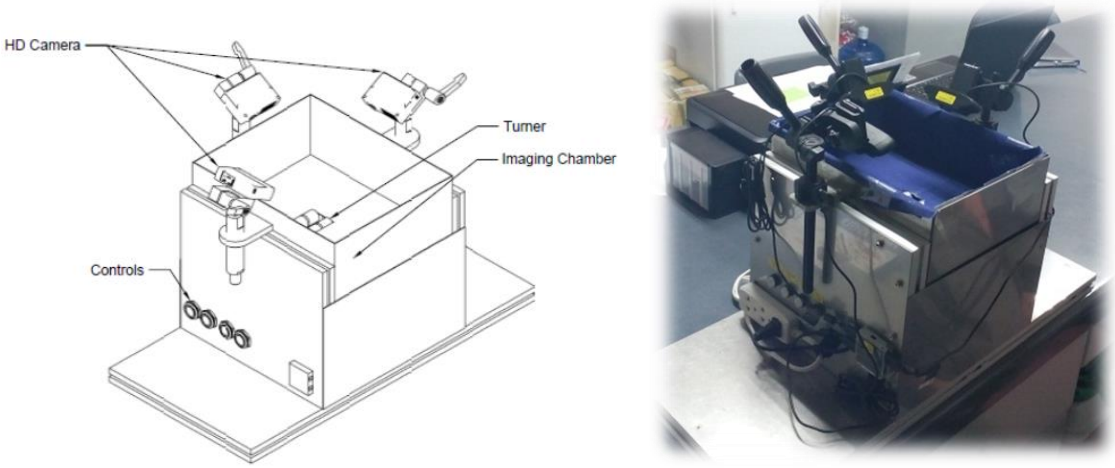

Figure 1. CAD-generated drawing and actual laboratory set-up of CVS mango sorting system

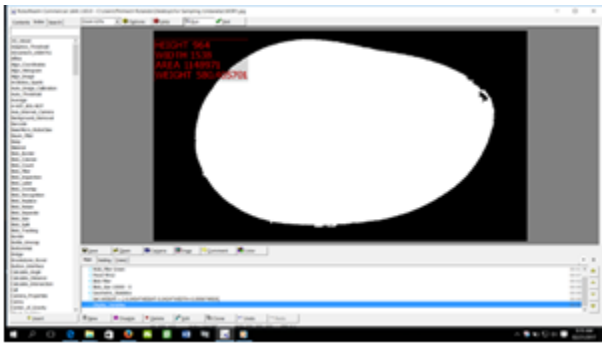

Figure 2. Screenshot of image processing and analysis software

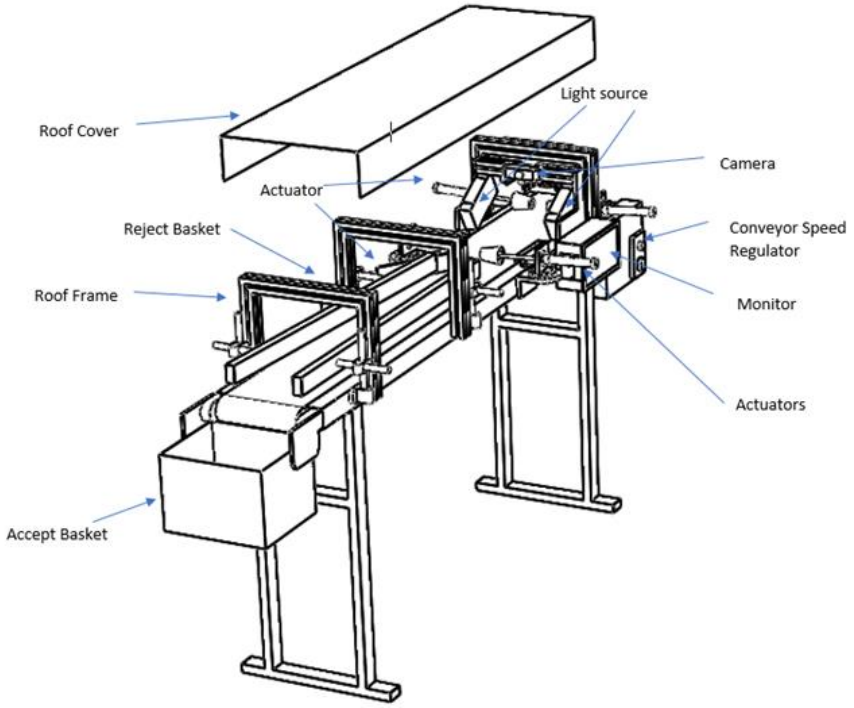

Figure 3. Initial prototype unit CVS-based mango sorting machine

Figure 4. Actual set-up and testing of the CVS-based mango sorting machine

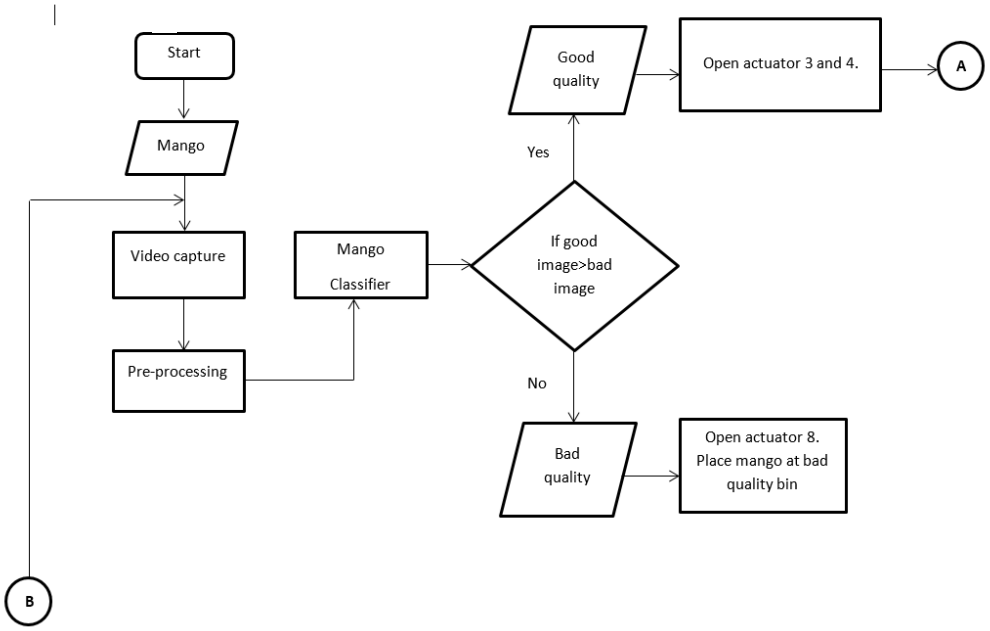

Figure 5a. Process flow of initial sorting and classification of mango fruit using the developed CVS-based mango sorting machine

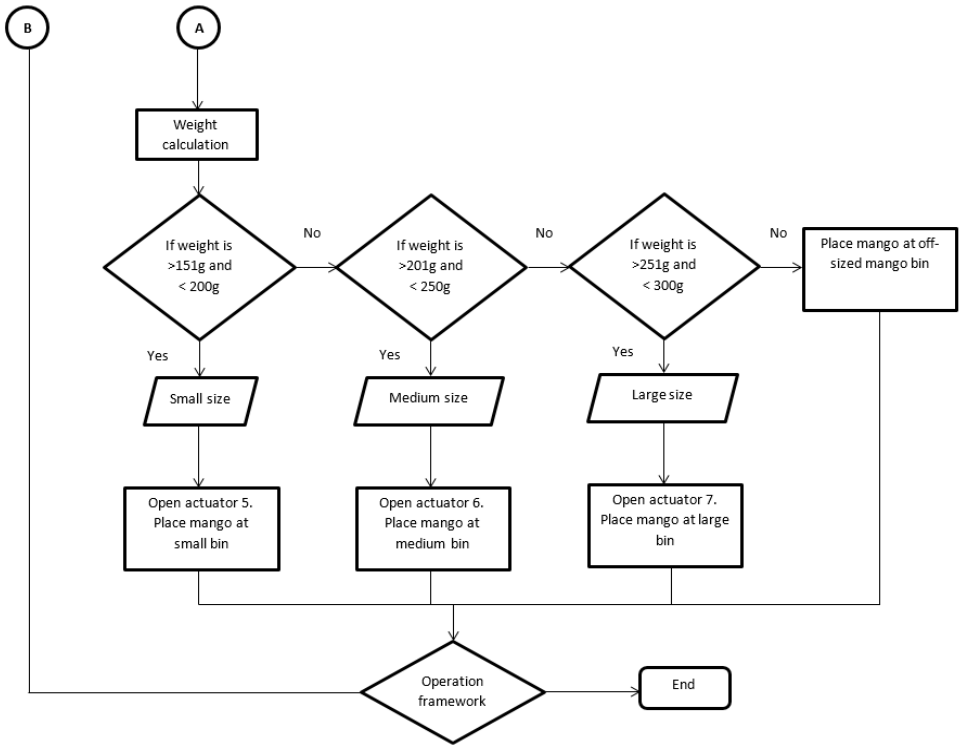

Figure 5b. Process flow of 2nd stage mango sorting using the developed CVS-based mango sorting machine

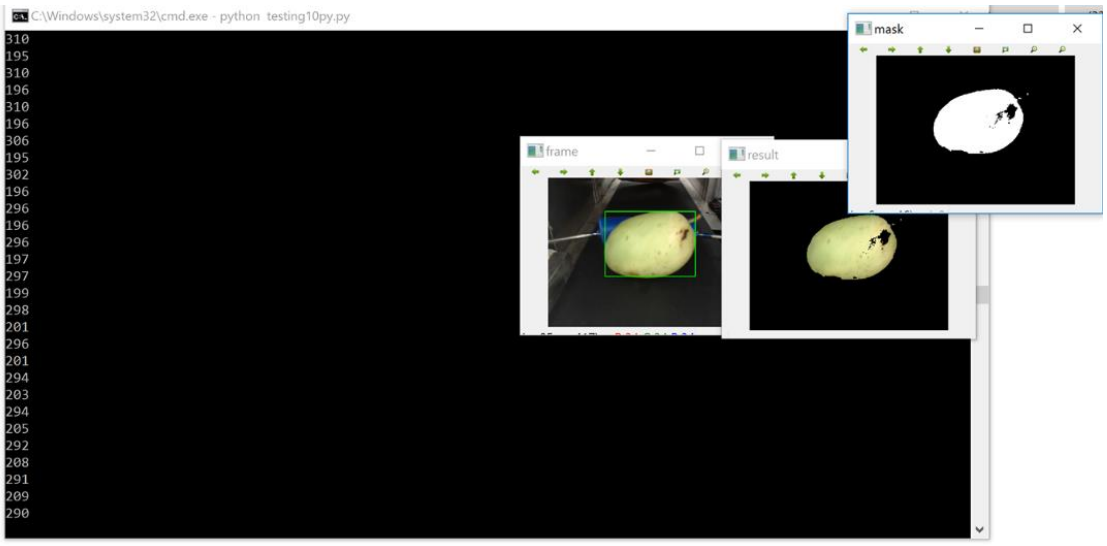

Figure 6. Screenshot of mango fruit image processing using the CVS-based mango sorting machine

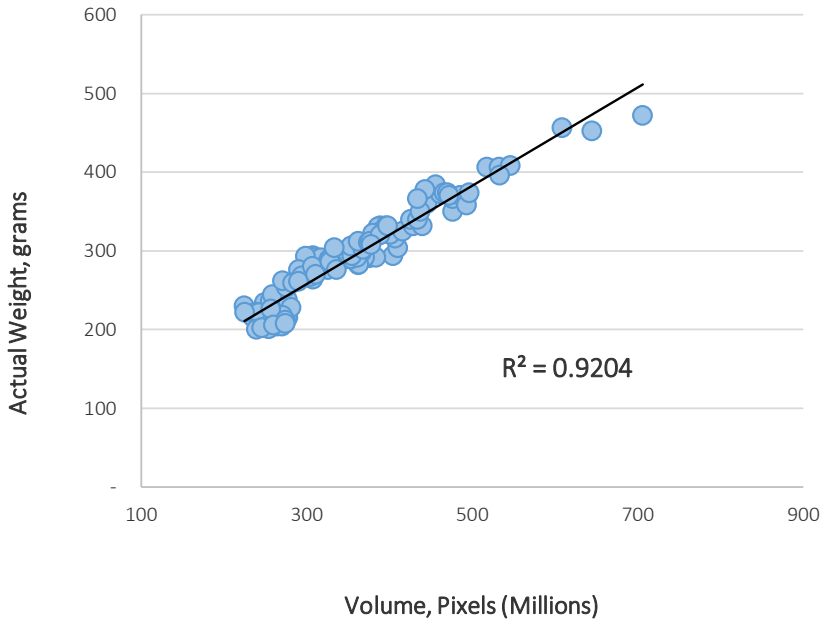

Figure 7. Calibration data generated between actual weight and volume of mango using the Initial prototype unit CVS-based mango sorting machine

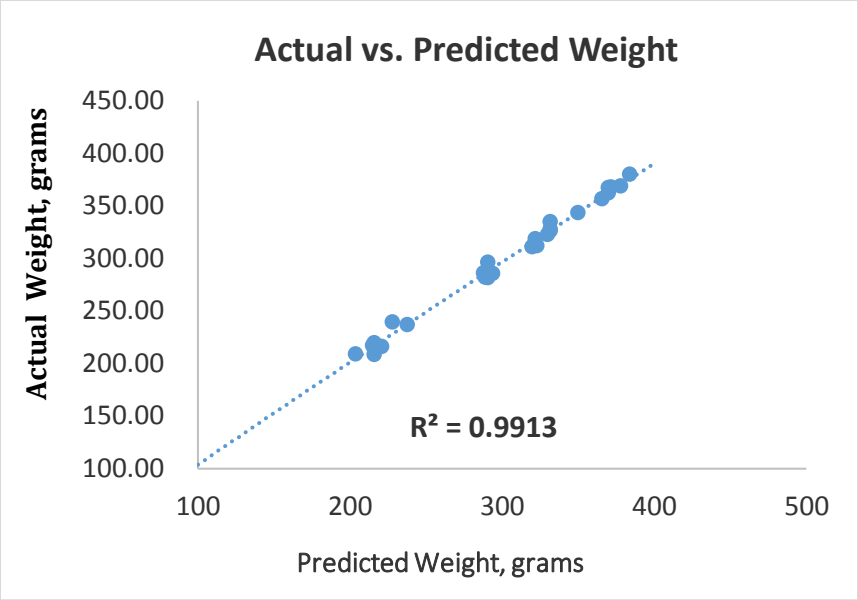

Figure 8. Validation data generated between actual and predicted weights of the laboratory set-up CVS-based mango sorting machine.

DEVELOPMENT OF AN ELECTRIC HAND TRACTOR (e-TRACTOR) FOR TRANSPORT

Rossana Marie C. Amongo[1], Erwin P. Quilloy[1],
Mark Angelo F. Ranches[1], Maria Victoria L. Larona[2] and Marish S. Madlangayan[3]

[1]Agricultural Machinery Division, Institute of Agricultural Engineering
[2]Center for Agri-Fisheries and Biosystems Engineering
[3]Associate Professor, Department of Civil Engineering
College of Engineering and Agro-industrial Technology
University of the Philippines Los Baños
College, Laguna, Philippines 4031

ABSTRACT

The study aims to develop an e-Tractor for the transport of agricultural products. A Needs and Design Assessment (NADA) of the intended beneficiary was initially conducted to match their needs. A loading requirement of 200 kg was obtained from NADA which was the basis for the e-Tractor design comprising of a 3-kW DC electric motor as the prime mover, a 5.76 kWh battery system as the power source, a hand tractor with automobile differential as transmission system and a trailer as the load carrier component. Initial tests showed that the system could be charged for 240 minutes using a 15-ampere charger and operate for around 115 minutes. The e-Tractor with three-speed settings: low (2 kph), medium (5 kph), high (7 kph) was tested against three loadings (0 kg, 200 kg, 400 kg) to optimize its performance. The e-Tractor can operate continuously for a maximum of 300 minutes at two kph (no load) and a minimum of 72 minutes at seven kph (400 kg). The maximum distance traveled was 21.53 km at seven kph (no load) and a minimum distance of 6.11 km at seven kph (400 kg). The obtained optimum speed of 7 kph and a load of 287.8 kg will result in an operational time of 127.5 minutes and distance traveled of 14.33 km. The potential of an operational e-Tractor for transport can move agricultural products faster to lessen spoilage contributing to food security and a healthier environment having no detrimental gas emissions from the machine.

Keywords*: electric hand tractor, e-Tractor, e-Tractor* speed, *agricultural product loading*

INTRODUCTION

In recent years, the promotion and utilization of agricultural mechanization technologies (AMTs) have been purposively implemented by the government and by different stakeholders in the food value chain to propel agricultural production. With the advancement of technology, most of the Research and Development

Institutions (RDIs) and Higher Education Institutions (HEIs) involved in the country's agricultural sector have been focusing on innovative technologies to cope with the demand of the ever-growing population.

Among the AMTs widely adopted and utilized in the agricultural production systems is the hand tractor or two-wheel tractor powered by small internal combustion engines. It is a single-axle machine powered by a three hp to 15 hp small internal combustion engine. It is commonly utilized for land preparation, planting, cultivating, harvesting, and transport. Amongo et al., (2011) revealed that among the farmer-operator of hand tractors in Laguna, Philippines, 68% used the machine for land preparation operation while the other 32% incorporates weeding and/or hauling and transport.

Hand tractors can be classified as either traction or pull-type, rotary type, or general-purpose type. The traction type hand tractor has a drawbar which provides a pulling power for implements. Rotary type tractors make use of rotating blades to cut through and pulverize the soil. General-purpose type, on the other hand, makes use of both the draw bar for traction and the power take-off (PTO) shaft for doing rotary work. The power from the engine on these hand tractors is transferred to the wheels or the PTO shaft through the transmission system which can be in the form of belt and pulleys assembly, chain and sprockets, gears or direct drive (Resurreccion, 2006).

The hand tractor becomes necessary machinery in today's agriculture. Its utilization primed with gasoline and diesel engines dominate the mobile operations in the agricultural production systems. However, its utilization has become more and more expensive because of the rising costs of fossil fuels. Moreover, the use of small internal combustion engines has been contributing to gas emissions polluting the air and the environment. To address these problems, researchers have focused on utilizing renewable energy or green energy as an alternative source of power on the farm.

This study focuses on developing an innovative technology utilizing green energy to power hand tractors intended for the mobility of agricultural products while also preventing the emission of harmful gasses that contribute to the pollution and degradation of the environment. The development of the electric hand tractor (e-Tractor) is seen as an innovative substitute for the conventional hand tractor which utilizes internal combustion engines. It uses an electric motor as a prime mover and a battery system as the power source. The use of electric motors is perceived for stationary operations in the agricultural production systems. Hence, this innovation will serve as a starting point for the use of electric motors for mobile applications in Philippine agriculture.

OBJECTIVES

The main objective of the study is to develop an electric hand tractor (e-Tractor) for transport. Specifically, it aims to:

a. establish the design parameters for the e-Tractor through the conduct of Needs and Design Assessment (NADA) of the intended beneficiaries;
b. design and fabricate an e-Tractor for transport and mobility of agricultural products;
c. evaluate the performance of the designed e-Tractor; and
d. determine the optimum working condition (speed [kph] and load [kg] settings) of the e-Tractor for transport.

MATERIALS AND METHODS

The development of the e-Tractor is part of the Green Spark Project for un-energized communities implemented through the collaboration of the Institute of Agricultural Engineering and the Civil Engineering Department of UP Los Baños and funded by the National Grid Corporation of the Philippines (NGCP).

Conduct of Needs and Design Assessment (NADA)

The Green Spark project site identified by NGCP is in Brgy. Macabud, Rodriguez, Rizal where the Needs and Design Assessment (NADA) was conducted. The project site is an agricultural-based area with no supply of electricity from the grid of NGCP. A questionnaire was crafted based on the needs of the intended beneficiaries on the utilization of hand tractor for agricultural applications. A total of 70 respondents were identified for the NADA survey taken from stratified random sampling calculated using equation 1:

$$ssf = \frac{sso}{1+\frac{sso-1}{pop}} \; ; \quad sso = \frac{z^2(P)(1-P)}{(C.I.)^2} \quad \text{(Equation 1)}$$

Where:

ssf is the sample size for finite population
sso is the sample size for considerably infinite population
pop is the population number

z is the z-value for a given confidence level (2.576 for 99% C.L.)
C.I. is the confidence interval
z is the z-value for a given confidence level (2.576 for 99% C.L.)
P is the percentage (0-1)

Design and Fabrication of the e-Tractor

Using the data obtained from the NADA, the e-Tractor was designed using computer-aided design software, AutoCAD ®. The main design consideration is the type and load of agricultural product to be transported. The prime mover power rating was based on the conventional small hand tractor primed with the small internal combustion engine and was computed using equation 2:

$$Motor\ Power = \left(\frac{2}{3}\right)\ x\ (Internal\ Combustion\ Engine\ Power) \quad \text{(Equation 2)}$$

The e-Tractor was fabricated at the Engineering Shop, College of Engineering and Agro-Industrial Technology, University of the Philippines Los Baños, Laguna. The fabrication materials were acquired from local suppliers while the electric motor components were imported from foreign suppliers.

Testing of e-Tractor

The e-Tractor was tested using three different speed and load settings as independent variables with distance and duration of travel as dependent or response variables. The test was conducted at the Pili Drive, College of Engineering and Agro-Industrial Technology, University of the Philippines Los Baños, Los Baños, Laguna. The speed of the e-Tractor varied from 2 kph (low), 5 kph (medium), and 7 kph (high). The load was varied from 0 kg, 200 kg, and 400 kg. A total of nine (9) trials was done for different speed and load settings.

Data Analysis

The data obtained from the test were analyzed using Design Expert 11. The optimum speed and load settings were determined by maximizing the distance and time of travel for the e-Tractor.

RESULTS AND DISCUSSION

Needs and Design Assessment (NADA)

At the start of project implementation, NADA was first conducted at Brgy. Macabud, Rodriguez, Rizal. Residents from the four sitios of the barangay (Proper I, Proper II, Udiongan, and Calumpit) served as the sampling population. A total of 70 respondents were interviewed for the survey. They were randomly selected and identified from the sampling population of the four sitios. The distribution of respondents was based on the population ratio for each sitio.

From the NADA, the project site is an agricultural-based community since 39% of the respondents were farmers and others were housewives (23%), laborers/skilled workers (11%), entrepreneurs (11%), government officials or employees (9%), while the rest had

no occupation (3%) as presented in Figure 1. The data indicates that agriculture plays a vital role for the whole community. Food crops such as rice, banana, cassava, and corn comprise 50% of the main crops planted in the area as presented in Figure 2. Other respondents do not have main crops while 10% had horticultural crops.

With regard to the availability of tractors in the area, the residents are not new in the use of agricultural machines. About 40% of the respondents noted that both two-wheel (2W) and four-wheel tractors (4W) are servicing the agricultural production area, 17% for 4W tractors, and 9% for 2W tractors (Figure 3). The rest of the respondents (34%) noted that they are not being serviced with any tractors. The availability of hand tractors in the area is an indication of its acceptability and that the residents are familiar with its utilization. The success of the introduction of new technology into a community is based on the acceptability of the intended end-users. The tractors in the area are used for land preparation, cultivation, and hauling/transport.

The introduction of the e-Tractor to the intended users in the project area gave an initial positive response. They responded that the machine can be used for hauling of agricultural products particularly from the remote farm areas or for human transport and may even be utilized for farming operations especially for land preparation (plowing) operation. Figure 4 shows the willingness of the respondents to use the e-Tractor for transport purposes. Thirteen percent of the residents strongly agreed to use the e-Tractor for transport and 24% agreed to do so. 7% said that they may or may not use the e-Tractor while 16% were unwilling. A total of 40% of the respondents were undecided. Those who agreed on using the e-Tractor for transport noted the weight of the products they wanted to load. The respondents agreed to use the e-Tractor for hauling of agricultural products such as rice (200 kg), cassava (200 to 500 kg), banana (40 kg, 300 kg, and 1000 kg), and other vegetables (ranging from 20 to 500 kg). Out of those who would use the e-Tractor for hauling, 56.25% had loads of at most 200 kg while 43.75% had loads of more than 300 kg. It is then necessary to design the e-Tractor to accommodate a minimum load of 200 kg.

Design and Fabrication of the e-Tractor

Figure 5 shows the rendered design using AutoCad ®. Table 1 shows the specifications of the e-Tractor. It has three main components namely the hand tractor, the prime mover and trailer as the load carrier. The trailer is designed based on the Philippine Agricultural Engineering Standards (PAES) 136:2004 or the Agricultural Trailer Specifications. The overall length of the trailer is 3120 mm while the overall width is 1470 mm. The overall platform dimension is 860 mm by 1680 mm. The height of the seats is 0.3 m and the backrest for the passengers is 0.23 m. The backrest can be dropped down while the rear cover is completely removable for easier loading of products. Like in common hand tractor trailers in the Philippines, the driver's seat also serves as a tool box. The trailer also has a roof which makes it possible to accommodate passengers especially during rainy seasons.

The e-Tractor's prime mover was matched based on the conventional hand tractors used in the Philippines. A small hand tractor has at least a 5-hp gasoline engine equivalent to 3.73 kW. An electric motor can produce a delivery rating of about 2/3 of the power of a small internal combustion engine. A 3.73 kW internal combustion engine is then as efficient as an electric motor with a power of 2.4867 kW or 2.5 kW power. Hence, the hand tractor was matched with a 3kW electric motor to compensate for the transmission and other losses. The wiring of the electrical components of the e-Tractor is shown in Figure 6. The electric motor was connected to the motor controller which commands voltage and current drawn from the battery system. The battery system is composed of four 12-V, 120-Ah sealed lead acid batteries connected in a series configuration. The battery system provides a total power of 5.76 kWh, but only 50% of this power was utilized to lengthen the useful life of the battery systems. The motor controller can change the motor speed through the speed controller lever. The operator can directly manipulate the speed control lever to the desired e-Tractor speed.

The transmission system of the e-Tractor was adopted from the original design of the UPLB Hand Tractor with Steering clutch Mechanism (Amongo et al., 2017) as presented in Figure 7. This design utilizes a surplus automotive differential. Two differentials were used as a transmission system for the e-Tractor where the upper differential was oriented vertically with respect to the ground and is connected to the belt and pulley transmission system powered by the electric motor. The lower differential connected to the vertically positioned differential was horizontally aligned serving as the axle of the wheels that provide traction. The upper and lower differentials are connected such that the speed ratio from the electric motor is reduced by 47 times with respect to the wheel speed. Simple costings on the fabrication of the e-Tractor including the trailer incurred a total cost of around Php 178,181.72. The fabricated e-Tractor with a trailer is presented in Figure 8.

Data Analysis

Testing the e-Tractor was done at the Pili Drive, University of the Philippines Los Baños, Laguna. A total of nine (9) runs was done where different speed and load settings were considered. Table 2 shows the results of the e-Tractor test. The e-Tractor was limited to three main speeds: the low speed at 2 kph, the medium speed at 5 kph, and the high speed at 7 kph. Three settings for the load were used namely no load, 200-kg load, and 400 kg load. Based on the data obtained, different speed and load settings resulted in a varying distance and time of travel. The maximum distance that the e-Tractor can travel is 21.533 km which is attained at 7 kph with no load. Without load, there is a lower current draw which also results in lower power consumption. The minimum distance traveled is 7.475 km recorded at 2 kph with a load of 400 kg. The maximum duration of travel was 299.7 minutes attained at 2 kph with no load. The minimum duration of travel was 73 minutes attained at 7 kph with 400 kg of load.

The data was optimized using Design Expert 11 with speed and load setting as the independent variables and distance and travel time as the responses. The speed was set in range and limited to 2 kph, 5 kph, and 7 kph while the load was set and ranged from 0 to

400 kg. The distance and duration of travel are the response variables that were both maximized to obtain the optimum condition of the performance of the e-Tractor. Three solutions were presented with different desirability as presented in Table 3. In the first solution, the load is 287.793 kg at the speed of 7 kph which will result in 14.326 km distance and 127.519 minutes of operation with the desirability of 0.391. The desirability presented is the combined desirability of the dependent or response variables. For every trial, the expected distance and operation time will occur 39.1% of the time. The second solution has 372.506 kg of load and 5 kph speed. This will result in 11.851 km and 95.353 minutes of operation with the desirability of 0.300. The third solution is a load of 247.891 kg and a speed of 2 kph, resulting in 8.921 km and 196.363 minutes of operation and desirability of 0.204. The first solution has the highest desirability. Figure 9 shows the location of the points obtained in the first solution.

CONCLUSION

An electric hand tractor (e-Tractor) was designed and developed to increase agricultural products' mobility in a community. The Needs and Design Assessment was conducted at Brgy. Macabud, Rodriguez, Rizal, which is an agricultural-based community. The majority of the respondents were farmers and food crop production dominate their fields. The residents were familiar with the use of both four-wheel and two-wheel tractors. On the introduction of the e-Tractor, 37% agreed to use the machine for transporting agricultural products. The load requirement based on the study was 200 kg. The e-Tractor was designed using AutoCAD ® where the trailer was based on PAES 136:2004 on the Agricultural Trailer Specifications. The trailer has features such as dropdown backrests and removable rear cover for easier loading of products. It also has a roof as protection during rainy seasons. The prime mover was designed based on the conventional small hand tractors. The e-Tractor was matched with a 3kW electric motor with the equivalent power of an internal combustion engine of 5 hp or 3.73 kW. The 3-kW electric motor is powered by a 5.76-kW sealed lead acid battery system. Only 50% of the battery capacity was utilized to lengthen battery systems' useful life. The transmission system of the e-Tractor is based on the original design of the UPLB Hand Tractor with a steering clutch mechanism. The test for the e-Tractor was conducted with a total of nine (9) runs. The speed settings varied from 2 kph, 5 kph, and 7 kph while the load settings were set at no load, 200 kg load, and 400 kg. The distance and duration of travel were then obtained as response variables. The maximum and minimum distance traveled were 21.5327 km and 7.4754 km, respectively. The maximum and minimum duration of travel was 299.7 minutes and 73 minutes, respectively. The load, distance, and duration of travel were maximized, and the speed was set in range to obtain the optimum solution using Design Expert 11. The solution with the best desirability was a load of 287.793 kg and a speed of 7 kph. In this setting, the resulting travel distance was 14.3256 km and the duration of travel of 127.519 minutes with combined desirability of 39.10%.

The study shows the potential use of electric motor in mobile applications for the agricultural production systems as exemplified in the development of an innovative e-

Tractor. The e-Tractor can be utilized not only for hauling and transport of agricultural products but may also be used in tillage and cultivation operations. It has paved the way for using electric motors as prime mover which counters the notion that electric motors are only good for stationary applications. The use of electric motors could be a potential prime mover for the different farming operations in the agricultural production systems which could enhance farming efficiencies because of the higher delivery ratings compared to fossil-fueled engines. Moreover, the use of the e-Tractor can mitigate further degradation of the environment because of the non-emission of harmful gases as contributed by fossil fuels. The use of green energy as a source of power to charge the battery for the e-Tractor also illustrates the potential applications of the clean and green energy source as alternative power on the farm. With the development of the innovative e-Tractor, this technology could contribute to the modernization of the agriculture and fisheries sector by utilizing a more efficient and environment-friendly technology in the agricultural production systems.

Acknowledgment

The research team acknowledges the National Grid Corporation of the Philippines (NGCP) for funding this study under the project entitled "The UPLB Un-energized Community-Based Sustainable Energy Research Program" where the e-Tractor is a component technology for development. The team is also grateful for the support of the Center for Agri-Fisheries and Biosystems Mechanization (BIOMECH) during the design and fabrication as well as the Agricultural Machinery and Testing Evaluation Center (AMTEC) during the testing of the e-Tractor. Appreciation is also extended to the officials of Brgy. Macabud Rodriguez, Rizal for their receptive acceptance of the Team and the technologies introduced in their community.

REFERENCES

Amongo R.M.C., O.F. Zubia, M.C. Petingco & P.S. Garcia. 2011. Design Improvement of the Local Two-Wheel Tractor using Anthropometry. Poster paper presented during the 61st Philippine Society of Agricultural Engineers (PSAE) Annual Convention, 9th International Conference and Exhibition and the 22nd Agricultural Engineering Week, April 25-29, 2011, Dapitan City, Zamboanga del Norte, Philippines.

Department of Trade and Industry. 2019. Gross Domestic Product (GDP). Retrieved March 25, 2019 from https://www.dti.gov.ph/resources/statistics/gross-domestic-product-gdp#graph

Philippine Agricultural Engineering Standards (PAES) 136:2004. Agricultural Machinery-Agricultural Trailer- Specifications.

Philippine Agricultural Engineering Standards (PAES) 109:2000. Agricultural Machinery-Walking-type Agricultural Tractor-Specifications Part 1: Pull-type.

Resurreccion A.N. 2006. Agricultural Machinery Lecture Notes. Los Baños, Laguna. College of Engineering and Agro-Industrial Technology. University of the Philippines Los Baños, Laguna.

Table 1. Specifications of the e-Tractor.

Item	Specification
Trailer	
Overall length, m	3120
Overall width, m	1470
Overall height (including roof), m	2400
Ground clearance, m	430
Seat height, m	300
Backrest height, m	230
Gross Weight, kg	342.4
Hand Tractor	
Overall length, m	2200
Overall height, m	1625
Overall width, m	900
Ground clearance, m	150
Gross weight, kg	372.2
Prime Mover	
Type	Direct current electric motor
Power, kW	3
Rated rpm, rpm	2500
Power source	Battery
Voltage, V	48
Battery Capacity, Ah	120

Table 2. Results of the test for the e-Tractor.

Run	Load (kg)	Speed (kph)	Distance travelled (km)	Operation time (min)
1	0	2 (Low)	14.186	299.7
2	0	5 (Medium)	9.872	126.0
3	0	7 (High)	21.533	178.0
4	200	2 (Low)	7.511	158.7
5	200	5 (Medium)	9.374	112.3
6	200	7 (High)	21.503	181.4
7	400	2 (Low)	7.475	157.9
8	400	5 (Medium)	12.678	145.7
9	400	7 (High)	8.514	73.0

Table 3. Obtained solutions using Design Expert 11.

Solution	Load (kg)	Speed (kph)	Distance travelled (km)	Length of operation (min)	Desirability
1	287.793	7 (High)	14.326	127.519	0.391
2	372.506	5 (Medium)	11.851	95.353	0.300
3	247.891	2 (Low)	8.921	196.363	0.204

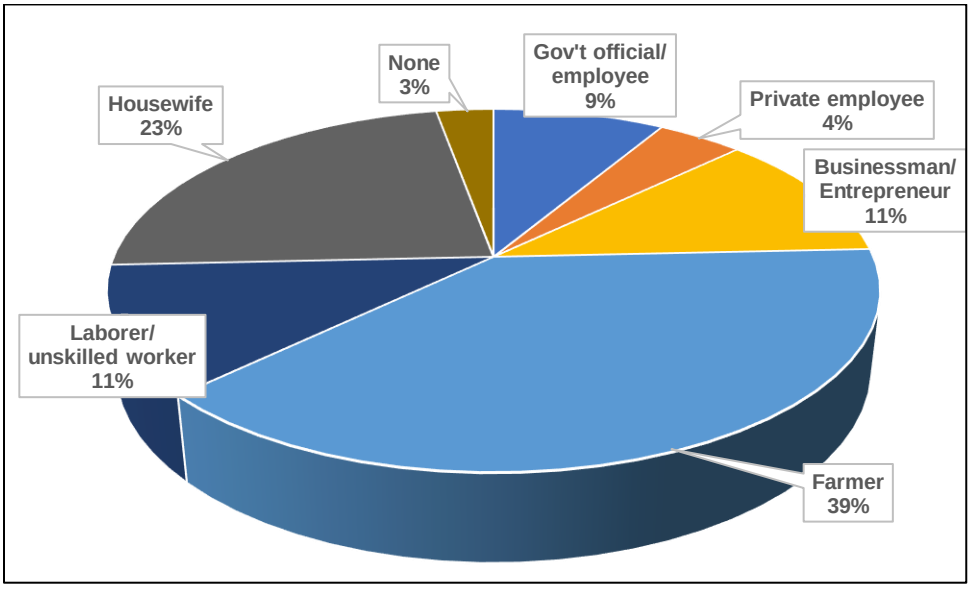

Figure 1. Main occupation of the respondents in Sito Proper I, Propper II, Udiongan, and Calumpit, Brgy. Macabud, Rodriguez, Rizal, October 2018.

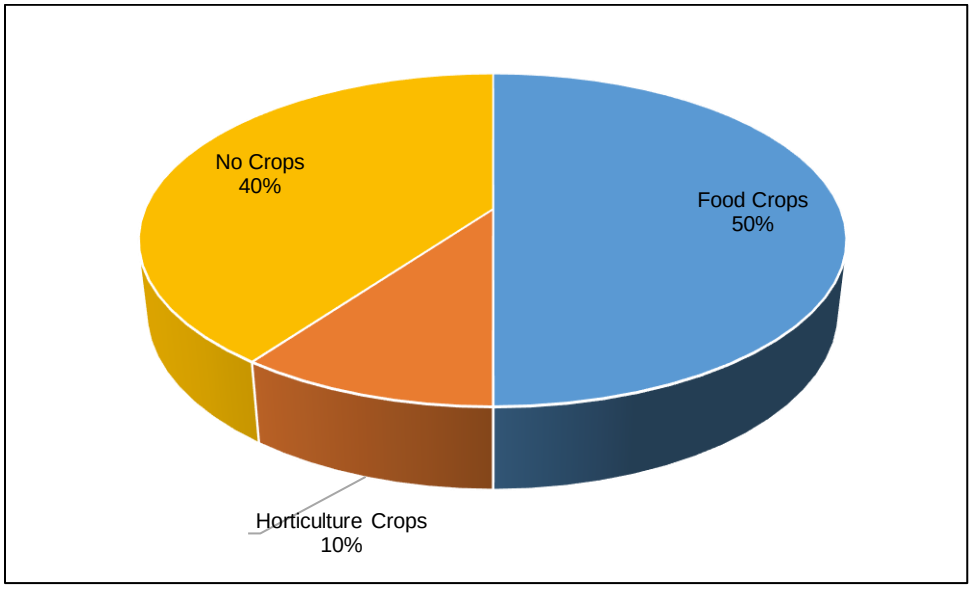

Figure 2. Main crops planted by the respondents in Sitio Proper I, Proper II, Udiongan, and Calumpit, Brgy. Macabud, Rodriguez, Rizal, October 2018.

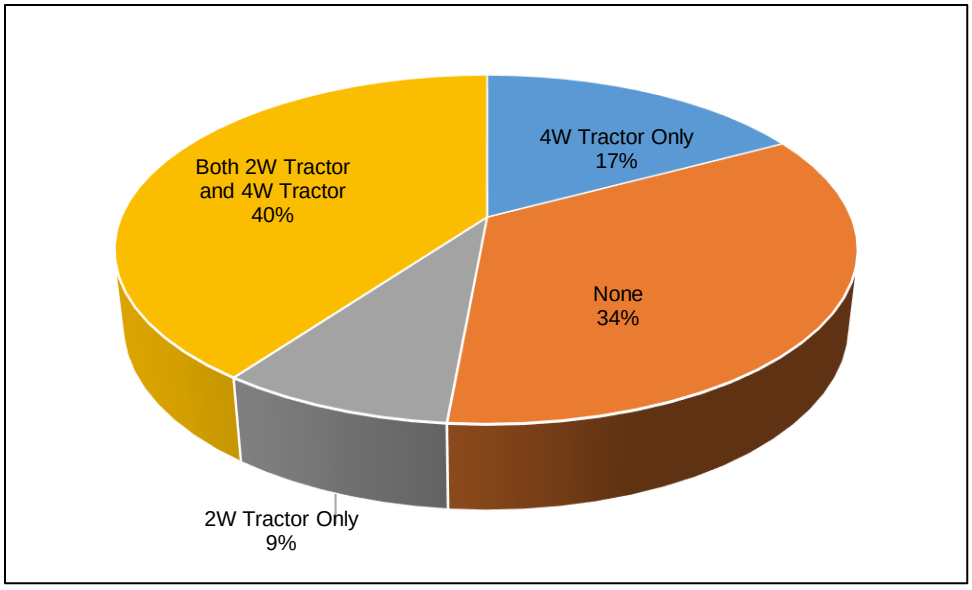

Figure 3. Availability of tractors in Sitio Proper I, Proper II, Udiongan, and Calumpit, Brgy. Macabud, Rodriguez, Rizal, October 2018.

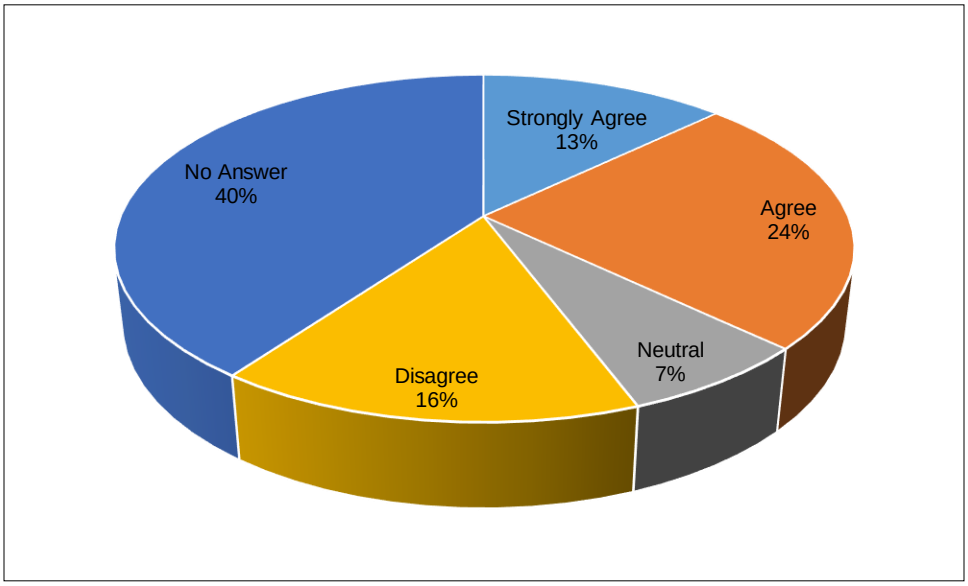

Figure 4. Willingness of the respondents to use the e-Tractor for transport in Sitio Proper I, Proper II, Udiongan, and Calumpit, Brgy. Macabud, Rodriguez, Rizal, October 2018.

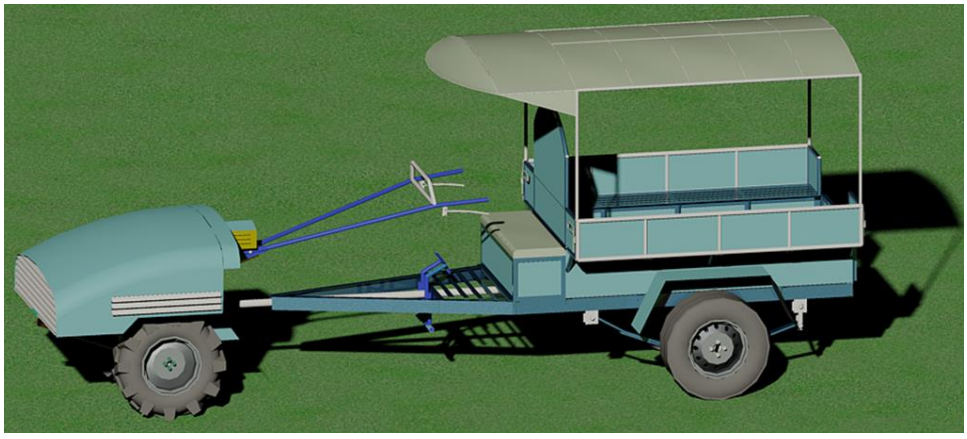

Figure 5. Rendered design of the e-Tractor using AutoCad ®.

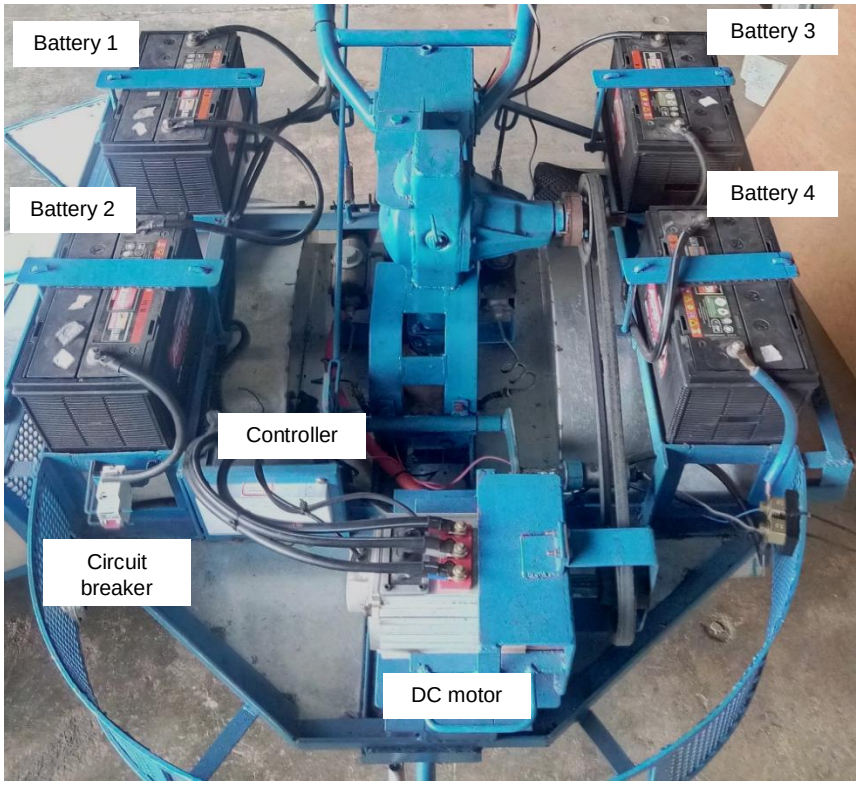

Figure 6. The wiring of the electrical components of the e-Tractor.

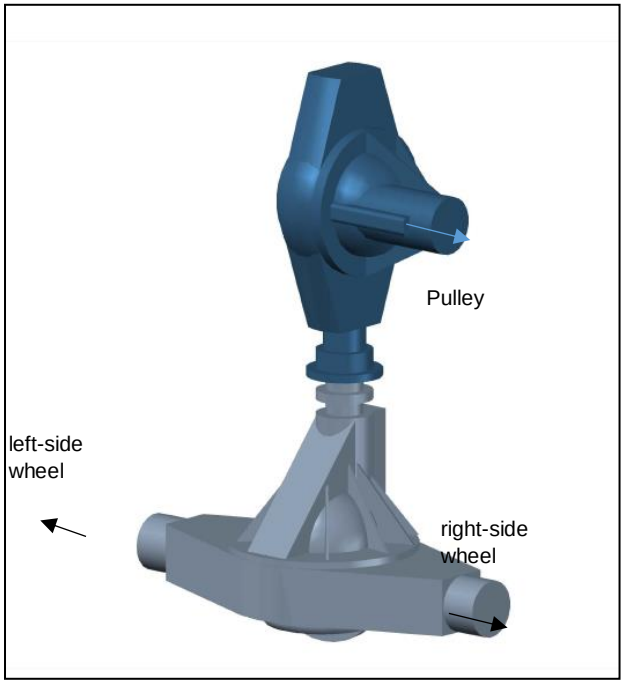

Figure 7. Rendered UPLB design for hand tractor transmission system.

Figure 8. Fabricated e-Tractor with trailer.

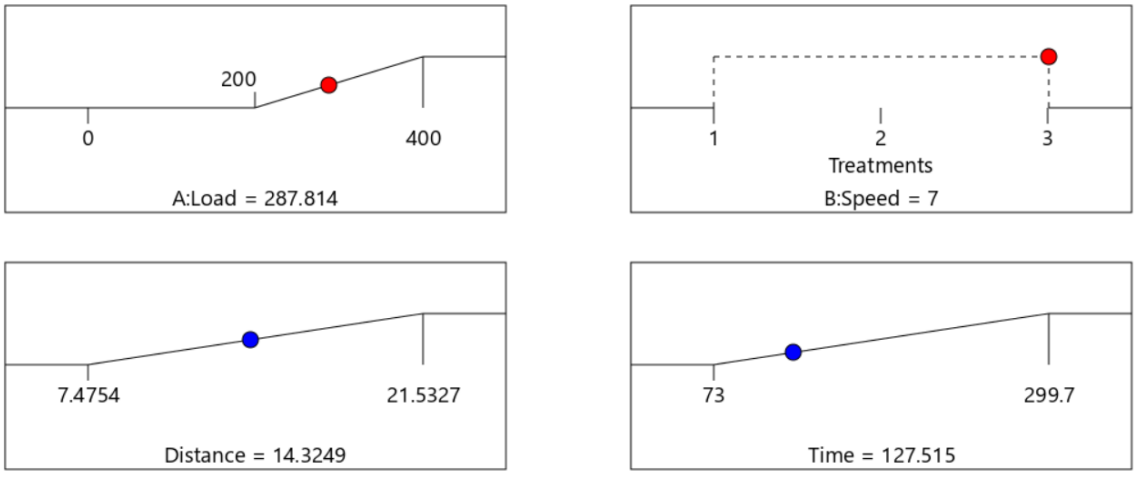

Figure 9. Solution obtained from Design Expert 11.

The papers published in this issue were judged Best Paper Award during the Philippine Society of Agricultural and Biosystems Engineers (PSABE) Annual Convention Technical Paper Presentation held at SMX Convention Center Bacolod City on April 25, 2019

PHILIPPINE SOCIETY OF AGRICULTURAL AND BIOSYTEMS ENGINEERS
793 UNIT 6B8 VICTORIA STATION 1, EDSA GMA KAMUNING
QUEZON CITY, PHILIPPINES